Behavioural and molecular phenotypes of mouse models for ASD

Sven Oliver Bachmann

A thesis submitted to Cardiff University in accordance with the requirements for the degree of Doctor in Philosophy in the discipline of Neuroscience

School of Biosciences, Cardiff University

June 2018

Declaration

This work has not been submitted in substance for any other degree or award at this or any other university or place of learning, nor is being submitted concurrently in candidature for any degree or other award.

Signed …… Date ……

STATEMENT 1

This thesis is being submitted in partial fulfillment of the requirements for the degree of a PhD.

Signed …… Date ……

STATEMENT 2

This thesis is the result of my own independent work/investigation, except where otherwise stated, and the thesis has not been edited by a third party beyond what is permitted by Cardiff University's Policy on the Use of Third Party Editors by Research Degree Students. Other sources are acknowledged by explicit references. The views expressed are my own.

Signed …… Date ……

STATEMENT 3

I hereby give consent for my thesis, if accepted, to be available online in the University's Open Access repository and for inter-library loan, and for the title and summary to be made available to outside organisations.

Signed …… Date ……

Acknowledgements

I would like to thank my supervisor Stéphane for giving me the opportunity to do my PhD in his lab. I`m extremely grateful for all the interesting and constructive discussion we had. I learned a lot from you and I appreciate your openness to share your thoughts. Further, I`m tremendously grateful for all your support, enthusiasm and positivity.

This project was funded by the Sêr Cymru programme, which was initiated by the Welsh Government. I would like to thank for supporting my PhD.

I would like to thank Adam Ranson and Fangli Chen for their expertise and help with the structural plasticity imaging and Sophie Waldron for the spine counting.

Thanks to all members of the group for your help, ideas and collaborative efforts on many projects. The working environment you created was truly encouraging and pleasant. I would like to extend my thanks to current and former members for the Barde lab and the Martinez-Garay lab for broadening the view on scientific topics and for contributing to the community on our floor. Special thanks to Katharina and Pedro for your friendship beyond the working environment.

At this point, I would like to thank all my friends and my family for their endless support. It was extremely encouraging to receive such an enormous support from home during the time of my PhD abroad. A special thanks to my friends Lucas and Philippe. Last but not least, thank you, mum and dad, for all your time and love. My warmest thanks to my brother Dani for the constant motivation.

Abstract

Autism spectrum disorders (ASD) are more prevalent in male than in female individuals and are characterised by clinical core symptoms such as impaired sociability, verbal communication and ritualistic behaviours. The gene encoding the cytoplasmic FMR1 interacting protein 1 (CYFIP1) has been associated with ASD in humans. At the molecular level, CYFIP1 has been demonstrated to negatively regulate protein synthesis and actin remodelling. At the neuronal level, *Cyfip1* haploinsufficiency leads to defects in synaptic plasticity associated with alteration of dendritic spine morphology, two pathophysiological features found in numerous mouse models of ASD. However, the consequences of *Cyfip1* deletion at the behavioural level remains unclear, limiting our understanding of the relationship between pathophysiology and behavioural phenotypes.

With this study, we aimed to characterise the behavioural phenotype of *Cyfip1*$^{+/-}$ mice and then to identify associated cellular phenotypes. The results we obtained revealed sex-specific defects in social interest and motor learning. In addition, motor learning deficits were observed in adult *Cyfip1*$^{+/-}$ mice but not earlier in development. Associated with motor learning deficits, we identified a brain region-specific neuronal phenotype with decreased dendritic spine densities and increased dendritic spine turnover in *Cyfip1*$^{+/-}$ mice. The dendritic spine formation and the *in vivo* protein synthesis rate were intact in *Cyfip1*$^{+/-}$ mice.

These results identified behavioural deficits in *Cyfip1*$^{+/-}$ mice, which relate to symptoms and comorbidities of ASD in human. The cellular phenotypes indicated an alteration of dendritic spine density and spine turnover, a phenotype found in several mouse models of ASD and in humans affected by the condition. Altogether, these findings indicate that *Cyfip1*$^{+/-}$ mice can represent a valuable model for the study of ASD pathophysiology and in particular the relationship between specific neuronal phenotypes and behavioural alterations.

Abbreviations

ABI1/2	ABI interactor 1/2
AMPARs	α-amino-3-hydroxy-5-methyl-4-isoxazolepropionic acid receptors
ANOVA	Analysis of variance
Arp2/3	Actin-related protein 2/3
ASD	Autism spectrum disorders
BDNF	Brain-derived neurotrophic factor
CA1	*Cornu Ammonis 1*
Cb	Cerebellum
cm	Centimetre/s
CNS	Central nervous system
Crhr2	Corticotropin releasing hormone receptor 2
CYFIP1	Cytoplasmic FMRP interacting protein 1
CYFIP2	Cytoplasmic FMRP interacting protein 2
Cyp2d9	Cytochrome P450, family 2, subfamily d, polypeptide
DHPG	Dihydroxyphenylglycine
DTI	Diffusor tensor imaging
EGFP	Enhanced green fluorescent protein
eIF4E	Eukaryotic translation initiation factor E
FMRP	Fragile X mental retardation protein
$GABA_AR$ β2/3	Gamma-aminobutyric acid type A receptor beta 2/3
GAPDH	Glyceraldehyde 3-phosphate dehydrogenase
GTP-Rac1	Guanosine triphosphate bound Rac1
h	Hour/s
Hpc	Hippocampus
HSPC300	Haematopoietic stem cell protein 300

Li	Liver
LTD	Long-term depression
LTP	Long-term potentiation
M1	Primary motor cortex
mCx	Motor cortex
mEPSC	Miniature excitatory postsynaptic currents
MGH	Mixed genotype housing
mGluR1	Metabotropic glutamate receptor 1
min	Minute/s
mIPSC	Miniature inhibitory postsynaptic currents
ml	Millilitre/s
mm	Millimetre/s
mM	Millimole/s
mRNA	Messenger ribonucleic acid
Mup	Major urinary protein
NCKAP1	Non-catalytic region of tyrosine kinase adaptor protein 1 associated protein 1
Nlgn3	Neuroligin-3
nm	Nanometre/s
P40	Postnatal day 40
P60	Postnatal day 60
PCR	Polymerase chain reaction
p-eIF4E	Phosphorylated eukaryotic translation initiation factor E
RNA	Ribonucleic acid
s	Second/s
S1/2	Social odour 1/2
sCx	Somatosensory cortex
SEM	Standard error of the mean

SGH	Single genotype housing
Str	Striatum
Temp.	Temperature
TUBGCP3	Tubulin gamma complex associated protein 3
V1	Primary visual area
WAVE1	Wiskott-Aldrich syndrome protein family verprolin homologous protein 1
WRC	Wiskott-Aldrich syndrome protein family verprolin homologous protein 1 regulatory complex
WRIS	WRC interacting receptor sequence
WT	Wild type
µl	Microlitre/s
µm	Micrometre/s
µM	Micromole/s

Contents

List of Figures

List of Tables

Chapter 1

Introduction

1.1. Microdeletions and microduplications of chromosome 15q11.2

This chapter summarises the role of *CYFIP1* in the context of the human pathology. *CYFIP1* is one of the genes encoded in the 11.2 region of chromosome 15, which can undergo structural rearrangements such as microdeletions and microduplications. 15q11.2 microdeletions and microduplications are associated with Prader-Willi and Angelman syndromes, which allow explaining the relationship between genetics and clinical relevance of *CYFIP1*.

Prader-Willi and Angelman syndromes arise from deletions of risk genes located on chromosome 15 (Nicholls & Knepper 2001). These deletions can be classified into two types. The genetic deletion between breakpoint 1 and breakpoint 2 is classified as Type I deletion of 6.58 megabases, whereas the Type II deletion of 5.33 megabases occurs between breakpoint 2 and breakpoint 3 (Amos-Landgraf et al. 1999; Butler et al. 2008). The larger Type I deletion is associated with more severe neurodevelopmental symptoms than the Type II deletion (Butler et al. 2004; Milner et al. 2005; Varela et al. 2005; Bittel et al. 2006). Both types of deletions are characterised by neurobehavioral deficits, developmental speech and motor delays, which are most commonly described manifestations in individuals with microdeletions in the 11.2 region (Cox & Butler 2015). Some of the 15q11.2 deletion carriers also show symptoms of autism (Sahoo et al. 2007; Burnside et al. 2011; Madrigal et al. 2012), schizophrenia (Kirov et al. 2009; Rees et al. 2014; Stefansson et al. 2014) or seizures (Valente et al. 2013). Individuals carrying 15q11.2 microduplications (Browne et al. 1997; Roberts et al. 2002) also show clinical symptoms including developmental, motor and speech delays (Burnside et al. 2011; Benítez-Burraco et

al. 2017) and, for some of them, autistic features (Van Der Zwaag et al. 2010; Burnside et al. 2011). 15q11.2 deletions were reported to occur at a frequency of 8 in 3,992 individuals (0.20%) and duplications at a frequency of 16 in 4,363 individuals (0.37%) whereas developmental delays are more likely upon 15q11.2 microdeletions than microduplications (Burnside et al. 2011).

Four genes were identified to be encoded in 15q11.2: tubulin gamma complex associated protein 3 (*TUBGCP3*), *CYFIP1* and non-imprinted in Prader-Willi/Angelman syndrome 1 and 2 (*NIPA1/2)* (Chai et al. 2003). Notably, Prader-Willi and Angelman syndromes are imprinted genetic disorders. The Prader-Willi syndrome results from the functional lack of paternally inherited genes, whereas the Angelman syndrome arises from the loss of maternally expressed genes on chromosome 15 (Nicholls & Knepper 2001). With regards to the genes located in the 11.2 region, *NIPA1/2* are non-imprinted genes and there is no evidence for *TUBGCP3 or CYFIP1* to be imprinted (Chai et al. 2003). *TUBGCP3* encodes a member of the gamma-tubulin small complex involved in microtubule nucleation and dynamics (Raynaud-Messina & Merdes 2007; Murphy et al. 2001). The proteins encoded by *NIPA1 and NIPA2* function as magnesium ion transporters (Goytain et al. 2007). The functions of the protein encoded by *CYFIP1* are summarised below (1.2 and 1.3.).

In order to understand the pathophysiologic contribution of *TUBGCP3*, *CYFIP1* and *NIPA1/2* the corresponding mRNA levels were determined in carriers of 15q11.2 deletion or duplication. Microdeletions of 15q11.2 correlated with decreased *TUBGCP3*, *CYFIP1* and *NIPA1/2* mRNA levels in lymphoblastoid cells derived from patients with Prader-Willi syndrome (Bittel et al. 2006). Decreased *CYFIP1* mRNA levels were also found in leukocytes obtained from patients diagnosed with Fragile X and Prader-Willi syndromes (Nowicki et al. 2007). However, the authors did not clarify whether 15q11.2 microdeletions or microduplications were involved. Nevertheless, decreased *CYFIP1* mRNA levels were detected in a subject that had been diagnosed with autism and carried an *SH3 and multiple ankyrin repeat domains 2* (*SHANK2)*

deletion (Leblond et al. 2012). On the other hand, *TUBGCP3* and *NIPA1/2* mRNA levels (Van Der Zwaag et al. 2010) and *CYFIP1* mRNA levels (Van Der Zwaag et al. 2010; Noroozi et al. 2018) were increased in whole blood RNA extracts from patients diagnosed with ASD.

Availability of patient-derived samples is restricted and limits the preclinical research. Therefore, investigating the mechanism that links dysregulated gene dosage of *TUBGCP3, CYFIP1* and *NIP1/2* with the symptoms required a model system. In the mouse, orthologues of *TUBGCP3, CYFIP1* and *NIPA1/2* were identified and on chromosome 7 (Chai et al. 2003).

1.2 Molecular functions of CYFIP1

This chapter summarises the molecular roles of CYFIP1. The focus is first set on CYFIP1 as an effector downstream of the small GTPase Rac1 and CYFIP1 as a member of the WAVE regulatory complex. Second, the role of CYFIP1 as a negative regulator of translation is described in chapter 1.2.2. Notably, *Cyfip1* is expressed in neurons but numerous insights into the molecular roles of CYFIP1 originate from studies using non-neuronal cells.

1.2.1 CYFIP1 as a regulator of actin dynamics

1.2.1.1 CYFIP1/Sra-1 association with Rac1 GTPase

CYFIP1 was initially named specifically Rac1-associated protein 1 (Sra-1) referring to its binding to the small GTPase Rac1. The small GTPase Rac1 is a member of the Rho family GTPases which regulates actin reorganisation (Hall 1998). In order to better understand Rac1 specific functions, a study was conducted to identify novel

targets of the small GTPase Rac1. Affinity purification was used to probe for Rac-1 interacting proteins in the bovine brain cytosol, which revealed a protein with a molecular weight of 140 kilodaltons (Kobayashi et al. 1998). Interestingly, this protein of 140 kilodaltons was specifically co-purified with the active guanosine triphosphate (GTP) bound form of Rac1, but not with Rac1 in its inactive guanosine diphosphate (GDP) bound state (Kobayashi et al. 1998). This was the first functional characterisation of a previously discovered protein of 1,253 amino acids encoded by the gene *shyc* involved in neuronal differentiation *in vitro* (Nagase et al. 1995; Köster et al. 1998). Moreover, the interaction between GTP-Rac1 and the identified interaction partner was demonstrated to be established by the N-terminus of the identified protein. This association was specific to GTP-Rac1 as other small GTPases such as cell cycle division control protein 42 homologue (Cdc42) or Ras homologue gene family member A (RhoA) did not bind the identified GTP-Rac1 interactor. Therefore, the characterised protein was named specifically Rac1-associated protein 1 (Sra-1) (Kobayashi et al. 1998), also known as CYFIP1.

Rac1 was reported to regulate the actin cytoskeleton dynamics associated with membrane ruffling in mouse-derived Swiss 3T3 and human-derived KB cells (Ridley et al. 1992; Nishiyama et al. 1994). In addition, CYFIP1 co-sedimented with filamentous actin in KB cells (Kobayashi et al. 1998). This suggested that the CYFIP1 as a Rac1 effector is potentially involved in actin filament organisation associated with membrane ruffling. However, the molecular pathway linking CYFIP1 to actin remodelling remained unclear up until the characterisation of the Wiskott-Aldrich syndrome protein family verprolin homologous protein (WAVE) regulatory complex.

1.2.1.2 CYFIP1 is a member of the WAVE regulatory complex

CYFIP1 is a member of the Wiskott-Aldrich syndrome protein family verprolin homologous protein (WAVE) regulatory complex (WRC). The WRC is an assembly of the proteins WAVE1/2/3, CYFIP1/2, Nck-associated protein 1 (NCKAP1), ABI interactor 1/2 (ABI1/2) and haematopoietic stem cell protein 300 (HSPC300) (Dai & Pendergast 1995; Shi et al. 1995; Eden et al. 2002; Kunda et al. 2003; Schenck et al. 2003; Chen et al. 2010). The assembled WRC inhibits the verprolin-homology central acidic regions (VCA) motif of WAVE1 which is required for the binding and activation of actin-related protein 2/3 (Arp2/3) (Takenawa & Suetsugu 2007; Chen et al. 2010; Padrick & Rosen 2010). Inhibition of the WRC relies on the binding of CYFIP1 to the WAVE1 VCA (Chen et al. 2010). Point mutations of CYFIP1 prevented Rac1 binding to the WRC (Chen et al. 2010) in agreement with the finding that Rac1 does not directly bind to the WRC (Pollard & Borisy 2003; Chen et al. 2010). This suggests that WRC-associated CYFIP1 serves as a binding site for Rac1 (Chen et al. 2010), which is supported by the reported Rac1-CYFIP1 interaction (Kobayashi et al. 1998).

These findings allow concluding on a working model in which the assembled WRC includes CYFIP1 as an inhibitor of the WAVE1 VCA (**Figure 1.1**). Binding of activated GTP-bound Rac1 triggers a conformational change in CYFIP1 (De Rubeis et al. 2013) and releases CYFIP1 from the WRC. Consequently, the inhibition of the WAVE1 VCA is abolished. As a result, the VCA motif can promote actin filament nucleation by V-region dependent recruitment of actin monomers and C- and A-region mediated conformational changes in Arp2/3 (Marchand et al. 2001; Goley et al. 2004).

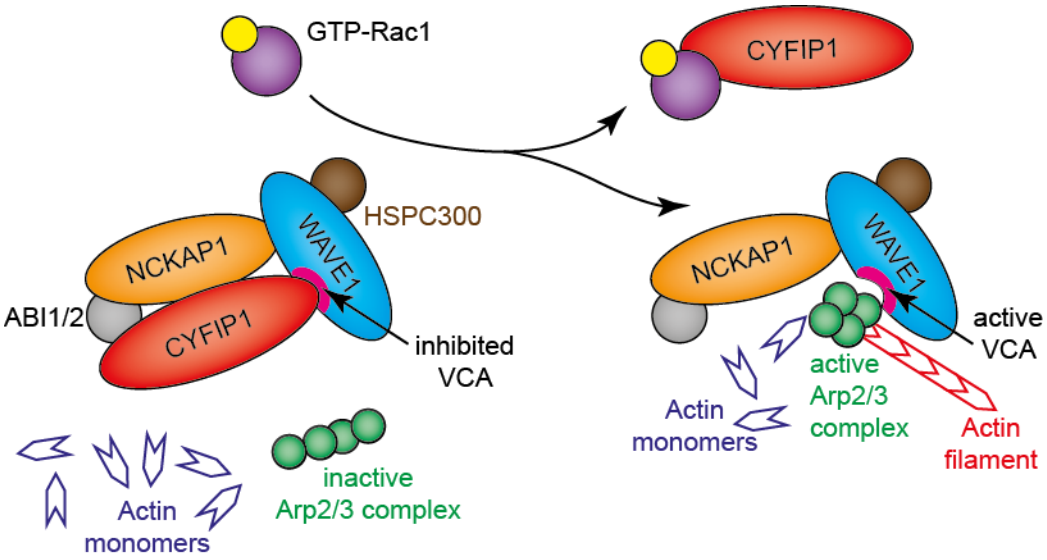

Figure 1.1 Schematic of CYFIP1 as a negative regulator of the WRC.
CYFIP1 is a member and negative regulator of the multiprotein WRC. Dissociation of CYIFP1 overcomes the WRC inhibition and the WAVE1 VCA promotes actin nucleation. Schematic adapted from Abekhoukh & Bardoni 2014.

1.2.2 CYFIP1 as a translational repressor

Despite the previous characterisation and terminology of the protein encoded by the mouse orthologue of human cDNA clone KIAA0068 as Sra-1 (Kobayashi et al. 1998) (as discussed in chapter 1.2.1.1), CYFIP1 became the commonly used annotation based on the findings described here.

A study was conducted to better understand the pathophysiology underlying the fragile X syndrome caused by mutations or loss of *fragile X mental retardation 1* (*FMR1)* (Verkerk et al. 1991). The aim of the study was to identify novel interaction partners of the *FMR1* encoded fragile X mental retardation protein (FMRP). Therefore, the N-terminal part of FMRP was used as a bait in a two-hybrid system to screen an embryonal mouse library (Schenck et al. 2001). The screening revealed the protein encoded by the mouse orthologue of human cDNA clone KIAA0068. The

identified FMRP interactor was denoted as cytoplasmic FMRP Interacting protein 1 (CYFIP1).

In the following, relevant FMRP functions are introduced to then explain the consequences of the FMRP-CYFIP1 interaction. FMRP is known to bind to RNAs either directly via G quartet structures and U-rich sequences or through noncoding RNAs (Ashley et al. 1993; Siomi et al. 1993). This enables FMRP to localise mRNAs as cargo to granules that are transported from the soma to dendrites (Kanai et al. 2004). In addition, FMRP can stabilise target mRNAs based on the finding that FMRP binds the 3` untranslated region of *postsynaptic density protein 95* (*PSD-95*) mRNA and increased *PSD-95* mRNA half-life upon pharmacological inhibition of transcription (Zalfa et al. 2007). The RNA binding properties also support the role of FMRP in translational repression (Brown et al. 2001; Qin et al. 2005; Bassell & Warren 2008; Darnell et al. 2011; Michalon et al. 2012). Translational repression is mediated by FMRP binding to the L5 protein on the ribosomal 80S subunit which hinders the binding of tRNA and translation elongation factors (Che et al. 2015). CYFIP1 as an identified FMRP interacting protein was therefore studied for its involvement in translational control. Translation initiation is established by a complex of the eukaryotic translation initiation factor (eIF) 4E, 4G and 4A (Sonenberg & Hinnebusch 2009). Inhibition of the assembly of this complex is a regulatory mechanism reducing translation initiation. 4E binding proteins are negative regulators of the assembly of the translation initiation complex by specifically interfering with the association of eIF4E with eIF4G (Richter & Sonenberg 2005). Pull-down experiments revealed that CYFIP1 binds directly to eIF4E (Napoli et al. 2008; Beggs et al. 2015). Therefore, FMRP can repress the translation of target mRNAs through CYFIP1 (**Figure 1.2**). Moreover, this process could be promoted by FMRP stabilising CYFIP1 at the 5` end of the target mRNAs (Napoli et al. 2008). Neuronal signalling can mediate the dissociation of the CYFIP1-eIF4E interaction as discussed in the following section.

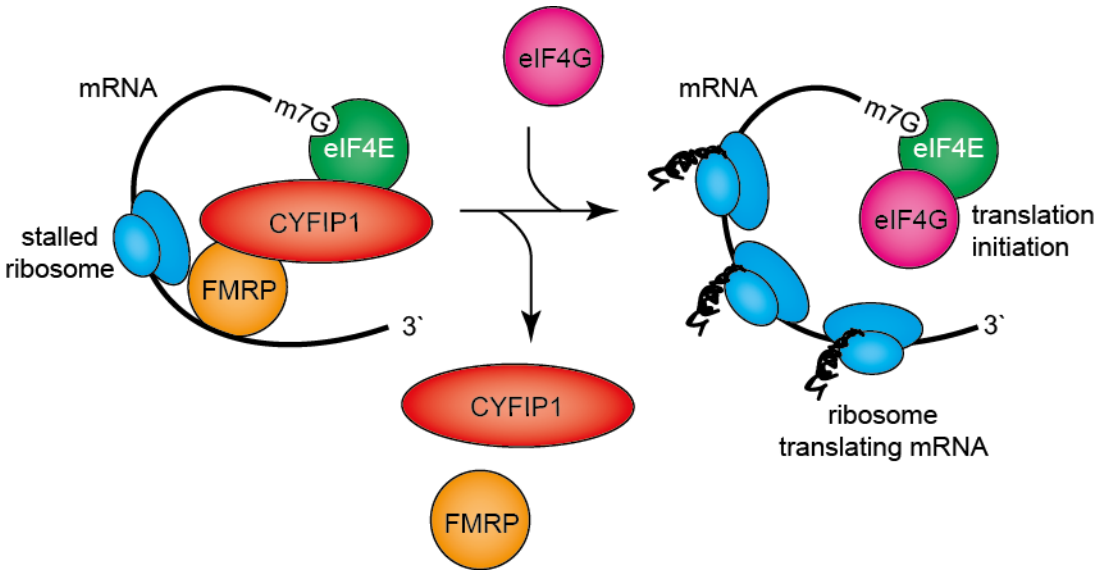

Figure 1.2 Schematic of CYFIP1 as a negative regulator of translation.
CYFIP1 mediates translational repression based on its interaction with eIF4E and FMRP. CYFIP1 interferes with the assembly of the translation initiation complex centred around eIF4E as whereas FMRP mediates stalling of the ribosomal unit 80S. Dissociation of the eIF4E-CYFIP1-FMRP interaction results in translation initiation and protein synthesis. Schematic adapted from De Rubeis et al. 2013.

CYFIP1 acting as a WRC regulator downstream of Rac1 and as a repressor of protein translation can be reconciled. The structure of the assembled CYFIP1 containing WRC complex does not enable CYFIP1 to simultaneously bind to eIF4E binding. This is supported by pull-down experiments which did not reveal WRC components associated with eIF4E bound CYFIP1 (Napoli et al. 2008). Thus, Rac1 has been suggested to regulate the mode of CYFIP1 function where activated Rac1 releases CYFIP1 from the WRC (Cory & Ridley 2002; Eden et al. 2002) which enables CYFIP1 to associate with FMRP and eIF4E to repress protein synthesis (De Rubeis et al. 2013).

1.3. Neuronal functions of CYFIP1

Cyfip1 is highly conserved in evolution and its expression in the central nervous system has been demonstrated in *Drosophila melanogaster* (Schenck et al. 2001), *Mus musculus* (Napoli et al. 2008), *Bos taurus* (Kobayashi et al. 1998) and *Homo sapiens* (Oguro-Ando et al. 2014). Neurons are polarised cells with a specific cellular biology and neuronal CYFIP1 functions have been studied. CYFIP1 has been implicated in the regulation of neuronal morphology and electrophysiologic properties. This chapter describes first CYFIP1 functions related to neuronal morphology and second CYFIP1 functions related to neuronal transmission.

1.3.1 Synaptic morphology

In *Drosophila melanogaster*, heterozygous *Cyfip1* deletion is associated with decreased size of the neuromuscular junction (Schenck et al. 2003; Zhao et al. 2013), increased number of boutons and increased filamentous actin assembly (Zhao et al. 2013). This suggests that lack of CYFIP1 as a repressor of actin dynamics leads to increased actin nucleation. This consequently promotes formation and stabilisation of growth cone protrusions (Gomez & Letourneau 2014) giving rise to aberrant neuromuscular junction size. Increased presynaptic filamentous-actin assembly, as well as increased protein synthesis, was observed in hippocampal neurons from heterozygous *Cyfip1* mice (Hsiao et al. 2016). Rac1 inhibition normalised actin nucleation, suggesting that the mechanism is independent of the increased protein synthesis rate (Hsiao et al. 2016). Thus, CYFIP1 at the presynapse controls actin dynamics through Rac1 which is associated with morphologic consequences.

Cyfip1 overexpression in mouse hippocampal neurons *in vitro* increased dendritic complexity accompanied by increased dendritic length, increased number of filopodia and increased numbers of long and thin spines whereas the spine density was remained unchanged (Pathania et al. 2014).

The dendritic architecture was also studied in the context of *Cyfip1* deletion using cultured hippocampal neurons heterozygous for *Cyfip1*. In contrast to *Cyfip1* overexpression, *Cyfip1* haploinsufficiency revealed decreased dendritic complexity comprising reduced dendritic length and number of branch points without affecting the dendritic density overall. Although, morphologic spine subtypes such as long and thin spines and filopodia were increased in *Cyfip1*$^{+/-}$ dendrites compared to wild type dendrites (Pathania et al. 2014). Decreased dendritic complexity and thin dendrites were also observed in fixed *Cyfip1*$^{+/-}$ *Cornu Ammonis 1* (CA1) neurons compared to wild type controls (Pathania et al. 2014). Hence, *Cyfip1* deletion results in decreased dendritic complexity and increased number of spines with morphologic properties associated with immaturity whereas the net dendritic density remained unchanged (Pathania et al. 2014). Similar observations were made in principal neurons originating from mice with a conditional homozygous *Cyfip1* deletion selectively in principal cells of the neocortex (Davenport et al. 2018). This suggests that altered spine morphology results from a cell-autonomous mechanism involving CYFIP1.

Alongside altered dendritic spine morphology upon *Cyfip1* deletion, increased assembly of filamentous actin was observed in cultured hippocampal *Cyfip1*$^{+/-}$ neurons compared to wild type controls (Pathania et al. 2014). This finding is not unexpected since CYFIP1 is a regulator of actin dynamics (section 1.2.1). Actin is localised at dendritic spines (Matus et al. 1982) and is crucial for development and maintenance of dendritic spines (Wegner et al. 2008; Hotulainen et al. 2009), structural plasticity (Halpain 2000; Matus et al. 2000; Kim et al. 2013) and the anchoring of postsynaptic receptors such as α-amino-3-hydroxy-5-methyl-4-isoxazolepropionic acid receptors (AMPARs) and *N*-methyl-D-aspartate receptors (NMDARs) at excitatory synapses (Allison et al. 1998). Formation of a dendritic spine has been suggested to be initiated by a dynamic filopodium, which cycles between elongation and shrinkage where actin polymerisation at the tip is independent of Arp2/3 activity but potentially occurring at the root of the filopodium. With the

beginning of spine head formation, Arp2/3 nucleates branched actin filaments that mediate spine head growth. During spine maturation, cofilin counteracts actin polymerisation to regulate the spine length. Actin polymerisation and disassembly at the surface of a mature dendritic spine allow morphologic plasticity (Hotulainen et al. 2009).

In the light of the relevance of actin dynamics in neurons, spine pathologies have been characterised in patients diagnosed with ASD (Hutsler & Zhang 2010), epilepsy (Bothwell et al. 2001), schizophrenia and bipolar disorder reviewed in (Glausier & Lewis 2013; Forrest et al. 2018). Since CYFIP1 regulates actin dynamics, dysregulated CYFIP1 levels might have consequences on stabilisation of dendritic spines (Luo et al. 1996; Nakayama et al. 2000). Thus, it is possible that CYFIP1 plays a role in the spine pathologies observed in different psychiatric conditions.

Dysregulated CYFIP1 protein levels might have more broad implications for the synaptic morphology since CYFIP1 is necessary for the recruitment and localisation of the WRC. The fully assembled WRC, but not any WRC subcomplex, enables association of CYFIP1 and ABI2 (Ismail et al. 2009; Chen et al. 2010). The CYFIP1-ABI2 interaction serves as a binding site for a specific motif named WRC interacting receptor sequence (WRIS) (Chen et al. 2014). Numerous adhesion proteins, receptors, ion channels and scaffolding proteins were identified to contain the WRIS sequence and were validated as WRC ligands (Nakao et al. 2008; Tai et al. 2010; Stavoe et al. 2012). WRIS containing proteins or synergistic protein complexes can recruit the WRC. For example clustering of WRIS motif containing membrane proteins at the cell membrane can recruit the WRC to the membrane. Interestingly, WRIS motifs were found in synaptic proteins such as neuroligins, protocadherins and G-protein coupled receptors (Chen et al. 2014). This suggests a role for CYFIP1 as a synapse-specific regulator of the WRC with implications in dendritic morphology. However, the effect of the WRC binding through WRIS motifs depends on WRIS neighbouring motifs which are likely to involve various regulatory functions.

1.3.2 Synaptic physiology

The postsynaptic proteome can be regulated by local translation (Steward & Schuman 2003; Glock et al. 2017) which is thought to be crucial for neuronal function and specification of neuronal networks (Martin et al. 2000; Pfeiffer & Huber 2006). Postsynaptic local protein translation is induced by two distinct mechanisms. Brain-derived neurotrophic factor (BDNF) binds and activates its receptor, tropomyosin receptor kinase B (TrkB) (Barbacid 1994), which in turn alleviates FMRP-dependent repression of translation. This leads to increased expression of specific proteins including the activity regulated cytoskeleton associated protein (Arc) and alpha Ca^{2+}/calmodulin-dependent protein kinase II (αCaMKII) (Aakalu et al. 2001; Yin et al. 2002; Schratt et al. 2004). Similarly, stimulation of the metabotropic glutamate receptor 1 (mGluR1) alleviates FMRP-dependent repression of translation (Weiler & Greenough 1993). Studies hypothesised that activation of TrkB or mGluR1 could modulate the binding between CYFIP1, FMRP and the translation initiation factor eIF4E to control protein translation. Using synaptosome preparations of primary cortical cultures it was demonstrated that BDNF activation of TrkB and dihydroxyphenylglycine (DHPG) stimulation of mGluR1 signalling decreases the interaction between CYFIP1 and eIF4E (Napoli et al. 2008; Panja et al. 2014; Genheden et al. 2015). TrkB signalling mediated CYFIP1-eIF4E dissociation requires the activation of mitogen-activated protein kinase interacting protein kinases, a mechanism also observed in non-neuronal cells (Panja et al. 2014; Beggs et al. 2015; Genheden et al. 2015). Further, sustained activation of mGluR1 can lead to synaptic plasticity such as long-term potentiation (LTP) or long-term depression (LTD). Hippocampal slices were prepared from *Cyfip1* haploinsufficient mice and Schaffer collateral - CA1 synapses were assessed by electrophysiologic recordings. LTD induction by paired pulse-low frequency stimulation or DHPG application revealed enhanced reductions in field excitatory postsynaptic potential slopes (Bozdagi et al.

2012). In wild type but not in *Cyfip1*$^{+/-}$ mice, inhibition of protein translation using cycloheximide or a mammalian target of rapamycin (mTOR) inhibitor prevented LTD induction (Bozdagi et al. 2012). Induction of LTP at Schaffer collateral - CA1 synapses was not affected by *Cyfip1* haploinsufficiency. Taken together, these results show that CYFIP1 is required for TrkB and mGluR1 activity-dependent regulation of protein synthesis and LTD (Bozdagi et al. 2012).

CYFIP1 localises at excitatory synapses and *Cyfip1* overexpression increased the number of excitatory synapses (Pathania et al. 2014; Davenport et al. 2018). *Cyfip1* overexpression also increased miniature excitatory postsynaptic current (mEPSC) frequencies (Davenport et al. 2018). The knockout of *Cyfip1* specifically in glutamatergic principal cells of the neocortex and hippocampus was demonstrated to increase miniature inhibitory postsynaptic current (mIPSC) amplitudes in CA1 pyramidal neurons. In contrast, AMPARs mediated mEPSCs remained unchanged despite increased AMPAR mobility at the synapse (Pathania et al. 2014; Davenport et al. 2018). The increased inhibitory transmission can be explained by increased levels of gamma-aminobutyric acid type A receptor beta 2/3 ($GABA_AR$ β2/3) that can serve as building blocks for $GABA_AR$ receptors expressed at the cell membrane (Lüscher et al. 2011). This finding illustrates that CYFIP1 can have cell non-autonomous effects on inhibitory synaptic transmission. In contrast to *Cyfip1* deletion, *Cyfip1* overexpression in cultured hippocampal neurons revealed decreased inhibitory synapse size and decreased mIPSC amplitudes (Davenport et al. 2018). Therefore, the bidirectional dosage of *Cyfip1* has opposite effects on synaptic excitation and inhibition. This indicates that CYFIP1 is involved in the regulation of inhibitory and excitatory synapses with consequences on synaptic transmission. The functional and structural consequences of *Cyfip1* overexpression point towards potential pathophysiologic mechanisms underlying the 15q11.2 microduplication. However, *Cyfip1* overexpression is not directly elucidating the physiologic function of CYFIP1. Notably, CYFIP1 localisation at excitatory and inhibitory synapses was

determined based on *Cyfip1* overexpression (Pathania et al. 2014; Davenport et al. 2018) which can lead to ectopic localisation of CYFIP1.

The specific molecular mechanisms underlying these neuronal CYFIP1 functions remain elusive. In addition, *Cyfip1* expression in the brain might not be restricted to neurons but up until now, there is no supportive literature on *Cyfip1* expression in glial cells.

1.4 The *Cyfip1* paralogue *Cyfip2*

Mouse *Cyfip1* shares high sequence homology (87.7% identity, 94.5% homology) with the gene encoding the human p53-mediated pro-apoptotic protein (PIR121) (Saller et al. 1999; Schenck et al. 2001). This observation was made alongside the characterisation of the Rac1-CYFIP1 interaction. Therefore, PIR121 was validated by pull-down experiments to bind to FMRP, which designated PIR121 as cytoplasmic FMRP interacting protein 2 (CYFIP2) (Schenck et al. 2001).

In human, *CYFIP2* is encoded on chromosome 5q33.3. *CYIFIP2* is a *CYFIP1* paralogue which is not associated with structural rearrangements of 15q11.2. *CYFIP2* has been related to neuropathologies such as schizophrenia, epilepsy, Alzheimer`s disease (Föcking et al. 2015; Tiwari et al. 2016; Nakashima et al. 2018). Outside of the central nervous system, *CYFIP2* characterised as a target of the tumour protein p53 in cells related to lung, colorectal cancer and gastric cancer (Saller et al. 1999; Jackson et al. 2007; Jiao et al. 2017). CYFIP2 interacts through its N-terminus with FMRP like CYFIP1 but CYFIP2 binds FMRP with a higher affinity. In addition to FMRP, CYFIP2 associates with the FMRP related proteins FXR1P, and FXR2P (Schenck et al. 2001). In addition, CYFIP2 was determined as a member of WRC

whereas the functional characterisation is restricted to CFYIP1 (Eden et al. 2002; Chen et al. 2010).

CYFIP2 localises to excitatory (Pathania et al. 2014) and inhibitory (Davenport et al. 2018) synapses. *Cyfip2* overexpression in cultured hippocampal neurons results in increased number of excitatory synapses and decreased the number inhibitory synapses. The functional consequences are increased mEPSCs and reduction in mIPSC amplitudes. In addition, *Cyfip2* overexpression increases the dendritic complexity based on increased dendritic length and number of branch points (Pathania et al. 2014). The increased dendritic outgrowth observed in *Cyfip2* overexpressing neurons was prevented when the phosphorylation-deficient CYFIP2^{T1067A} was overexpressed (Lee et al. 2017). Heterozygous loss of *Cyfip2* resulted in increased number of immature spines and decreased number of mature spines in the cortex whereas the dendritic organisation was unchanged in CA1 neurons compared to wild type controls (Han et al. 2014). Moreover, structural plasticity upon DHPG stimulation of mGluR1 signalling was absent in cortical *Cyfip2*$^{+/-}$ neurons. In wild type cortical neurons, DHPG activation of mGluR1 signalling increased the number of mature dendritic spines and moreover increased *Cyfip2* mRNA levels independent from translation (Han et al. 2014). This suggests that CYFIP2 function is required for the regulation of dendritic morphology, mGluR1 induced structural plasticity and translational control of its own target mRNA.

Mice heterozygous for *Cyfip2* were hyperactive and showed decreased startle responses for auditory stimulus and enhanced prepulse inhibition (Han et al. 2014). In zebrafish, CYFIP2 deletion increases the activity of spiral fibre neurons resulting in enhanced startle sensitivity (Marsden et al. 2018). CYFIP1 and CYFIP2 have distinct roles in the axon of retinal ganglion cell in zebrafish. CYFIP2 controls filamentous actin dynamics in the growth cone upon axon-axon contact which mediates axon guidance whereas CYFIP1 regulates axon growth (Cioni et al. 2018). The presynaptic function of CYFIP2 has not been studied in the mouse, which makes it difficult to

argue that divergent functions of CYFIP1 and CYFIP2 are a presynaptic feature or specific to zebrafish.

Cyfip2 overexpression phenocopies structural and functional changes found by *Cyfip1* overexpression indicating an overlap of CYFIP1 and CYFIP2 functions (Pathania et al. 2014; Davenport et al. 2018). Nevertheless, *Cyfip2* is not compensating the embryonic lethal consequences of homozygous *Cyfip1* deletion in the mouse (Bozdagi et al. 2012; Pathania et al. 2014) and fly (Schenck et al. 2003; Zhao et al. 2013). This could be due to the fact that *Cyfip1* and *Cyfip2* have non-overlapping expression patterns in cell populations vital to the developing embryo.

1.5 Behaviour of mice heterozygous for *Cyfip1*

In human, *CYFIP1* is encoded in the chromosome 15q11.2 which can be affected by microdeletions leading to neurological symptoms (section 1.1). The mouse orthologue of *CYFIP1* is located on chromosome 7 (Chai et al. 2003). For the study of *Cyfip1* function and consequences of *Cyfip1* deletion, mutant mice for *Cyfip1* have been generated. Homozygous knockout of *Cyfip1* was reported to be embryonically lethal in the mouse (Bozdagi et al. 2012; Pathania et al. 2014) and fly (Schenck et al. 2003; Zhao et al. 2013). Therefore, mouse mutants heterozygous for *Cyfip1* *(Cyfip1*$^{+/-}$*)* have been generated and used for molecular and cellular experiments as well as for behavioural assessments. The behavioural characterisation of two independently generated mouse lines with *Cyfip1* haploinsufficiency is summarised in this chapter.

Embryonic stem cells (129SvEvBrd strain) were targeted in order to insert a trapping cassette inserted into intron 1 of one *Cyfip1* allele. Successfully targeted stem cells

were delivered into preimplantation stage embryos and obtained mosaic mice were backcrossed to a C57Bl/6Tac background. Generated male *Cyfip1*$^{+/-}$ mice were assessed at four months of age for their behaviours (Bozdagi et al. 2012). The only phenotype reported by this study is that *Cyfip1*$^{+/-}$ mice showed enhanced extinction of inhibitory avoidance compared to wild type mice in a fear conditioning test. The general locomotor behaviour in the open-field was similar compared to wild type control mice. The behaviour in an elevated zero maze and transitions between light and dark compartments were comparable between *Cyfip1*$^{+/-}$ and wild type mice. *Cyfip1*$^{+/-}$ and wild type mice showed similar behaviours in a Morris Water maze and a contextual fear conditioning paradigm, indicating that hippocampus-dependent learning was intact in *Cyfip1*$^{+/-}$ mice.

Independently, *Cyfip1* was targeted in AB2.1 embryonic stem cells with a construct containing exon 5 of *Cyfip1* and a puromycin selection cassette. The generated chimaeras were bread and backcrossed to C57BL/6J for more than 7 generations (Chung et al. 2015). Behavioural assessment of the obtained *Cyfip1*$^{+/-}$ mice was performed between 2 and 3 months of age. The focus of this study was on the comparison of the maternal and paternal contribution of *Cyfip1*. In an open-field assay, *Cyfip1* mutation with maternal origin caused hypoactivity compared to wild type controls, without affecting anxiety or hippocampus-dependant learning. Mice with a paternal *Cyfip1* deletion showed increased anxiety and increased fear-conditioning compared to wild type mice, but no alteration of their activity behaviour. In an elevated zero paradigm paternal *Cyfip1*$^{+/-}$ mutants showed less incomplete transitions between open and closed arms compared to wild type mice. However, this phenotype seems subtle since the time spent in the open arms and completed transitions were comparable between paternal *Cyfip1*$^{+/-}$ mutant and wild type mice. In addition, the phenotype seems to be driven by the wild type control mice used as a control for the paternal *Cyfip1*$^{+/-}$ mutants. These control mice seem to show more incomplete transitions compared to paternal and maternal *Cyfip1*$^{+/-}$ mutants and wild

types controls used for maternal *Cyfip1*$^{+/-}$ mutants. Fear conditioning and contextual fear responses were similar between *Cyfip1*$^{+/-}$ mutant mice independent from the parental *Cyfip1* origin and wild type mice. However, paternal *Cyfip1*$^{+/-}$ mutants showed increased freezing behaviour during cued fear testing compared to wild type control mice (Chung et al. 2015).

In summary, the behaviour of the independently generated *Cyfip1*$^{+/-}$ mutants is not grossly altered and does not highlight a shared phenotypic behaviour.

1.6 Aims and objectives

The aim of this PhD project was to characterise the behavioural and molecular phenotypes of *Cyfip1*$^{+/-}$ mice. To achieve this aim we first investigated the impact of *Cyfip1* haploinsufficiency on *Cyfip1* mRNA and CYFIP1 protein levels in different anatomical brain regions. Next, we assessed the social behaviour of male and female *Cyfip1*$^{+/-}$ mice which has not been done despite the association of CYFIP1 with ASD in human (Nishimura et al. 2007; Van Der Zwaag et al. 2010; Leblond et al. 2012; Pinto et al. 2014). In addition, we characterised the activity and anxiety behaviour of *Cyfip1*$^{+/-}$ mice. In human, impaired motor learning behaviour can be a comorbidity of ASD (Moraes et al. 2017). To test for a reminiscent motor learning phenotype in a mouse model for ASD, our study aimed to assess the motor learning behaviour of male and female *Cyfip1*$^{+/-}$ mice over the development.

Following the behavioural characterisation of *Cyfip1*$^{+/-}$ mice, we investigated the molecular consequences of *Cyfip1* haploinsufficiency in specific brain regions including the motor cortex, striatum, hippocampus and cerebellum. Using *in vivo* techniques we studied effects of *Cyfip1* haploinsufficiency on the protein synthesis rate and dendritic spine dynamics. The dendritic spine density has already been

studied in *Cyfip1*$^{+/-}$ mice but the underlying spine dynamics remained unknown (Pathania et al. 2014; Davenport et al. 2018). Therefore, we analysed the neuronal phenotype of *Cyfip1*$^{+/-}$ mice in vivo and in particular quantified the dendritic spine turnover at baseline and upon motor training in the motor cortex.

Chapter 2

Material and methods

2.1 Animal husbandry and legislation

All animals were maintained on a 12 h light/dark cycle (beginning of light cycle 06.00, end of light cycle 18.00). The holding room temperature was maintained at 21°C. All animals had free access to food and water and were housed with at least one cardboard tube, one wooden chew stick and nesting material. Animals were weaned between P28 and P30. Health checks were made on a regular basis and only healthy animals were used for behavioural testing or tissue collection and subsequent analysis. Animal husbandry and experiments were performed in compliance with the Animal Scientific Procedures Act (ASPA, Home Office 1986).

The Cyfip1$^{tm2a(EUCOMM)Wtsi}$ (EUCOMM) mouse line was either bred with C57Bl/6 mice (The Jackson Laboratory) to obtain *Cyfip1*$^{+/-}$ and *Cyfip1*$^{+/+}$ mice (wild type mice) and or crossed with Tg(Thy1-EGFP)MJrs/J (The Jackson Laboratory) to obtain Thy1-EGFP-*Cyfip1*$^{+/-}$ and Thy1-EGFP-*Cyfip1*$^{+/+}$ mice.

2.2 Genotyping

Upon weaning ear notches were collected and stored at -20°C or processed on the same day. For DNA extraction the ear notch biopsies were incubated in 150 µl NaOH 50 mM for 1 h at 90°C. 50 µl Tris 1 M, EDTA 4 mM pH 7.5 were added to the suspension. For a PCR reaction of 25 µl, 1.5 µl of the extraction suspension were mixed with 2.5 µl 10x Standard Taq Buffer (NEB), 0.5 µl 10 mM deoxynucleotides (dNTPs) (Promega), 0.5 µl 10 µM of each primer (Table 2.1), 0.125 µl 5`000 U/ml Taq DNA polymerase and 19.375 µl water. PCR was performed using a T100 Thermal

Cycler (Biorad) with the according thermocycler program (Table 2.1). After completion of the thermocycler programme the reaction mixtures were loaded on a 2% agarose gel in 1x TBE buffer (5x stock: 54 Tris base, 27.5 g boric acid, 20 ml of 0.5 M EDTA pH 8.0) containing 5 µl SaveView nucleic acid stain (NBS Biologicals) per 50 ml gel for visualisation of the DNA products. Agarose gel electrophoresis was performed at 100 V for ~25 min. Reactions with DNA extracts originating from animals from the *Cyfip1*$^{+/-}$ colony revealed either only wild type band at 273 bp, determined as wild type, or a mutant band at 146 bp and a wild type band at 273 bp determined as heterozygous for *Cyfp1*. Animals of the *Cyfip1-Thy1EGFP* line were additionally tested for the expression of Thy1-EGFP by testing for the transgene band at 415 bp whereas a positive control was included with a band size of 324 bp.

Target	**Primer 5`-3`**	**Programme**		**Band size**
		Temp.	Time	
Cyfip1	Wild type forward: CAGGCTGTCTTTTCCTCCTG Wild type reverse: ACTGCAAACATCCCCTTCAG Mutant reverse: GAACTTCGGAATAGGAACTTCG	1) 95°C 2) 95°C 3) 60°C 4) 68°C 5) 2)-4) 6) 68°C 7) 4°C	1 min 30 s 40 s 1 min 40 x 5 min Hold	Mutant: 146 bp WT: 273 bp
Thy1-EGFP	Transgene forward: CTAGGCCACAGAATTGAAAGATCT Transgene reverse: CGGTGGTGCAGATGAACTT Internal control forward: CTAGGCCACAGAATTGAAAGATC Internal control reverse: GTAGGTGGAAATTCTAGCATCAT	1) 95°C 2) 95°C 3) 60°C 4) 68°C 5) 2)-4) 6) 68°C 7) 4°C	1 min 30 s 40 s 1 min 34 x 5 min Hold	Mutant: 415 bp Control: 324 bp

Table 2.1 Primers and thermocycler programmes for used for genotyping.

2.3 Behaviour

All behaviours were assessed during the light cycle. Test animals were handled to the same standard that mice could be hold in open hands. All mice were habituated for at least 30 min to the testing room prior to behavioural testing. Not more than one behaviour test was performed on a day with exception of marble burying followed by open-field testing with at least 2 h in between. All experimental equipment was cleaned between testing of individual animals. The experimenter was blind to the genotype during the behavioural testing and during the scoring of pictures or video recordings. Tested animals were not older than 12 weeks of age.

2.3.1 Interest for social odours

Before the behavioural testing, social odours were collected by scraping the bottom of a home cage with a cotton swap. Social odours were collected from cages containing male C57Bl/6 mice unfamiliar to the subject mouse. For the behavioural testing the subject mouse was habituated for 2 min to a clean cotton swab in the test arena (40 cm x 20 cm). After 2 min the clean cotton swab was removed and a social odour was presented twice for 2 min in sequence with a 30 s delay. For the second presentation of the social odour a different cotton swab with the same social odour was used. The mice were able to move freely during the test phase. The behaviour was video recorded and the time the animals explored the odour with nose contact was manually scored. The procedure was adapted from (Yang & Crawley 2009).

2.3.2 Social odour discrimination

Based on the three chamber assay for social discrimination (Moy et al. 2004) and the ability of mice to discriminate between different social odours (Mihalick et al. 2000; Ferkin & Li 2005; Arbuckle et al. 2015) we developed a social discrimination task relying on social odours. Before the behavioural testing, social odours (S1 and S2)

were collected from two different cages containing male C57Bl/6 mice unfamiliar to the subject mouse. An unfamiliar social odour S1 and a clean cotton swab were presented simultaneously for 10 min in opposite corners of the testing arena (40 cm x 40 cm). After 10 min mice were returned to their home cage for 30 min. To test for the discrimination behaviour, S1 and S2 were presented at the same time over 4 min in opposite corners of the arena. The behaviour was recorded using infrared illumination from the bottom (Tracksys) and a computer-linked video camera (The Imaging Source) placed above the arena. EthoVision XT (Noldus) software was used to track and quantification of the total time the animal spent in proximity to the odour, which was defined as sixteenth of the entire arena. The mice were tested in the dark and were able to freely explore the arena.

2.3.3 Ultrasonic courtship vocalisation

Prior to the experiment female C57Bl/6 mice in estrus were identified by testing for the stage of the estrus cycle. Vaginal smears were stained with modified Giemsa solution (fixative, blue/azure dye and xanthene dye, Polysciences Inc.) (Caligioni 2009). Male mice were first habituated for 3 min to the arena (20 cm x 40 cm). Following the habituation, an unfamiliar female mouse in estrus was added to the same arena for 3 min. During this time the mice could interact with each other and move freely. The vocalisation behaviour was recorded by a preamplifier (UltraSoundGate 416H, Avisoft Bioacustics) connected microphone (UltraSoundGate CM16, Avisoft Bioacustics) placed above the arena. Vocalisation events within the frequency range of 30 hertz – 200 hertz (Holy & Guo 2005) were recorded and analysed for the total time of duration of emitted calls using SASLabPro (Avisoft Bioacustics).

2.3.4 Tube test

The tube test was initially described as dominance tube (Lindzey et al. 1961) or Lindzey tube and has been used to evaluate the social dominance of mice (Wang et al. 2011). Social dominance within cages was assessed using the tube test apparatus (Noldus). The tube test apparatus consists of a smooth transparent acrylic tube (length: 30 cm; internal diameter 3.5 cm) with automatic doors at each end of the tube as well as in the centre of the tube. Before hierarchal assessment, all mice were trained over 4 days to the same standard to move through the tube without stopping or walking backwards. At the beginning of the test mice were placed at opposite ends of the tube and the doors at each end of the tube were opened. As soon as both mice reached the centre of the tube the door at the tube centre was opened. The two mouse encountered each other and aimed to push the opponent out of the tube. The mouse that got pushed out of the tube was declared as submissive of that trial whereas the mouse that won the direct encounter was declared as dominant. The trial was repeated with alternating sides of entry until one of the mice won two encounters. The assessment was repeated three times with five days between the tests. The total number of wins or the percentage of wins determined as (number of wins/total number of encounters) x 100 was used for analysis.

2.3.5 Open-field

The open-field maze was first used to test rats for anxiety-associated behaviours such as locomotor activity (Hall 1934). For this study, the spontaneous locomotor activity of mice was tested in an open field arena (40 cm x 40 cm) for 20 min in the dark. The mice were able to freely move and explore the environment during the test. The arena was infrared illuminated from the bottom (Tracksys) to enable video recordings by a computer-linked video camera (The Imaging Source) placed above the arena. The trajectory travelled by each individual subject mouse was tracked and quantified for the average velocity in cm/s using the EthoVision XT software (Noldus).

Increased anxiety in mice has been associated with the animal`s preference to stay close to the walls of the open field arena (Simon et al. 1994), which is also known as thigmotaxis. This behaviour can be determined by analysing the time mice spent in the centre of the open-field arena. The centre of the open-field area was defined as 5 cm from the wall. Using this parameter the open-field recordings were re-analysed for the time an individual animal spent in the defined area of the open field using EthoVision XT (Noldus) software.

2.3.6 Marble burying

Marble burying has been associated with anxiety (Broekkamp et al. 1986) and repetitive behaviour (Thomas et al. 2009). A clean box (28 cm x 17 cm) was 4 cm deep filled bedding (same type of bedding as used in the holding cage) to allow burying the marbles (1.25 cm in diameter). 20 marbles were arranged in 4 rows of 5 marbles on top of the bedding. The individual subject mouse was put into the box which was closed with a lid. The subject mouse moved freely in the box over the test period of 30 min. The testing room used was dimly lit, with equal light distribution for all mice that were tested. After the test period the subject mouse was returned to the home cage. The bedding was replaced and the box and marbles were cleaned between tests. Marbles were manually counted based on photographs of the test box taken at the end of a test period. A buried marble was defined as marble with half or more of its volume buried in the bedding.

2.3.7 Rotarod

The rotarod paradigm is based on an accelerating rod which allows testing for motor learning (Brooks & Dunnett 2009; Costa et al. 2004). During a trial the rod of the apparatus (Ugo Basile 7650) accelerated from 0 rpm to 40 rpm within 5 min. The latency to fall off the rod was evaluated over 7 subsequent trials with rests of 5 min in

between. During the 5 min between test trial mice were at the base of the apparatus and were able to freely move. The latency to fall was determined based on the time spent on the rod until the test mouse fell off, gripped to the rod and followed the rod for a full rotation or the testing trial end after 5 min. The measured latency to fall was used for the analysis.

2.4 Dissections

Mice were culled by cervical dislocation and confirmed by decapitation in accordance to Schedule 1 (ASPA, Home Office 1986). Collected peripheral tissues, liver and spleen, were immediately snap frozen in liquid nitrogen and stored at -80°C. The brain was placed in brain matrice (Electron Microscopy) on ice and sliced with pre-chilled blades (Electron Microscopy). The brain was cut coronally from anterior to posterior. The olfactory bulb was cut first following by cuts with the following spacing relative to the initial cut: 1.5 mm, 1 mm, 1 mm, 1.5 mm, 1.5 mm, 1.5 mm. The resulting slices were micro dissected in PBS on ice as illustrated (Figure 2.1) and snap frozen in liquid nitrogen followed by storage at -80°C.

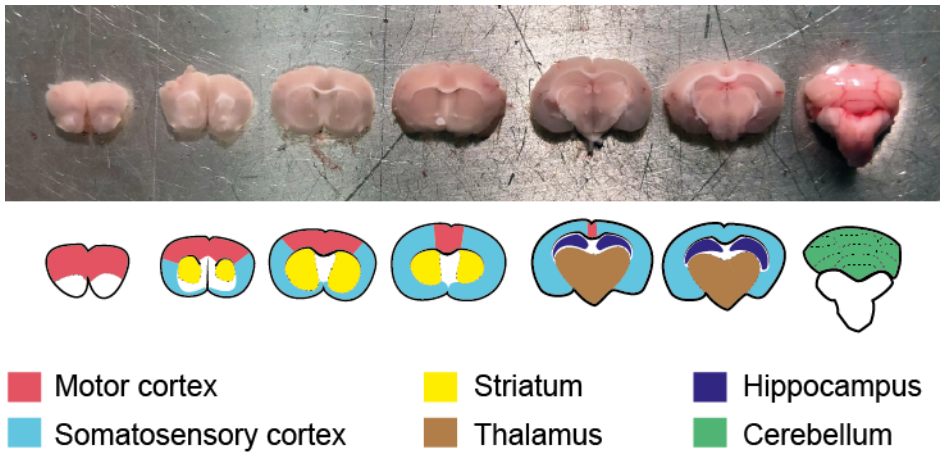

Figure 2.1 Schematic of microdissection.
Anatomical brain regions were microdissected as illustrated. The depicted nomenclature was used to refer to the given tissue samples.

2.5 RNA extraction and quantitative real-time PCR

Collected tissue (Chapter 2.4.1) was triturated in 1 ml with TRIzol reagent (Thermo Fisher Scientific) using a 25 gauge needle and syringe. The suspension was centrifuged for 10 s at 12,000 g to pellet the tissue pieces. The liquid was transferred into a new tube and 200 µl chlorophorm (Merck) were added. After repeated inverting over 15 s, the sample was centrifuged at 12`000 g for 15min at 4°C. The aqueous phase was transferred in a new tube and 0.5 ml of 100% isopropanol (Merck) were added. After repeated inverting over 15 s, sample was loaded onto a column for purification using the RNeasy kit (Qiagen). After an initial centrifugation of 15 s at 12,000 g the flow through was discarded and 350 µl Buffer RW1 RNeasy kit (Qiagen) was added to the column followed by centrifugation for 30 s at 12`000 g. To remove DNA from the sample the column was incubated with 75 µl of DNaseI mix (Qiagen) (10 µl DNase I stock solution in 70 µl RDD Buffer) for 15 min. The column was washed with 350 µl RW1 buffer (RNeasy kit, Qiagen) by centrifugation for 20 s at 12,000 g. A second was wash was performed with a volume of 700 µl RW1 buffer. Next, two additional washing steps with 500 µl RPE buffer (RNeasy kit, Qiagen) with centrifugation for 20 s at 12,000 g in between followed. After a final centrifugation a for 1 min at 12,000 g the column bound RNA was eluted using 30 µl RNAse free water (Qiagen). After elution RNA was kept on ice and RNA concentration was determined using a BioSpectrometer® (Eppendorf). If the concentration was too high to be determined the sample was diluted in RNAse free water (Qiagen). Only contamination free samples with a 260/280 nm absorbance ratio between 1.8 and 2.0 were used for reverse transcription.

1 mg of extracted RNA were used for reverse transcription using SuperScript® III reverse transcriptase (Thermo Fisher Scientific). The RNA was diluted with RNAse free water to a final volume of 11 µl and 1 µl Random Hexamer Primers (Promega) and 1 µl 1 mM of dNTP mix (prepared from dATP, dCTP, dGTP and dTTP, Promega)

were added. The sample was incubated at 65°C for 5 min. 4 µl 5x First-Strand Buffer (Thermo Fisher Scientific), 1 µl 0.1 M DTT, 1 µl 20 – 40 U/µl RNasin® Ribonuclease Inhibitor (Promega) and 1 µl 200 U/µl SuperScript® III reverse transcriptase were prepared as a master mix and added to the sample. This reaction was incubated at 50°C for 2 h followed by heat inactivation at 70°C for 15 min. The obtained complementary DNA (cDNA) was directly used or stored at -20°C if necessary.

Prior real-time PCR testing of the samples, each primer primer (Table 2.2) was tested for specificity and efficiency. To test specificity the melt curve was generated by performing a real-time-PCR reaction including a temperature raise of 1°C per minute up to 99°C. The melt curve was assessed for a single sharp peak. The efficiency of each primer pair was tested by testing for a linearity between obtained cycle of signal detection and the logarithm of the amount of cDNA used in the reaction (15 ng – 125 ng). Linearity was tested by a liner regression data fitting and the slope was determined (Excel). The efficiency was calculated as 10((-1/(slope))-1) x 100. Only primer pairs with an efficiency of over 65% were used. Primers were designed using https://www.genscript.com/tools/real-time-pcr-tagman-primer-design-tool and tested for specificity using https://blast.ncbi.nlm.nih.gov/Blast.cgi unless primer sequences were previously published (Table 2.2 Legend).

For each real-time PCR reaction 15-50 ng cDNA was used. Per reaction the cDNA was mixed with 12.5 µl FAST SYBR® Green master mix (Thermo Fisher Scientific), 0.625 µl 10 µM forward primer (Table 2.2), 0.625 µl 10 µM reverse primer (Table 2.2) and water up to a volume of 25 µl. All reaction were prepared as a master mix of duplicates or triplicates. Individual reactions were load into a MicroAmp® Fast Optical 96-well plate (Thermo Fisher Scientific) whereas all plates contained control reactions amplifying *18S* cDNA. Using StepOnePlus™ Real-Time PCR system (Thermo Fisher Scientific) the plate was ran using the following programme: 1) 10 min at 95°C, 2) 30 sec at 95°C, 3) 30 sec at 57°C, 4) 1 min at 70°C, whereas steps 2) – 4) were repeated 39 times. The results were analysed by the $2^{-\Delta\Delta CT}$ method using 18S as a control.

Target	Primer 5`-3`	
	Forward	Reverse
18S	GTCTGTGATGCCCTTAGATG	AGCTTATGACCCGCACTTAC
Crhr2	GCATCACCACCATCTTCAAC	GAATGCACCATCCAATGAAG
Cyfip1	CTGCATATAAGAGGGCTGCTCA	GGCCAGGAACATGGACAGAT
Cyp2d9	AGTCTCTGGCTTAATTCCTGAT	CGCAAGAGTATCGGGAATGC
Mup4	ATGAAGCTGCTGCTGTGT	TCATTCTCGGGCCTTGAG
Mup6	ATGAAGCTGCTGCTGCTGT	TCATTCTCGGGCCTGGAG
Mup20	CTGCTGCTGTGTTTGGGACT	TCTTTTGTCAGTGGCCAGCA

Table 2.2 Primers for real-time PCR.
Primers for *Cyp2d9* primers (Sato et al. 2017), Primers for *Mup20* (Guo et al. 2015)

2.6 CYFIP1 immunoprecipitation

Tissue was triturated in lysis buffer (25 mM Tris-HCl, pH 8, 50 mM KCl, 0.2 mM EDTA, 1% Triton, supplemented with protease and phosphatase inhibitor cocktails (Merck) and 1 µl NaF 1 M and 5 ul $NaVO_4$ 100 mM per 1 ml lysis buffer) using a 25 gauge needle and syringe. The homogenate was incubated on a rotator for 1 h at 4°C and then centrifuged for 10 min at 94 g at 4°C. The supernatant was re-centrifuged for 10 min at 9,391 g at 4°C. The protein concentration of the lysate was determined using the Pierce™ BCA Protein Assay kit (Thermo Fisher Scientific) according to the manufacture`s manual and BSA standards ranging from 5.5 mg/ml to 0.5 mg/ml including a blank control. Aliquots of the lysate were stored at -20°C and later analysed (input). 630 µg of protein lysate were incubated with 4 µg of anti-PIR121/Sra- 1 antibody (Cat. No 07-531, Millipore) or 4 µg of rabbit IgG (Merck) as a negative control on a rotator overnight at 4°C. Prior the precipitation, 20 µl of protein

A sepharose beads slurry (nProtein A Sepharose 4 Fast Flow, GE Healthcare) were saturated in 1% BSA (Merck) in PBS (Thermo Fisher Scientific) on the rotator for 1 h at 4°C. The sepharose beads were then washed twice with 500 µl lysis buffer and centrifugation for 2 min at 2,000 g at 4°C. For the precipitation the antibody incubated lysates were added to the prepared sepharose beads and incubated on a rotator for 2h at 4°C. For the elution the samples were centrifuged for 2 min at 2,000g at 4°C. The supernatant was removed and the sepharose beads were washed twice with 500 µl lysis buffer with centrifugation for 2 min at 2`000g at 4°C in between. A final wash was made with 500 µl lysis buffer (without Triton) followed by centrifugation for 2 min at 2,000 g at 4°C. After removal of the supernatant, 25 µl 2x sample buffer (212 mM Tris HCl, 182 mM Tris base, 4% LDS, 20% Glycerol, 1.02 mM EDTA, 0.44 mM Brilliant Blue G250, 0.350 mM Phenol Red, pH 8.5) and 100 mM DTT were added. The samples were incubated for 10 min at 70°C. After centrifugation for 2 min at 2000 g the supernatant was transferred into a new tube and analysed by Western blotting (chapter 2.7) at which anti-CYFIP1 (Cat. No ab ab156016, Abcam) was used for CYFIP1 detection.

2.7 Western blotting

Per mg of tissue, 10ul of lysis buffer (1% sodium dodecyl sulfate, 10mM Hepes, NaF 1mM, $NaVO_4$ 1mM, supplemented with complete protease and phosphatase inhibitor cocktails, Merck) was used. The tissue was triturated in the lysis buffer using a 25 gauge needle and syringe. The homogenate was incubated on a rotator for 1 h at 4°C and then centrifuged for 15 min at 15`000 g at 4°C. The supernatant was transferred into a new tube and mixed with sample buffer (106 mM Tris HCl, 141 mM Tris base, 2% LDS, 10% Glycerol, 0.51 mM EDTA, 0.22 mM Brilliant Blue G250,

0.175 mM Phenol Red, pH 8.5) and 50 mM DTT and boiled for 10 min at 70°C. Samples were directly used or stored at -20°C and boiled for 10 min at 70°C prior to further processing. Lysates were loaded on NuPAGE™ Novex™ 4-12% Bis-Tris gels with 10 wells or 15 wells (lysates subsequently analysed for puromycin were exclusively loaded on 10 well gels). Gels were ran in running buffer (50 mM MES, 50 mM Tris base, 0.1% SDS, 1 mM EDTA, pH 7.3) at 120 V for about 1 h 30 min. To transfer the proteins from the gel onto Amersham™ Protan™ 0.2 µm nitrocellulose membranes (GE Healthcare) a wet transfer was used. For transfer buffer consisted of 25 mM Bicine, 25 mM Bis-Tris, 1 mM EDTA and 20% isopropanol, Merck). After the transfer, the membrane was incubated in 5% Blotting-Grade Blocker (Biorad) in TBS-T (24.7 mM Tris base, 137 mM NaCl, 2.6 mM KCl, 0.1 % Tween-20, pH 7.5.). For immunoprobing, the membrane was incubated in 5% Blotting-Grade Blocker (Biorad) in TBS-T containing the primary antibody at given dilution (Table 2.3) overnight at 4°C. The membrane was washed three times for 15 min with TBS-T and then incubated with the secondary antibody at given dilution (Table 2.4) for 2 h at room temperature. The membrane was washed three times for 15 min with TBS-T. The membranes were developed using 1 ml Western blotting luminol reagent (Santa Cruz biotechnology) or WesternBright™ ECL (Advansta) for an incubation time of 1 min. The excessive substrate was removed and the signals were detected by a digital ChemiDoc™ MP system (Biorad) and the Image Lab™ software (Biorad). All signals were acquired without signal saturation. For blots tested for puromycin, Pierce™ Reversible Protein Stain Kit (Thermo Fisher Scientific) (Antharavally et al. 2004) was used as a normaliser and acquired by a GenoSmart2 system (VWR). The densitometric analysis of Pierce™ staining was performed using Fiji (Schindelin et al. 2012).

Antibody	Type	Species	Dilution	Cat. no	Distributor
anti-βIII-tubulin	mAb	mouse	1:5‘000	801202	Biolegend
anti-CYFIP1	mAb	rabbit	1:1‘000	ab156016	Abcam
anti-GAPDH	pAb	chicken	1:5‘000	83956	Abcam
anti-WAVE1	mAb	mouse	1:1‘000	MABN503	Millipore
anti-Phospho-eIF4E (Ser209)	pAb	rabbit	1:1‘000	07-823	Millipore
Anti-PIR121/ Sra-1	pAb	rabbit	1:1`000	07-531	Millipore
Anti-Puromycin	mAb	mouse	1:1‘000	MABE343	Millipore

Table 2.3 Primary antibodies used for Western blotting.

Monoclonal (mAb) and polyclonal (pAb) antibodies used for Western blotting.

Antibody	Species	Dilution	Cat. No	Distributor
anti-chicken IgY-HRP	goat	1:20‘000	ab6877	Abcam
anti-goat IgG-HRP	donkey	1:20‘000	sc-2020	Santa Cruz
anti-mouse IgG-HRP	goat	1:20‘000	W401B	Promega
anti-rabbit IgG-HRP	goat	1:20‘000	W402B	Promega

Table 2.4 Secondary antibodies used for Western blotting.

2.8 Puromycin incorporation *in vivo*

Male mice were anesthetised using isoflurane (UWH Phamacy) at 5% for induction, 2.5% for maintenance and head fixed in a stereotaxic frame. An aseptic surgical procedure procedures were applied, a heat mat (Vet Tech) was used during the surgery and the respiration was monitored by eye. The animal`s head was then shaved and the eyes covered with Viscotears® liquid gel (Alcon). The mouse was injected subcutaneously with Metacam (100 µl 0.66 mg/ml per 30g body weight, Boehringer Ingelheim) and a mid-saggital incision was made to expose the cranium. A dental drill, which was connected to the stereotaxic frame, and burr (Cat. no 500 204, Meisinger), was used to drill a hole into the cranium at the coordinates - 1 mm mediolateral and – 0.22 mm anteroposterior relative to bregma (Santini et al. 2013). A 5 µl Hamilton microliter syringe (Hamilton) with a 26 gauge needle was lowered by 2.4 mm relative to the brain surface in order to inject 0.5 µl of 50 µg/µl puromycin into the ventricle. After injection, the needle was left in place for 4 min, then withdrawn by 1.2 mm and left in place for another 4 min before complete removal. The incision was closed with three silk sutures. Over the course of the surgery, the mouse was injected subcutaneously with 1 ml of saline using a 1 ml syringe and 26 gauge needle. The animal recovered in a heated cage and was used for tissue collection (chapter 2.4) 1 h after the ventricular injection. The tissues were further analysed by Western blotting (chapter 2.7).

2.9 Histology

Thy1-EGFP-*Cyfip1*$^{+/-}$ and Thy1-EGFP-*Cyfip1*$^{+/+}$ adult male mice (n = 4 for both genotypes) were anesthetised with an intraperitoneal injection of 100 µl Euthanal (Merial animal health) and perfused with 4% paraformaldehyde (Electron microscopy

sciences) in 0.1 M phosphate buffer. Brains were post-fixed overnight in 4% paraformaldehyde in 0.1 M phosphate buffer at 4°C and then stored for 1 day in a 30% sucrose (Merck) in PBS solution. Brains were embedded in OCT (Scigen) and stored at -80°C. Using a cryostat (Leica Biosystems) coronal sections of 50 µm were cut and mounted on glass slides (VWR). Images of the primary motor and visual cortices were acquired by confocal microscopy on a Zeiss LSM700 upright confocal microscope (Carl Zeiss) with a 43x water immersion objective (numerical aperture = 1.3). At least 10 Z-stack images (2048 x 2048 pixels) were acquired with a spacing of 0.5 µm. The stacks were processed by Y-stack projections of maximum intensity in ImageJ (NIH). Focusing on secondary branching, dendrite stretches of 60 µm – 150 µm were identified and the spines were manually counted. The number of spines was determined in 24 dendrites per animal. The spine density was calculated as number of spines per 100 µm dendrite.

2.10 Craniotomy and structural imaging

Dendritic spine imaging was performed in awake and head fixed Thy1-EGFP-*Cyfip1*$^{+/-}$ and Thy1-EGFP-*Cyfip1*$^{+/+}$ adult male mice with implanted cranial windows. Aseptic surgical procedures were conducted based on previously described protocols (Goldey et al. 2014; Ranson 2017). Approximately one hour prior to cranial window surgery, animals were injected subcutaneously with the antibiotic Baytril (5 mg/kg, Henry Schein Animal Health) and the anti-inflammatory drugs Rimadyl (5 mg/kg, injected, UWH Phamacy) and Dexafort (0.15 mg/kg, intramuscularly injected, Henry Schein Animal Health). Anaesthesia was induced then maintained using Isoflurane (UWH Phamacy) at concentrations of 4%, then 1.5% - 2% respectively. After animals were secured in a stereotaxic frame, the scalp and periosteum were removed from the dorsal surface of the skull, and a custom head plate was attached to the cranium

using dental cement (Super Bond C&B), with an aperture approximately centred over right M1. A 3 mm circular craniotomy was next performed, centred over the forelimb area using stereotaxic coordinates 1.3 mm anterior to the bregma and 1.2 mm lateral from the midline. The craniotomy was then closed with a glass insert constructed from 3 layers of circular no 1 thickness glass (1 mm x 5 mm, 2 mm x 3 mm diameter) bonded together with optical adhesive (Norland Products; catalogue no. 7106).

Mice were imaged one week post surgery. Initial dendritic spine imaging was followed up after two, seven and nine days. *In vivo* 2-photon imaging was performed using a resonant scanning microscope (Thorlabs, B-Scope) with a 16x objective (numerical aperture = 0.8) with 3 mm working distance (Nikon). EGFP was excited at 980 nm using a Ti:sapphire laser (Coherent, Chameleon) with a maximum laser power at sample of 20 milliwatt. Z stacks were acquired at a frame rate of approximately 30 hertz, with 20 frames per depth, from 15 depths spaced by 2 µm. Recordings were targeted to stretches of dendrite close to parallel to the imaging plane. Cortical surface vascular landmarks were used to locate the same stretches of dendrite between sessions. During 2-photon imaging animals were free to run on a custom designed fixed axis cylindrical treadmill, and data collection was limited to stationary periods to avoid locomotion related brain movement. Imaging data was acquired using Scanimage 4.1. Imaging data was first corrected for brain motion using an automated rigid registration algorithm (Guizar-Sicairos et al. 2008) implemented in Matlab (MathWorks). The 20 frames from each depth were then averaged and a maximum intensity projection calculated over the Z planes which encompassed the stretch of dendrite of interest.

For baseline spine turnover dendrites of interest were imaged four times over the time period of nine days. The same animals were later trained on the rotarod and imaged two days after motor training. Formed and eliminated spines were manually counted

and normalised to 100 µm of dendrite (Thy1-EGFP-*Cyfip1*$^{+/-}$ n = 36, from 4 mice; Thy1-EGFP-*Cyfip1*$^{+/+}$ n = 40, from 4 mice).

2.11 Statistical analysis

Statistical details are attached in the appendix (Table A.1) Statistical analysis was performed using SPSS Statistics® 23 software (IBM). For pairwise comparisons the data was tested for normal distribution using the Shapiro-Wilk test and equality of variances by Levene`s test. Normal distributed data with equal variances was analysed by one or two-tailed Student`s *t*-test. Pairwise comparisons of nonparametric data was analysed by the one or two-tailed Mann-Whitney *U*-test. For repeated measures ANOVA data was analysed for normal distribution using the Shapiro-Wilk test and for equal variances using the Mauchly`s test of sphericity. Violation of Mauchly`s test of sphericity was analysed by Greenhouse-Geisser estimate of sphericity and if $\varepsilon < 0.75$ Greenhouse-Geisser correction was applied. Pillai`s Trace test was used as a multivariate test of repeated measures ANOVA. If significant single comparison post hoc test were made using Bonferroni tests. For multicomparisons one-way or multi-way ANOVAs were used followed by Bonferroni or Sidak`s tests when appropiate. All statistical data is presented as mean ± SEM. Power analysis was performed using G*Power (Faul et al. 2007).

Chapter 3

Effects of *Cyfip1* haploinsufficiency on *Cyfip1* mRNA and CYFIP1 protein levels in adult *Cyfip1*$^{+/-}$ mice

3.1 Introduction

The focus of this chapter is on the characterisation of *Cyfip1* mRNA and CYFIP1 protein levels in the *Cyfip1*$^{+/-}$ mouse model used in this study in comparison to wild type littermate mice. We hypothesised that the genetic *Cyfip1* haploinsufficiency directly compromises *Cyfip1* mRNA levels, which consequently diminishes CYFIP1 protein levels. We quantified *Cyfip1* mRNA and CYFIP1 protein levels in tissues from adult *Cyfip1*$^{+/-}$ and wild type mice using quantitative real-time PCR and Western blotting techniques following analysis for an effect of genotype on *Cyfip1* mRNA and CYFIP1 protein levels.

3.2 *Cyfip1* mRNA levels in *Cyfip1*$^{+/-}$ mice

We used quantitative real-time PCR using the $2^{-\Delta\Delta CT}$ method to quantify *Cyfip1* mRNA levels in tissues from adult *Cyfip1*$^{+/-}$ and wild type mice. The normalised *Cyfip1* mRNA levels in adult *Cyfip1*$^{+/-}$ mice were significantly decreased in the motor cortex (WT n = 11; *Cyfip1*$^{+/-}$ n = 11; one-tailed Student`s *t*-test, $P = 0.006$), striatum (WT n = 12; *Cyfip1*$^{+/-}$ n = 12; one-tailed Mann-Whitney *U*-test, $U = 11.000$, $P = 0.000$) cerebellum (WT n = 11; *Cyfip1*$^{+/-}$ n = 9; one-tailed Student`s *t*-test, $P = 0.006$) and liver (WT n = 10; *Cyfip1*$^{+/-}$ n = 9; one-tailed Mann-Whitney *U*-test, $U = 13.000$, $P = 0.004$) compared to normalised *Cyfip1* mRNA levels determined in wild type mice (**Figure 3.1**).

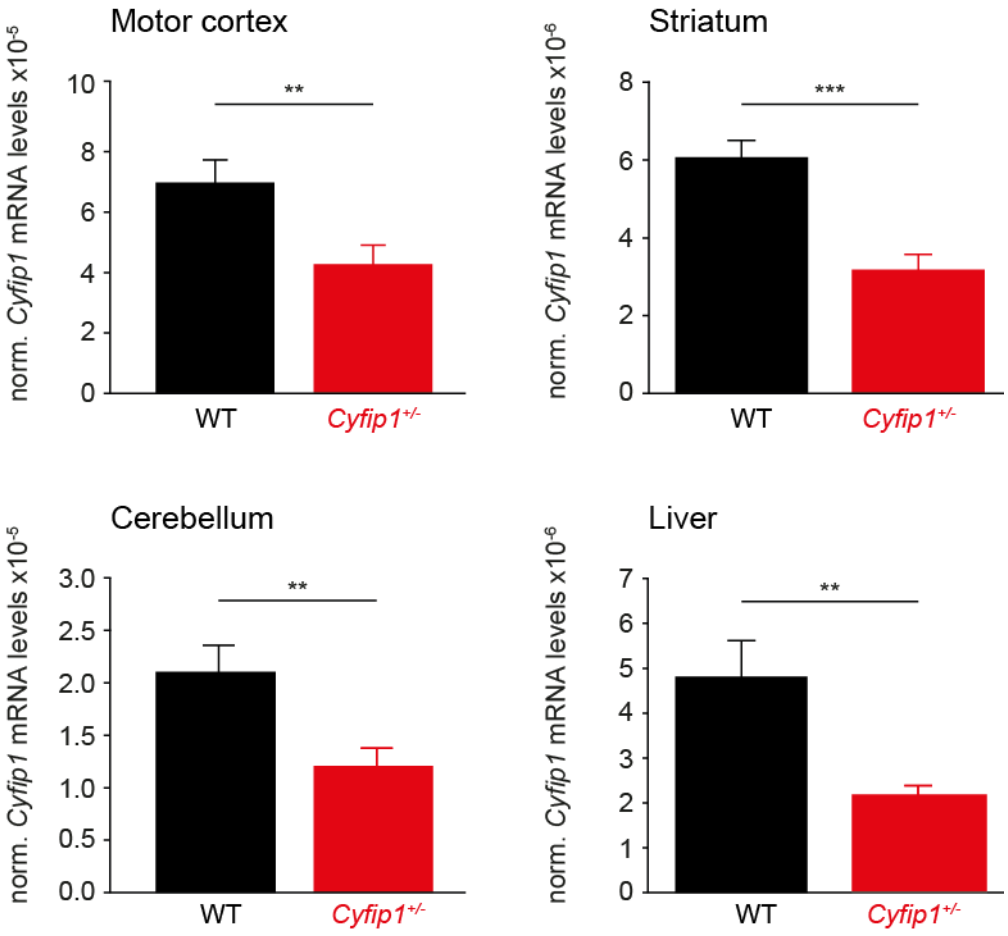

Figure 3.1 Relative *Cyfip1* mRNA levels in *Cyfip1*$^{+/-}$ and wild type tissues.
Cyfip1 mRNA levels were significantly decreased in the adult *Cyfip1*$^{+/-}$ motor cortex, striatum, cerebellum and liver compared to wild type control tissues. *Cyfip1* mRNA levels were normalised to *18S* mRNA levels. All values presented as mean ± SEM. Statistical significance was tested by one-tailed Student`s *t*-test or one-tailed Mann-Whitney *U*-test. $^{**}P < 0.01$; $^{***}P < 0.001$.

3.3 CYFIP1 protein levels in *Cyfip1*$^{+/-}$ mice

CYFIP1 protein levels in tissues from adult *Cyfip1*$^{+/-}$ and wild type mice were determined by Western blotting using an antibody specific for CYFIP1 and antibodies against βIII-Tubulin and GAPDH as loading controls for neuronal and non-neuronal tissues respectively. Lysates from the *Cyfip1*$^{+/-}$ motor cortex (WT n = 20; *Cyfip1*$^{+/-}$ n = 20; one-tailed Student`s *t*-test, $F = 0.967$, $P = 0.017$) and hippocampus (WT n = 13; *Cyfip1*$^{+/-}$ n = 12; one-tailed Student`s *t*-test, $F = 2.682$, $P = 0.002$) revealed significantly decreased CYFIP1 protein levels compared to wild type control lysates. In contrast, similar CYFIP1 protein levels were obtained between *Cyfip1*$^{+/-}$ and wild type tissues in the striatum (WT n = 16; *Cyfip1*$^{+/-}$ n = 16; one-tailed Mann-Whitney *U*- test, $U = 88.000$, $P = 0.069$), thalamus (WT n = 11; *Cyfip1*$^{+/-}$ n = 9; one-tailed Student`s *t*-test, $F = 0.703$, $P = 0.332$), somatosensory cortex (WT n = 5; *Cyfip1*$^{+/-}$ n = 9; one-tailed Mann-Whitney *U*-test, $U = 22.000$, $P = 0.500$) and cerebellum (WT n = 13; *Cyfip1*$^{+/-}$ n = 12; one-tailed Mann-Whitney *U*-test, $U = 58.000$, $P = 0.148$) (**Figure 3.2**). In addition, CYFIP1 protein levels obtained in the peripheral tissues liver and spleen were comparable between *Cyfip1*$^{+/-}$ and wild type mice (Liver: WT n = 11; *Cyfip1*$^{+/-}$ n = 9; one-tailed Mann-Whitney *U*-test, $U = 48.500$, $P = 0.471$; Spleen: WT n = 11; *Cyfip1*$^{+/-}$ n = 9; one-tailed Student`s *t*-test, $F = 1.721$, $P = 0.478$) (**Figure 3.2**).

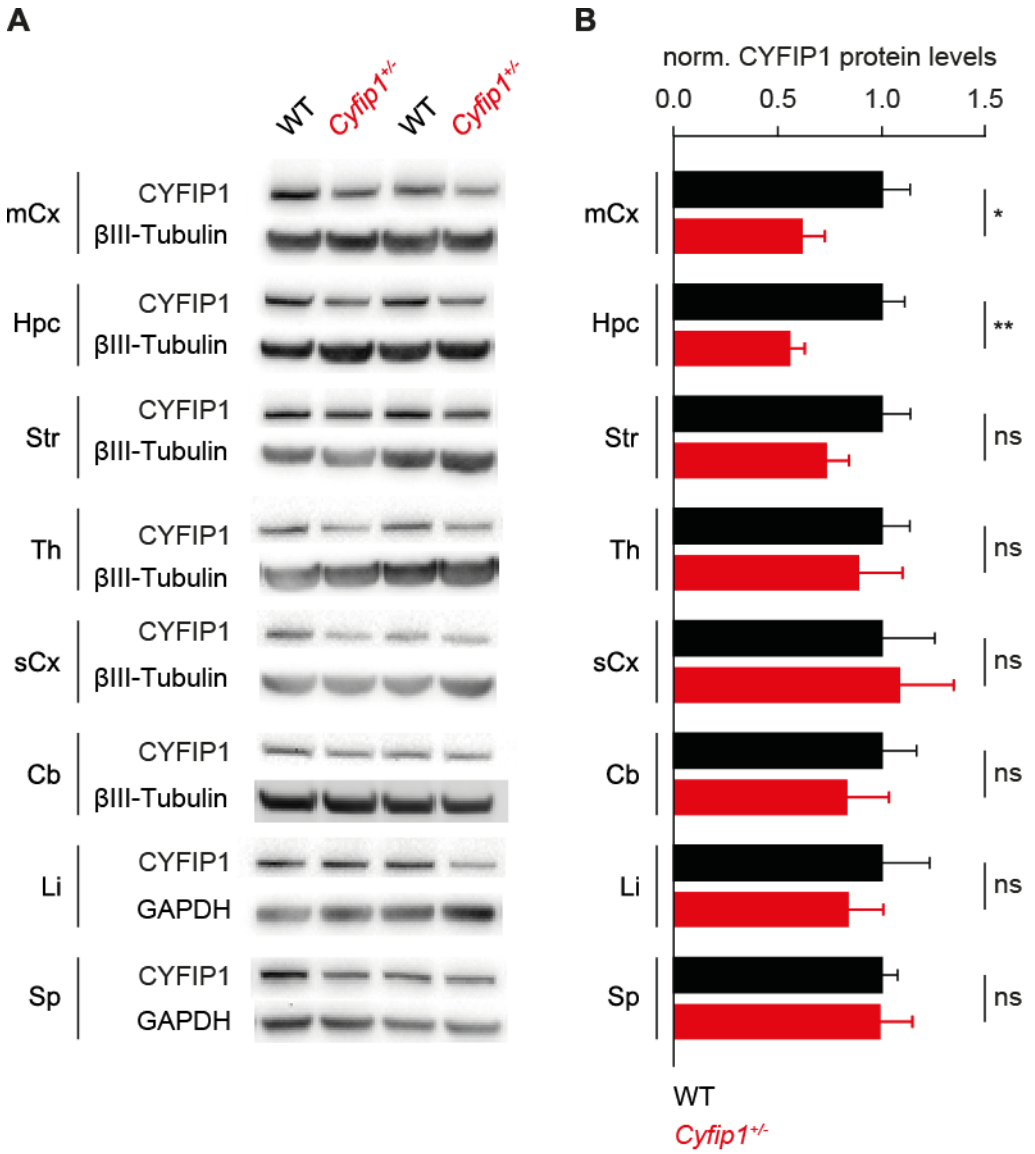

Figure 3.2 CYFIP1 protein levels in *Cyfip1*$^{+/-}$ and wild type tissues.

A, Wild type and *Cyfip1*$^{+/-}$ tissue lysates from the motor cortex (mCx), hippocampus (Hpc) , striatum (Str), thalamus (Th), somatosensory cortex (sCx), cerebellum (Cb), liver (Li) and spleen (Sp) analysed by Western blotting for CYFIP1 and βIII-Tubulin or GAPDH as loading controls. **B**, Quantification of Western blots. CYFIP1 levels were normalised to βIII-Tubulin or GAPDH. All values presented as mean ± SEM. Statistical significance was tested by one-tailed Student`s *t*-test or one-tailed Mann-Whitney *U*- test. ns $P > 0.05$; *$P < 0.05$; **$P < 0.01$.

3.4 Discussion

The quantification of *Cyfip1* mRNA levels relative to *18S* mRNA levels and the subsequent comparison between *Cyfip1*$^{+/-}$ mutant and wild type tissue revealed a significant reduction of *Cyfip1* mRNA levels across different brain regions, namely the motor cortex, striatum and cerebellum. Furthermore, *Cyfip1* mRNA levels in the peripheral liver tissue were significantly decreased in *Cyfip1*$^{+/-}$ mice compared to wild type mice. In addition, the magnitude of *Cyfip1*$^{+/-}$ specific reduction in *Cyfip1* mRNA levels was about 50 per cent across all tested tissues. Taken together, the results indicate that *Cyfip1* haploinsufficiency leads to reduced *Cyfip1* mRNA levels as hypothesised. Thus, both *Cyfip1* alleles contribute to *Cyfip1* mRNA levels suggesting a biallelic expression of *Cyfip1*.

CYFIP1 protein levels were significantly decreased in the motor cortex and hippocampus of *Cyfip1*$^{+/-}$ mice compared to wild type mice. Surprisingly, CYFIP1 protein levels were similar between mice heterozygous for *Cyfip1* and wild type control mice in the striatum, cerebellum, somatosensory cortex and thalamus. Similarly, peripheral CYFIP1 protein levels in liver and spleen were comparable between *Cyfip1*$^{+/-}$ and wild type mice. In certain *Cyfip1*$^{+/-}$ tissues such as the striatum, cerebellum, somatosensory cortex, thalamus, liver and spleen there was a discrepancy between *Cyfip1* mRNA levels, which were reduced by 50%, and CYFIP1 protein levels which were similar to wild type levels. This highlights an uncharacterised post-transcriptional compensatory mechanism, which gave rise to wild type CYFIP1 levels despite the underlying *Cyfip1* haploinsufficiency. In addition, the mechanism seemed not to be mediated by a neuronal network effect since CYFIP1 protein levels were also compensated in the peripheral *Cyfip1*$^{+/-}$ tissues such as the liver and spleen. As potential mechanisms, we propose an increased stability of *Cyfip1* mRNA or CYFIP1 protein due to an altered expression of microRNAs or CYFIP1 interaction partners (Fabian et al. 2018; Catalanotto et al. 2016) or an

increased translation of *Cyfip1* mRNA in *Cyfip1*$^{+/-}$ mice compared to wild type mice (Hsiao et al. 2016), which we addressed *in vivo* (chapter 6). We next assessed whether the brain region-specific decrease in CYFIP1 protein levels in *Cyfip1*$^{+/-}$ mice had consequences on the behaviour of *Cyfip1*$^{+/-}$ mice as presented in the next chapter.

Chapter 4

Behavioural characterisation of *Cyfip1*$^{+/-}$ mice

4.1 Introduction

This chapter outlines the behavioural characterisation of mice heterozygous for *Cyfip1*. In these experiments, we tested adult *Cyfip1*$^{+/-}$ and wild type littermate mice using behavioural paradigms for social behaviour, repetitive behaviour, anxiety-related behaviour, activity and motor learning behaviour.

4.2 Social behaviours of *Cyfip1*$^{+/-}$ mice

Cyfip1 has been associated with ASD in humans (Leblond et al. 2012; Nowicki et al. 2007; Nishimura et al. 2007; Van Der Zwaag et al. 2010; Noroozi et al. 2018; Pinto et al. 2014) which is characterised by impairments in sociability, verbal communication and ritualistic behaviours (*Diagnostic and statistical manual of mental disorders.* 5th ed., Washington, DC). ASD is more prevalent in male than female individuals (male/female ratio of 4.5:1) (Christensen et al. 2016). Despite the association of *Cyfip1* with ASD, the social behaviour of *Cyfip1*$^{+/-}$ mice has not been characterised yet. Social behaviours in mice are differentially manifested between male and female mice, for example, territorial and aggressive behaviours are more pronounced in males than in females (Wu et al. 2009) which in turn show specific maternal social behaviours (Lonstein & De Vries 2000). We therefore analysed the social behaviour of male and female mice separately.

We first tested adult wild type and *Cyfip1*$^{+/-}$ male mice for their interest in unfamiliar social odours collected from wild type male mice. Male wild type mice spent significantly more time in proximity to the social odour than a control consisting of the odour carrier without any additional odours, whereas *Cyfip1*$^{+/-}$ male mice spent similar

time exploring the control and social odour (WT n = 9; *Cyfip1*$^{+/-}$ n = 12; repeated measures ANOVA, main effect of odour, $F_{2, 18}$ = 11.177, P = 0.001; interaction odour x genotype, $F_{2, 18}$ = 3.776, P = 0.043, Bonferroni Post-hoc test) (**Figure 4.1A**). In a social discrimination task relying on social odours *Cyfip1*$^{+/-}$ and wild type male mice spent significantly more time with an unfamiliar social odour as opposed to a previously presented and therefore familiar social odour (WT n = 9; *Cyfip1*$^{+/-}$ n = 12; repeated measures ANOVA, main effect of odour, $F_{1, 19}$ = 27.792, P = 0.000, interaction odour x genotype, $F_{1, 19}$ = 0.647, P = 0.428) (**Figure 4.1B**). Next, *Cyfip1*$^{+/-}$ and wild type male mice were exposed to an unfamiliar adult female wild type mouse in estrus and ultrasonic vocalisations were recorded. Recordings analysed for the total duration of ultrasonic calls revealed that adult *Cyfip1*$^{+/-}$ and wild type male mice vocalised to similar extents towards the female wild type mouse (WT n = 18; *Cyfip1*$^{+/-}$ n = 10; two-tailed Student`s *t*-test P = 0.698) (**Figure 4.1C**). To test for dominance behaviour adult *Cyfip1*$^{+/-}$ and wild type male were assessed in the tube test. *Cyfip1*$^{+/-}$ male mice won 40.74% of the direct encounters with wild type males representing an equal distribution of dominance behaviour over the male *Cyfip1*$^{+/-}$ and wild type population (**Figure 4.1D**).

In addition, female C*yfip1*$^{+/-}$ and wild type mice were tested for their social interest. Adult C*yfip1*$^{+/-}$ and wild type female mice spent significantly more time in proximity to the social odour than to a control (WT n = 8; *Cyfip1*$^{+/-}$ n = 10; repeated measures ANOVA, main effect of odour, $F_{2, 15}$ = 6.306, P = 0.010; interaction odour x genotype, $F_{2, 15}$ = 0.654, P = 0.534, Bonferroni Post-hoc test) (**Figure 4.1E**). In contrast to the social discrimination behaviour of *Cyfip1*$^{+/-}$ and wild type male mice, female *Cyfip1*$^{+/-}$ and wild type female mice did not show a preference for an unfamiliar social odour over a familiar social odour (WT n = 8; *Cyfip1*$^{+/-}$ n = 10; repeated measures ANOVA, main effect of odour, $F_{1, 16}$ = 1.601, P = 0.224; interaction odour x genotype, $F_{1, 16}$ = 0.031, P = 0.862, Bonferroni Post-hoc test) (**Figure 4.1F**). Taken together, the assessment of social behaviours of adult *Cyfip1*$^{+/-}$ mice in comparison to wild type

control mice revealed a decreased interest in social odours specifically in *Cyfip1*$^{+/-}$ male mice.

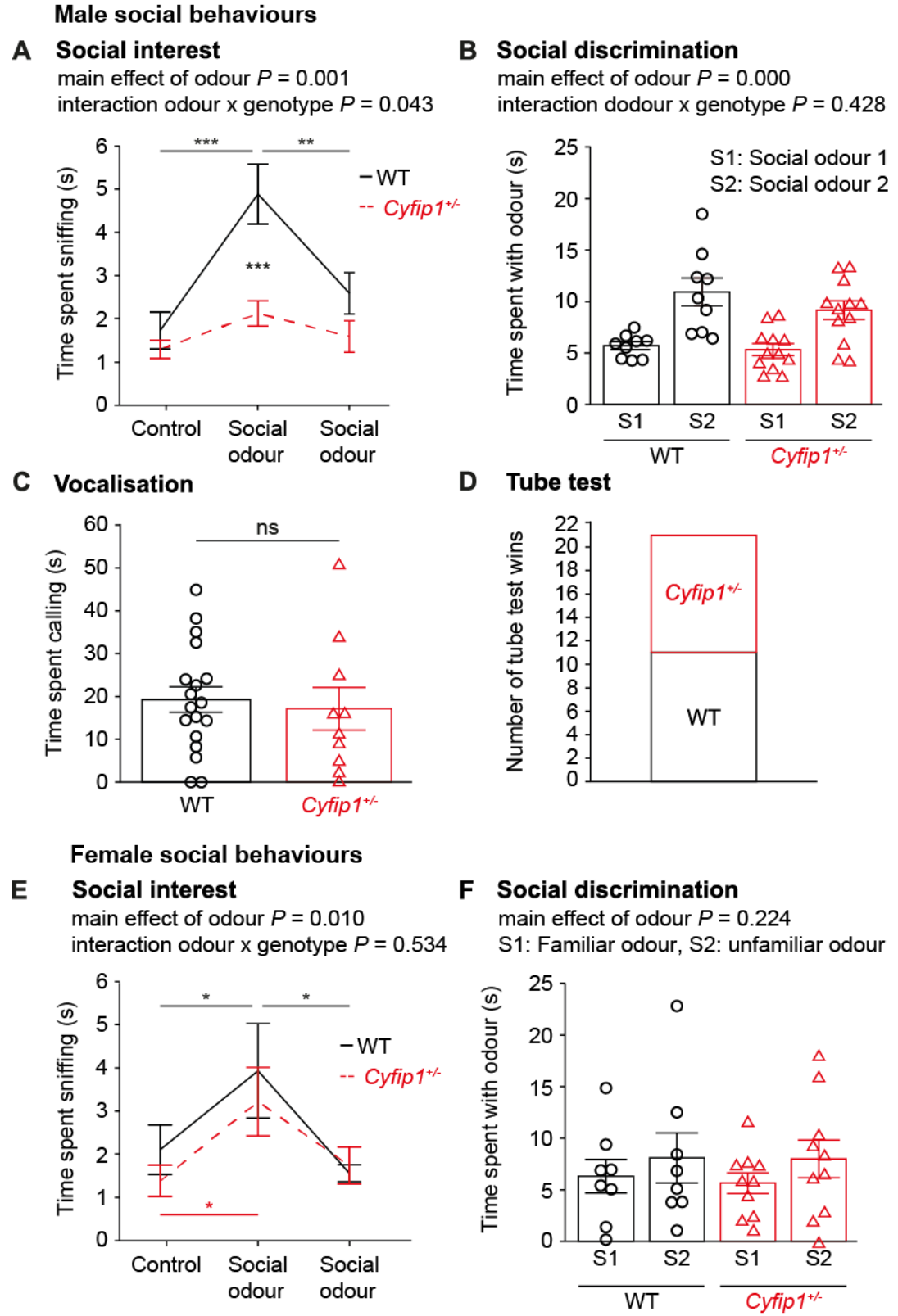

Figure 4.1 Reduced social interest but normal social discrimination, courtship and dominance behaviour of *Cyfip1*$^{+/-}$ male mice.

A, Adult *Cyfip1*$^{+/-}$ male mice spent less time exploring an unfamiliar social odour than wild type male mice. **B**, Adult *Cyfip1*$^{+/-}$ and wild type male mice spent more time with an unfamiliar social odour than a familiar social odour in a discrimination paradigm. **C**, Adult male *Cyfip1*$^{+/-}$ and wild type mice vocalised to comparable extends towards an adult female mouse in estrus. **D**, *Cyfip1*$^{+/-}$ and wild type mice won and lost similar number of direct tube test encounters. **E**, Adult *Cyfip1*$^{+/-}$ and wild type female mice showed interest in social odours. **F**, *Cyfip1*$^{+/-}$ and wild type female mice did not discriminate between familiar and unfamiliar social odours. Except from D all values presented as mean ± SEM. Statistical significance was tested by repeated measures ANOVA followed by Bonferroni Post-hoc test (A-B, E-F) or two-tailed Student`s *t*-test (C). ns $P > 0.05$; *$P < 0.05$; **$P \leq 0.01$; ***$P < 0.001$.

4.3 General locomotor activity and anxiety-related behaviours of *Cyfip1*$^{+/-}$ mice

In contrast to social behaviours, locomotor activity behaviours of two different *Cyfip1*$^{+/-}$ mouse lines have been reported with different results. Using open-field tests either similar activity levels between *Cyfip1*$^{+/-}$ mutant and wild type mice were reported (Bozdagi et al. 2012) or an imprinting specific hypoactivity in maternally heterozygous *Cyfip1* mice was observed compared to wild type mice (Chung et al. 2015). In addition, anxiety-related behaviours were demonstrated to be similar between *Cyfip1*$^{+/-}$ and wild type mice (Bozdagi et al. 2012) with the exception of a subtle effect on the anxiety behaviour of paternal *Cyfip1*$^{+/-}$ mutant mice (Chung et al. 2015). We tested adult male *Cyfip1*$^{+/-}$ and wild type mice in the open-field for their general locomotor activity. In addition, anxiety-related behaviours were assessed by the time the animals spent in the centre of the open-field arena and the marble burying behaviour. Using the same behaviour paradigms we then tested adult female *Cyfip1*$^{+/-}$ and wild type mice.

The observed activity behaviour of adult *Cyfip1*$^{+/-}$ male mice was comparable to the behaviour of wild type male mice (WT n = 10, *Cyfip1*$^{+/-}$ n = 17; two-tailed Student`s

t- test, *P* = 0.540) (**Figure 4.2A**). Moreover, adult *Cyfip1*$^{+/-}$ and wild type male mice spent similar amount of time in the centre of the open-field arena (WT n = 9, *Cyfip1*$^{+/-}$ n = 12; two-tailed Mann-Whitney *U*-test, *U* = 47.000, *P* = 0.651) (**Figure 4.2B**). In addition, the marble burying paradigm revealed that *Cyfip1*$^{+/-}$ and wild type mice buried comparable number of marbles (WT n = 15, *Cyfip1*$^{+/-}$ n = 15; two-tailed Student`s *t*-test, *P* = 0.243) (**Figure 4.2C**).

Next, female *Cyfip1*$^{+/-}$ and wild type mice were tested for their behaviours in the open-field and marble burying paradigm. Adult *Cyfip1*$^{+/-}$ female mice showed a tendency towards a hypoactivity phenotype in the open-field (WT n = 9, *Cyfip1*$^{+/-}$ n = 8; two-tailed Mann-Whitney *U*-test, *U* = 18.000, *P* = 0.093) (**Figure 4.2D**). Therefore, we determined whether an increased number of *Cyfip1*$^{+/-}$ and wild type female mice would allow detecting the assumed difference in activity between *Cyfip1*$^{+/-}$ and wild type mice. Thus, the measured mean velocities, standard deviations and the effect size were used as input for a power analysis. The power analysis revealed that a total of at least 19 *Cyfip1*$^{+/-}$ and 19 wild type female mice would be needed for the postulated hypoactivity in *Cyfip1*$^{+/-}$ female mice to reach statistical significance (Mann-Whitney *U*-test, two-tailed, *P* = 0.05, power (1-β) = 0.80). Notably, this power analysis underlies the assumption that the experimental data is representative for the entire population of *Cyfip1*$^{+/-}$ and wild type female mice and that female *Cyfip1*$^{+/-}$ mice are indeed hypoactive compared to wild type controls. In addition, female *Cyfip1*$^{+/-}$ and wild type mice spent similar amount time in the centre of the open-field arena (WT n = 10, *Cyfip1*$^{+/-}$ n = 9; two-tailed Student`s *t*-test, *P* = 0.806) (**Figure 4.2E**). The marble burying assay revealed that female *Cyfip1*$^{+/-}$ and wild type mice buried comparable number of marbles (WT n = 15, *Cyfip1*$^{+/-}$ n = 15; two-tailed Mann-Whitney *U*-test, *U* = 102.500, *P* = 0.683) (**Figure 4.2F**). In summary, adult *Cyfip1*$^{+/-}$ male and wild type mice have a similar activity and anxiety-related behaviours, whereas adult female *Cyfip1*$^{+/-}$ mice are potentially hypoactive but show anxiety-related behaviours similar to wild type female mice.

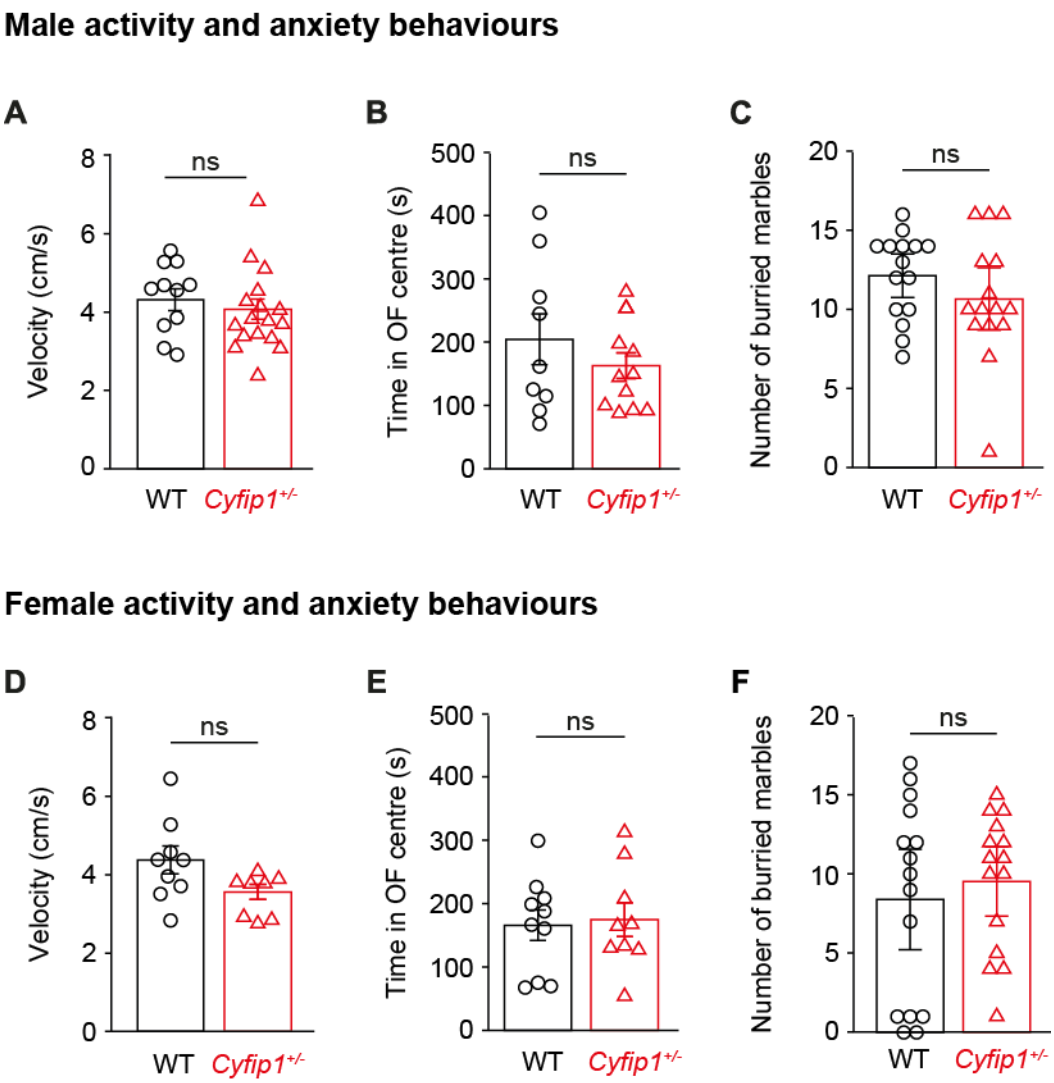

Figure 4.2 Similar activity and anxiety-related behaviours between adult *Cyfip1*$^{+/-}$ and wild type mice.

A-B, Open-field behaviour of adult male *Cyfip1*$^{+/-}$ and wild type mice. **C**, Marble burying behaviour of male *Cyfip1*$^{+/-}$ and wild type mice. **D-E**, *Cyfip1*$^{+/-}$ and wild type female behaviour in the open-field. **F**, Marble burying behaviour of female *Cyfip1*$^{+/-}$ and wild type mice. All values presented as mean ± SEM. Statistical significance was tested by two-tailed Student`s *t*-test or two-tailed Mann-Whitney *U*-test. ns $P > 0.05$.

4.5 Motor learning behaviour of *Cyfip1*$^{+/-}$ mice

General locomotor activity and moreover the ability to improve motor accuracy and motor coordination is required for motor learning. Motor learning in rat, monkey and human is associated with neuronal activity (Debaere et al. 2004; Wise et al. 1998; Jenkins et al. 1994) and connectivity (Gandolfo et al. 2000; Karni et al. 1995; Seitz et al. 1990). In mice, motor learning has an impact on neuronal activity specifically in the motor cortex and striatum (Costa et al. 2004). Interestingly, the motor cortex showed decreased CYFIP1 protein levels in adult *Cyfip1*$^{+/-}$ adult mice compared to wild type mice. Using an accelerating rod (rotarod) protocol, that has been demonstrated to mediate neuronal activity in the murine motor cortex and striatum (Costa et al. 2004). Thus, consequences of *Cyfip1* haploinsufficiency on motor learning behaviour were assessed.

Using a rotarod paradigm *Cyfip1*$^{+/-}$ and wild type male mice were tested for their ability to stay on the accelerating rod by analysing the latencies to fall over 7 subsequent trials. In order to validate our experimental design as a read-out for motor learning, we first we tested whether male wild type mice increased their latencies to fall over the seven test trials. As expected, adult male wild type mice increased their performance over the sequence of trials significantly (WT n = 17; repeated measure ANOVA, main effect of Trial $F_{6, 11}$ = 16.094, P = 0.000; Bonferroni Post-hoc test). In contrast, the performance of adult *Cyfip1*$^{+/-}$ male mice was unchanged over the trials (*Cyfip1*$^{+/-}$ n = 15; repeated measure ANOVA, main effect of Trial $F_{6, 9}$ = 1.092, P = 0.434) (**Figure 4.3A**) despite a similar baseline performances on trial 1 between male *Cyfip1*$^{+/-}$ and wild type mice (WT n = 17; *Cyfip1*$^{+/-}$ n = 15; Student`s *t*-test, two-tailed, P = 0.169) (**Figure 4.3B**). Next, we tested adult female *Cyfip1*$^{+/-}$ and wild type mice. Female wild type mice increased their performances with training (WT n = 12; repeated measure ANOVA, main effect of Trial $F_{6, 66}$ = 15.395, P = 0.000; Bonferroni Post-hoc test) as well as *Cyfip1*$^{+/-}$ female mice (*Cyfip1*$^{+/-}$ n = 10; repeated measure

ANOVA, main effect of Trial $F_{6, 54}$ = 3.409, P = 0.006; Bonferroni Post-hoc test) (**Figure 4.3C**). Baseline performance during trial 1 were similar between female *Cyfip1*$^{+/-}$ and wild type mice (WT n = 12; *Cyfip1*$^{+/-}$ n = 10; Student`s *t*-test, two-tailed, P = 0.332) (**Figure 4.3D**).

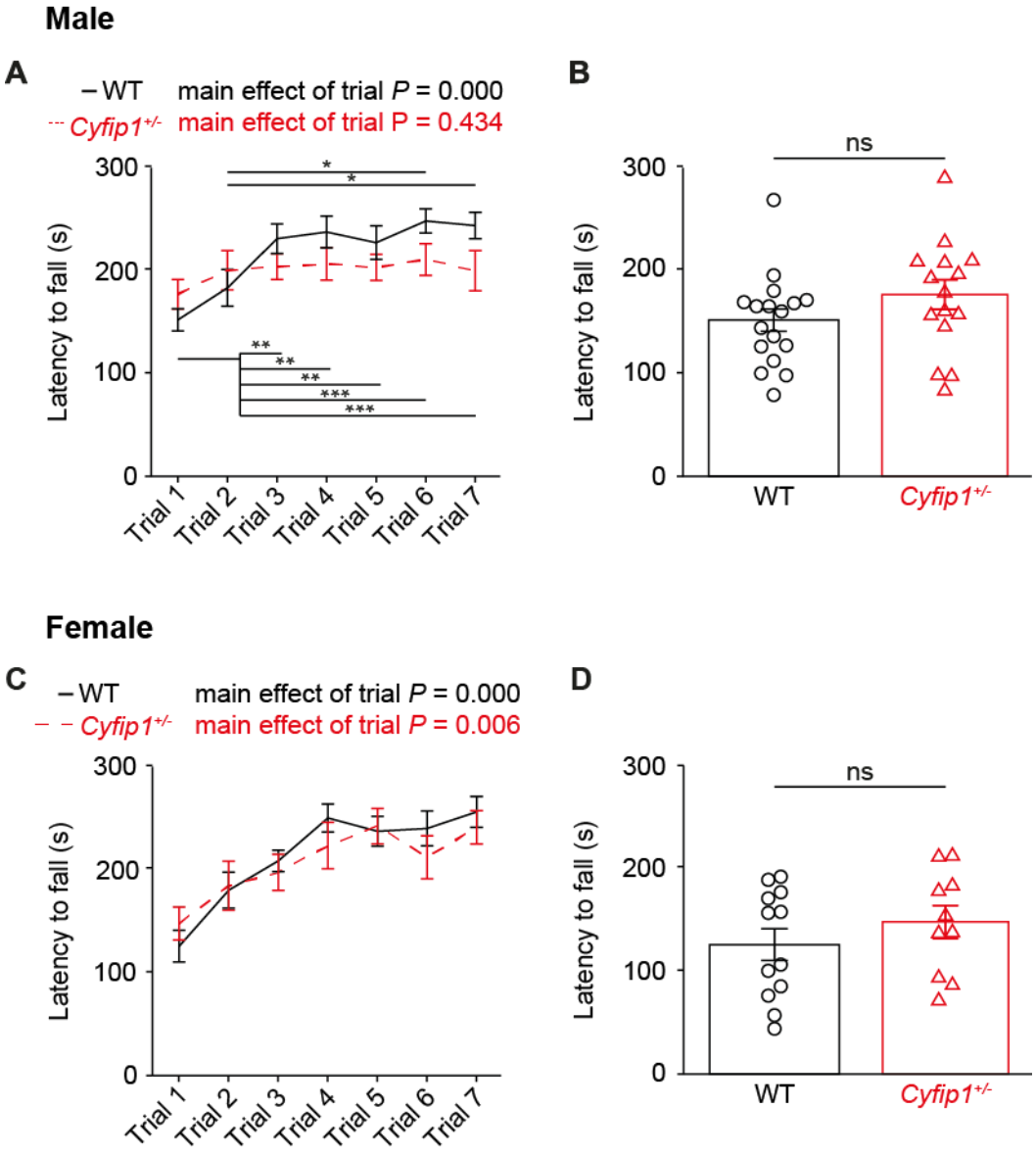

Figure 4.3 Impaired motor learning in adult *Cyfip1*$^{+/-}$ male mice.

A, Adult male wild type but not adult *Cyfip1*$^{+/-}$ male mice increased their performances over the sequence of seven trials of the rotarod protocol. **B**, Baseline performances during the first trial were similar between male *Cyfip1*$^{+/-}$ and wild type male mice. **C**, Adult female *Cyfip1*$^{+/-}$ and wild type mice increased their latency to fall from the

accelerating rod over the seven subsequent trials. **D**, *Cyfip1*$^{+/-}$ and wild type female mice showed comparable baseline performances during the first trial. All values presented as mean ± SEM. Statistical significance was tested by two-tailed Student`s *t*-test (C and D right). or by repeated measures ANOVA followed by Bonferroni Post-hoc test. ns $P > 0.05$, *$P < 0.05$, **$P < 0.01$, ***$P < 0.001$.

4.6 Discussion

We tested for the first time social behaviours of a mouse model for *Cyfip1* haploinsufficiency. Our results revealed a reduced interest in social odours specifically in adult *Cyfip1*$^{+/-}$ male mice. Nevertheless, social discrimination between familiar and unfamiliar social odours was intact in adult *Cyfip1*$^{+/-}$ male mice. In addition, dominance behaviour was not affected in *Cyfip1*$^{+/-}$ male mice. Anxiety-related behaviours were comparable between *Cyfip1*$^{+/-}$ and wild type mice.

The assessment of the activity behaviour revealed a potential hypoactivity specific to adult female *Cyfip1*$^{+/-}$ mice whereas male *Cyfip1*$^{+/-}$ and wild type mice showed similar activity behaviours. Altered social dominance and anxiety behaviours can have an effect on other behaviours (Vargas-Pérez et al. 2009; Van Loo et al. 2003). Our results allowed us to exclude the possibility of a cascade of behavioural consequences due to social or anxiety-related deficits of *Cyfip1*$^{+/-}$ mutant mice and demonstrate specificity of the described phenotypes. In order to test for further consequences of activity behaviour, we tested *Cyfip1*$^{+/-}$ and wild type mice for motor learning. Interestingly, we found a significant motor learning impairment specific to *Cyfip1*$^{+/-}$ male mice. Taken together, we found male-specific social and motor learning phenotypes in adult *Cyfip1*$^{+/-}$ mice.

4.7 Developmental characterisation of the male-specific *Cyfip1*$^{+/-}$ motor learning impairment

The phenotypic characterisation of adult *Cyfip1*$^{+/-}$ and wild type mice revealed a male-specific motor learning impairment in adult *Cyfip1*$^{+/-}$ mice. This phenotypic behaviour can be specific to adult *Cyfip1*$^{+/-}$ mice or can arise earlier in development. To test between these possibilities we focussed on the developmental assessment of the motor learning behaviour in *Cyfip1*$^{+/-}$ male and wild type mice.

Rotarod testing of mice earlier in development demonstrated that the postnatal day 40 (P40) was the earliest time point juvenile animals complied with the rotarod protocol. P40 accounts for a developmental time point after weaning and at the onset of sexual maturation. Wild type male mice at P40 increased their motor performances during the rotarod task (WT n = 7; repeated measures ANOVA, main effect of trial $F_{6, 36}$ = 15.261, P = 0.000, Bonferroni Post-hoc test) (**Figure 4.4A**). Interestingly, *Cyfip1*$^{+/-}$ male mice at P40 increased their ability to stay on the accelerating rod as observed in wild type control mice (*Cyfip1*$^{+/-}$ n = 10; repeated measures ANOVA, main effect of trial $F_{6, 54}$ = 7.716, P = 0.000, Bonferroni Post-hoc test) (**Figure 4.4B**). Next, the motor learning behaviour of male *Cyfip1*$^{+/-}$ and wild type mice at P40 was compared to the behaviour obtained from rotarod testing of adult *Cyfip1*$^{+/-}$ male and wild type mice at postnatal day 60 (P60). The rotarod behaviour of wild type male mice was comparable between the developmental time points P40 and P60 (WT P40 n = 7; WT P60 n = 17; repeated measures ANOVA, main effect of trial $F_{6, 17}$ = 23.515, P = 0.000, interaction trial x age $F_{6,17}$ = 0.815, P = 0.573) (**Figure 4.4C**, data from wild type mice at P60 replotted from **Figure 4.3A**). In contrast, *Cyfip1*$^{+/-}$ male mice performed significantly better at P40 than at P60 (*Cyfip1*$^{+/-}$ P40 n = 10; *Cyfip1*$^{+/-}$ P60 n = 15; repeated measures ANOVA, main effect of Trial $F_{6, 138}$ = 6.692, P = 0.000, Interaction Trial x Age $F_{6, 138}$ = 3.000, P = 0.009; Bonferroni Post-hoc test) (**Figure 4.4D**, data from *Cyfip1*$^{+/-}$ mice at P60 replotted from **Figure 4.3A**).

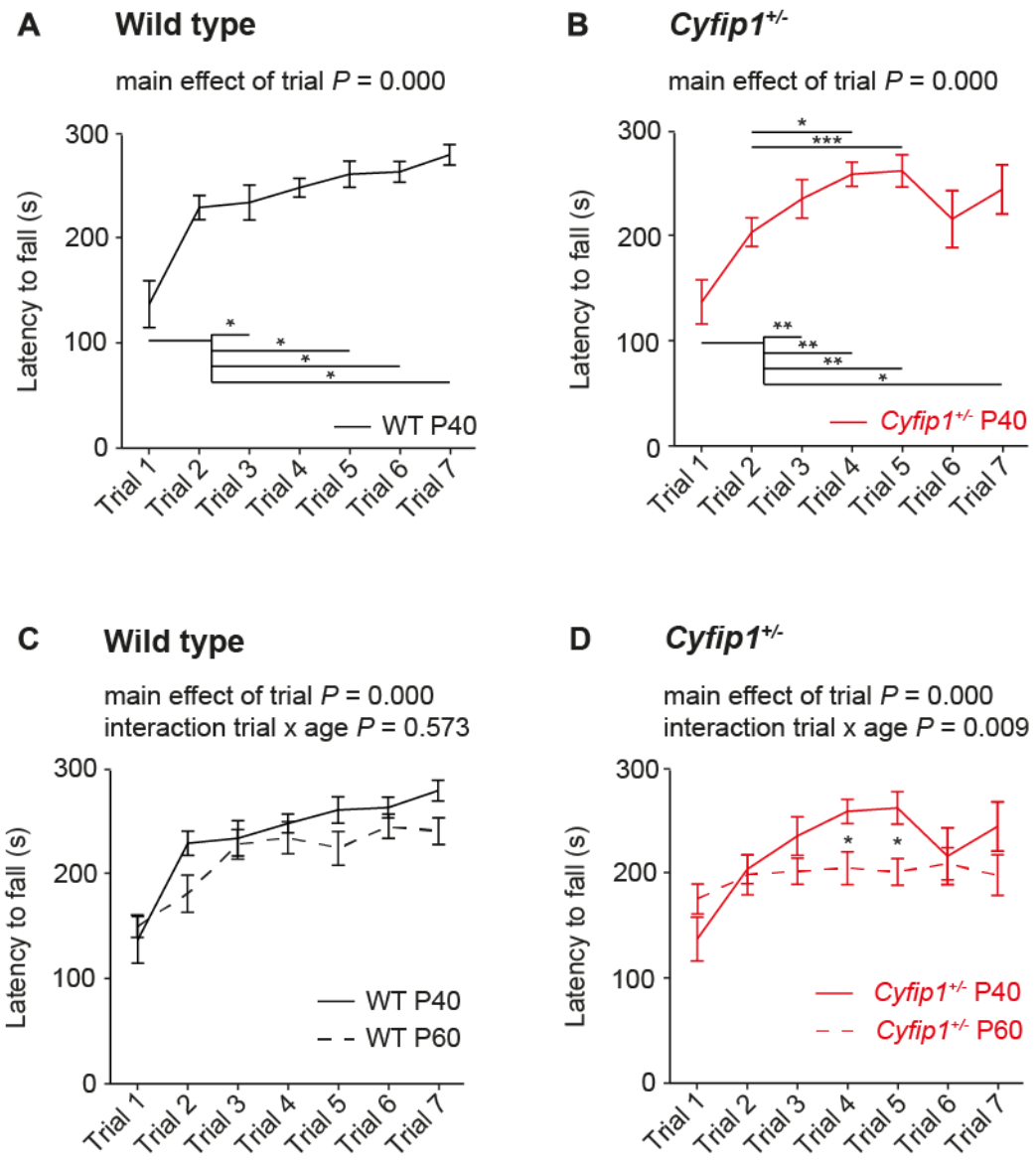

Figure 4.4 *Cyfip1*$^{+/-}$ mice show motor learning behaviour at P40.

A-B, Wild type and *Cyfip1*$^{+/-}$ male mice increased their latency to fall off the accelerating rod at P40. **C**, Male wild type mice at P40 and P60 show similar motor learning behaviour. **D**, Male *Cyfip1*$^{+/-}$ mice performed the rotarod task significantly better at P40 than at P60. All values presented as mean ± SEM. Statistical significance was tested by repeated measures ANOVA followed by Bonferroni Post-hoc test. *$P < 0.05$; **$P < 0.01$; ***$P < 0.001$.

The motor learning behaviour of *Cyfip1*$^{+/-}$ male mice was similar to the wild type behaviour at P40 whereas adult *Cyfip1*$^{+/-}$ male mice showed a motor learning impairment compare to adult wild type mice. We next assessed whether motor learning behaviour acquired during the development had a sustained effect on the motor behaviour of adult wild type and *Cyfip1*$^{+/-}$ male mice.

Male wild type and *Cyfip1*$^{+/-}$ mice were trained using the same rotarod protocol at postnatal days 40, 50 and 51 (in the following referred to as `trained` mice) and retested for their motor behaviour at P60. Testing for the motor behaviour of trained wild type male mice at P60 revealed constant performances over the seven test trials (Trained WT n = 6; repeated measures ANOVA, main effect of Trial, $F_{6, 36} = 2.053$, $P = 0.084$) (**Figure 4.5A**). In comparison to rotarod-untrained male wild type mice at P60, trained wild type mice showed significantly increased performances on the first two trials and similar performance levels on subsequent trials of the rotarod testing at P60 (Trained WT n = 7; Untrained WT n = 17; repeated measures ANOVA, main effect of Trial $F_{6, 17} = 3.260$, $P = 0.025$; interaction Trial x Training $F_{6, 17} = 2.650$, $P = 0.047$; Bonferroni Post-hoc test) (**Figure 4.5B**, data from rotarod untrained wild type replotted from **Figure 4.3A**). Interestingly, trained adult *Cyfip1*$^{+/-}$ male mice increased their motor performance during the rotarod task at P60 (*Cyfip1*$^{+/-}$ n = 6; repeated measures ANOVA, main effect of Trial $F_{6, 30} = 13.465$, $P = 0.000$; Bonferroni Post-hoc test) (**Figure 4.5C**). Compared to rotarod untrained *Cyfip1*$^{+/-}$ male mice, trained *Cyfip1*$^{+/-}$ male mice increased their performances significantly at P60 (Trained *Cyfip1*$^{+/-}$ n = 6; untrained *Cyfip1*$^{+/-}$ n = 15; repeated measures ANOVA, main effect of Trial $F_{6, 114} = 6.269$, $P = 0.000$; Interaction Trial x Training $F_{6, 114} = 2.872$, $P = 0.030$; Bonferroni Post-hoc test) (**Figure 4.5D**, data from rotarod untrained *Cyfip1*$^{+/-}$ mice replotted from **Figure 4.3A**).

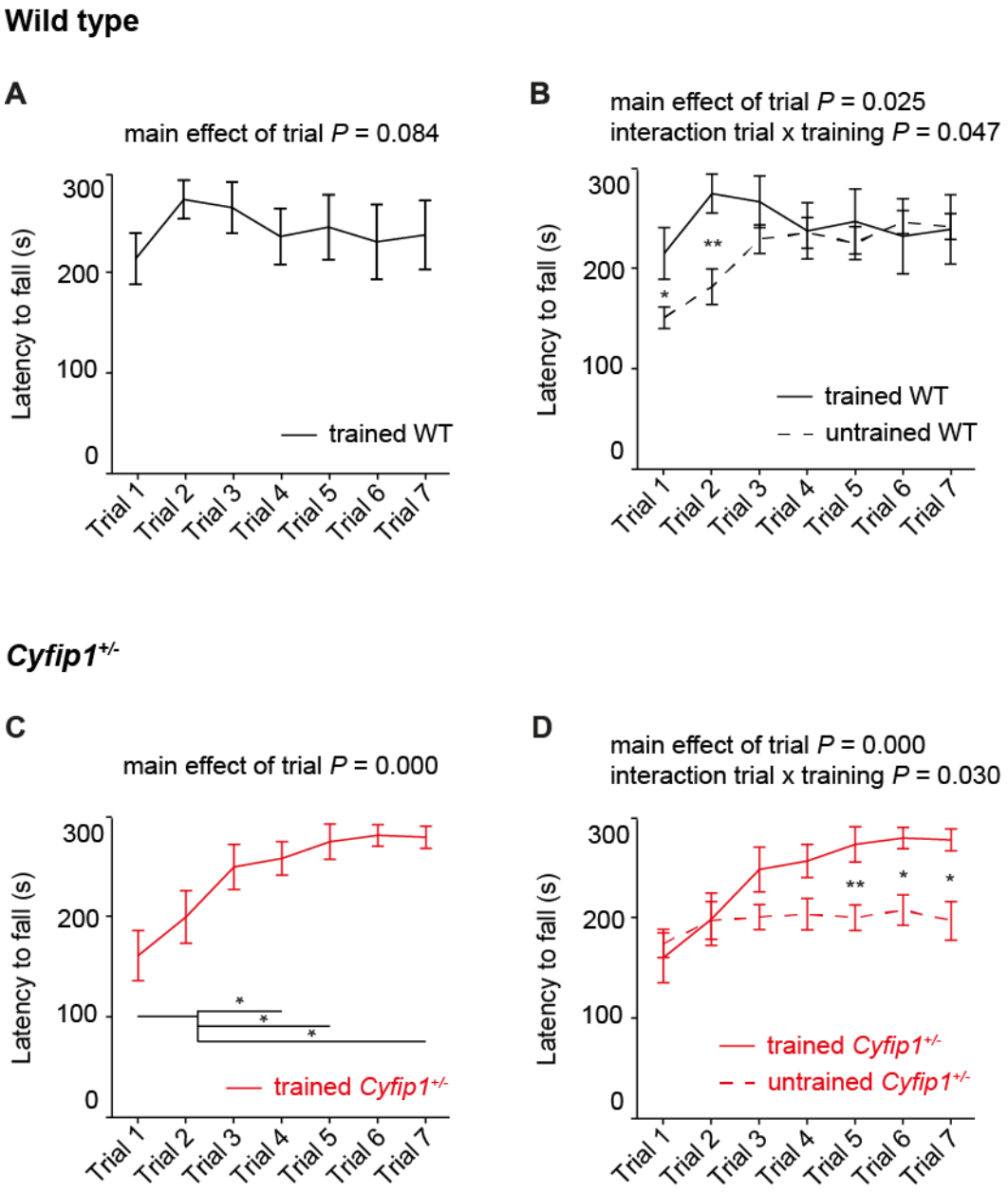

Figure 4.5 Motor training during the development improves *Cyfip1*$^{+/-}$ motor performance at P60.

A, P40 trained wild type male mice showed similar motor behaviour performance during the rotarod task at P60. **B,** Male wild type mice motor trained at P40 showed significantly increased motor performances during the first two trials during the behavioural assessment at P60 compared to untrained adult wild type mice. **C,** P60 *Cyfip1*$^{+/-}$ males increased the latency to stay on the rod over seven trials when trained earlier in development at P40. **D**, P40 motor trained *Cyfip1*$^{+/-}$ male mice in increased

their motor performances during the rotarod testing at P60**.** All values presented as mean ± SEM. Statistical significance was tested by repeated measures ANOVA followed by Bonferroni Post-hoc test. *$P < 0.05$; **$P < 0.01$.

4.8 Discussion

Like wild type mice, *Cyfip1*$^{+/-}$ male mice showed increased rotarod performance at P40. This observation is in contrast to the results obtained from adult *Cyfip1*$^{+/-}$ male mice, which revealed a motor learning impairment compared to adult wild type male mice. Therefore, we concluded that the *Cyfip1*$^{+/-}$ male-specific motor learning impairment occurs after a certain age, between P40 and P60.

Next, we tested whether the motor learning of juvenile wild type and *Cyfip1*$^{+/-}$ male mice was sustained over time and had an effect on the motor behaviour of adult wild type and *Cyfip1*$^{+/-}$ male mice. In wild type male mice, developmental motor training enabled trained wild type male mice to reach faster high performance levels similar to levels observed in untrained wild type mice in the last trials of the paradigm. In comparison, the performance of developmentally trained *Cyfip1*$^{+/-}$ male mice was significantly increased and allowed the mice to reach performance maxima that were not observed in untrained *Cyfip1*$^{+/-}$ male mice. Therefore, our results suggest a disrupted motor behaviour acquisition as a potential mechanism leading to impaired motor learning behaviour of adult *Cyfip1*$^{+/-}$ male mice.

Chapter 5

Molecular consequences of *Cyfip1*$^{+/-}$ deletion

5.1 Effect of sex on *Cyfip1* mRNA and CYFIP1 protein levels in adult *Cyfip1*$^{+/-}$ and wild type mice

5.1.1 Introduction

The characterisation of CYFIP1 protein levels in adult *Cyfip1*$^{+/-}$ mice revealed a significant decrease in CYFIP1 protein levels the motor cortex and hippocampus compared to wild type CYFIP1 levels. The main findings of the behavioural assessment of *Cyfip1*$^{+/-}$ and wild type mice were a motor learning deficit and a decreased interest in social odours (chapters 4.2, 4.5 and 4.7). Interestingly, both phenotypic behaviours were male-specific whereas female *Cyfip1*$^{+/-}$ mice behaved similarly to female wild type mice. The observed sex-specific *Cyfip1*$^{+/-}$ phenotypes lead to the question whether *Cyfip1* expression levels differed between adult male and female *Cyfip1*$^{+/-}$ mice. Therefore, *Cyfip1* mRNA and CYFIP1 protein levels were first compared between tissues from adult male and female *Cyfip1*$^{+/-}$ mice and second between tissues from adult male and female wild type mice.

5.1.2 Results

Brain tissues from adult *Cyfip1*$^{+/-}$ male and female mice were analysed for *Cyfip1* mRNA levels by real-time PCR using the $2^{-\Delta\Delta CT}$ method. Obtained *Cyfip1* mRNA levels in the male *Cyfip1*$^{+/-}$ motor cortex were significantly higher compared to the female *Cyfip1*$^{+/-}$ motor cortex (female n = 6; male n = 5; two-tailed Student`s *t*-test, $P = 0.003$) whereas male and female *Cyfip1*$^{+/-}$ tissues from the striatum (female n = 6; male

n = 6; two-tailed Mann-Whitney *U*-test, *U* = 16.000, *P* = 0.818), cerebellum (female n = 3; male n = 6; two-tailed Student`s *t*-test, *P* = 0.643) and liver (female n = 3; male n = 6; two-tailed Student`s *t*-test, *P* = 0.192) showed similar *Cyfip1* mRNA levels (**Figure 5.1A**). In adult wild type mice, motor cortical *Cyfip1* mRNA levels were significantly increased in male mice compared to females mice (female n = 6; male n = 5; two-tailed Student`s *t*-test, *P* = 0.012). In contrast, male and female *Cyfip1* mRNA levels were similar in wild type tissues collected from the striatum (female n = 6; male n = 6; two-tailed Mann-Whitney *U*-test, *U* = 10.000, *P* = 0.240), cerebellum (female n = 6; male n = 4; two-tailed Student`s *t*-test, *P* = 0.167) and liver (female n = 6; male n = 4; two-tailed Student`s *t*-test, *P* = 0.596) (**Figure 5.1B**).

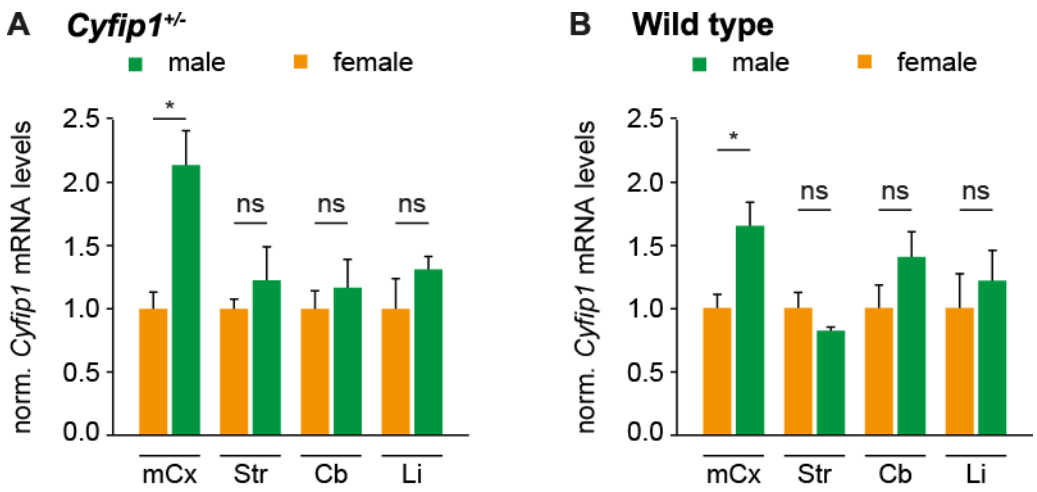

Figure 5.1 Male and female *Cyfip1* mRNA levels across different *Cyfip1*$^{+/-}$ and wild type brain regions.

A and **B**, Male and female *Cyfip1* mRNA levels in the *Cyfip1*$^{+/-}$ and wild type motor cortex (mCx), striatum (Str), cerebellum (Cb) and liver (Li). *Cyfip1* mRNA levels were normalised to *18S* mRNA levels. All values presented as mean ± SEM. Statistical significance was tested by two-tailed Student`s *t*-test or two-tailed Mann-Whitney *U*- test. ns $P > 0.05$; *$P < 0.05$.

Male and female CYFIP1 protein levels in *Cyfip1*$^{+/-}$ brain tissues were determined by Western blotting using CYFIP1 and βIII-Tubulin specific antibodies. Male and female CYFIP1 protein levels were similar between lysates from the motor cortex (female n = 6; male n = 7; two-tailed Student`s *t*-test, *P* = 0.715), striatum (female n = 4; male n = 7; two-tailed Mann-Whitney *U*-test, *U* = 12.000, *P* = 0.788), hippocampus (female n = 7; male n = 7; two-tailed Student`s *t*-test, *P* = 0.182) and cerebellum (female n = 7; male n = 7; two-tailed Mann-Whitney *U*-test, *U* = 22.000, *P* = 0.805) (**Figure 5.2A**). CYFIP1 protein levels in wild type mice were comparable between male and female brain tissues from the motor cortex (female n = 6; male n = 7; two-tailed Mann-Whitney, *U* = 14.000, *P* = 0.366), striatum (female n = 7; male n = 7; two-tailed Student`s *t*-test, *P* = 0.261), hippocampus (female n = 7; male n = 7; two-tailed Student`s *t*-test, *P* = 0.387) and cerebellum (female n = 7; male n = 7; two-tailed Student`s *t*-test, *P* = 0.749) (**Figure 5.2B**).

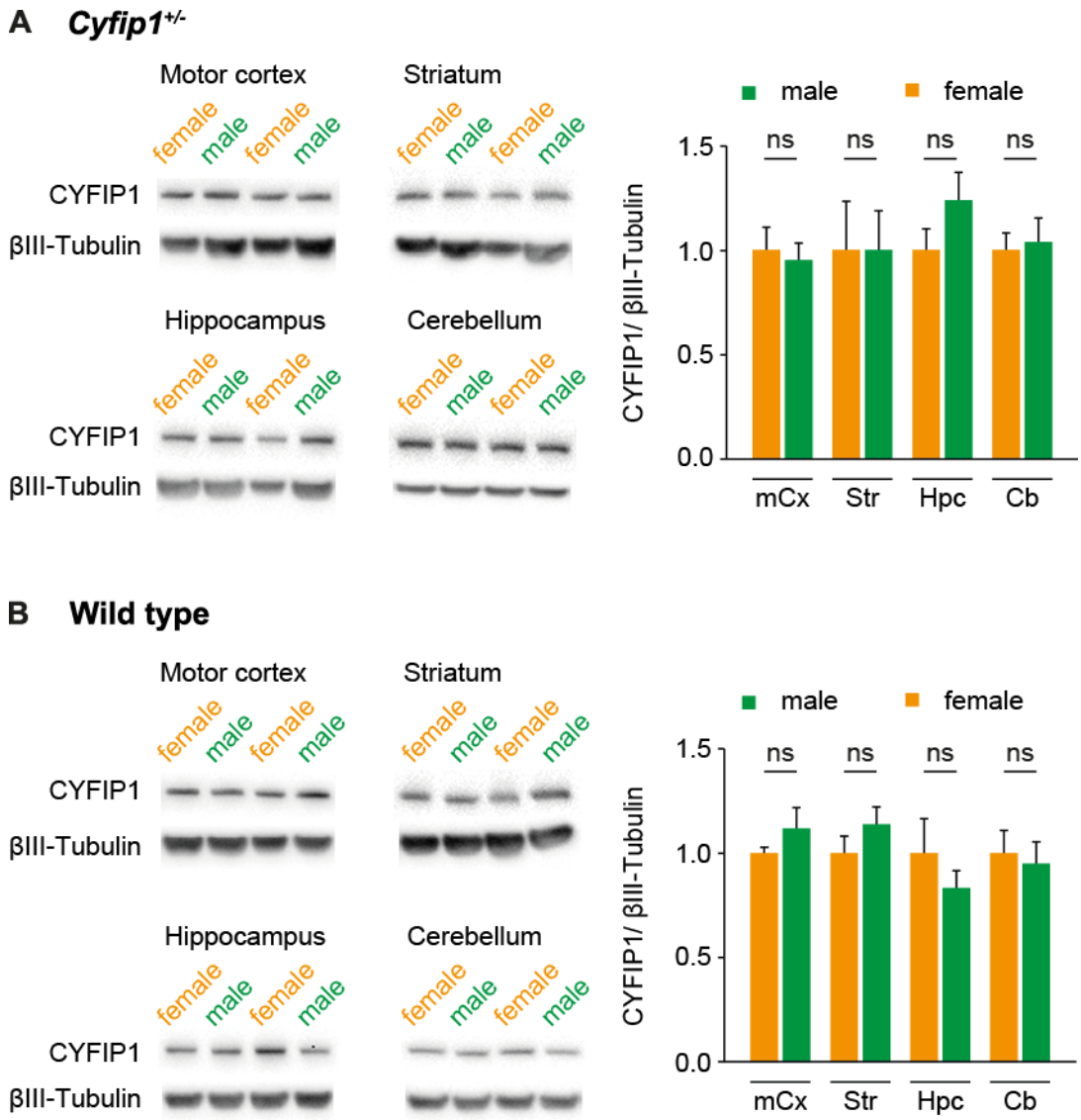

Figure 5.2 Male and female CYFIP1 protein levels across different *Cyfip1*$^{+/-}$ and wild type brain regions.

A and **B**, Male and female CYFIP1 protein levels in motor cortex (mCx), striatum (Str), hippocampus (Hpc) and cerebellum (Cb) of adult *Cyfip1*$^{+/-}$ and wild type mice. CYFIP1 levels were normalised to βIII-Tubulin levels. All values presented as mean ± SEM. Statistical significance was tested by two-tailed Student`s *t*-test or two-tailed Mann-Whitney *U*-test. ns $P > 0.05$.

5.1.3 Discussion

Cyfip1 mRNA levels were higher in male than in female mice in the motor cortex whereas *Cyfip1* mRNA levels were similar between the male and female striatum, cerebellum and liver. Similarly, *Cyfip1* mRNA levels were increased in the motor cortex of wild type male mice compared to wild type female mice and *Cyfip1* mRNA levels obtained in the male and female striatum, cerebellum and liver were comparable. Therefore, the sex had a similar effect on *Cyfip1* mRNA levels in *Cyfip1*$^{+/-}$ and wild type mice.

CYFIP1 protein levels in the *Cyfip1*$^{+/-}$ and wild type motor cortex, striatum, hippocampus and cerebellum were similar between male and female mice. Hence, the male-specific increase in *Cyfip1* mRNA levels in the *Cyfip1*$^{+/-}$ and wild type motor cortex did not result in a male-biased increase in CYFIP1 protein levels. In summary, the obtained results allowed excluding a genotype and sex-specific effect on *Cyfip1* mRNA and CYFIP1 protein level as an underlying of the sex-biased phenotypic *Cyfip1*$^{+/-}$ behaviours.

5.2 WAVE1 expression in the CNS of adult *Cyfip1*$^{+/-}$ mice

5.2.1 Introduction

CYFIP1 is a component of the WAVE complex which is involved in promoting actin nucleation which mediates cytoskeletal remodelling (Kunda et al. 2003; Eden et al. 2002; Chen et al. 2010). In the mouse, WAVE1 was confirmed as a CYFIP1 interactor by CYFIP1 co-immunoprecipitates (De Rubeis et al. 2013). Moreover structural analysis of the WAVE regulatory complex highlighted a direct interaction between the C-terminus of WAVE1 and CYFIP1 which is central for the regulation of the WRC activity (Chen et al. 2010).

We assessed WAVE1 protein levels and the CYFIP1-WAVE1 association in order to probe for molecular consequences of *Cyfip1* haploinsufficiency on WAVE1 protein levels and WRC regulation. *Cyfip1*$^{+/-}$ and wild type brain tissue extracts were analysed by CYFIP1 immunoprecipitation and/or Western blotting.

5.2.2 Results

In order to test for WAVE1 protein levels we performed biochemical analysis of different anatomical brain tissues of adult *Cyfip1*$^{+/-}$ and wild type mice. Obtained WAVE1 protein levels were similar between adult *Cyfip1*$^{+/-}$ and wild type lysates from the motor cortex (WT n = 5; *Cyfip1*$^{+/-}$ n = 5; two-tailed Student`s *t*-test, two-tailed $P = 0.553$), striatum (WT n = 5; *Cyfip1*$^{+/-}$ n = 5; two-tailed Student`s *t*-test, two-tailed $P = 0.957$), hippocampus (WT n = 5; *Cyfip1*$^{+/-}$ n = 3; two-tailed Student`s *t*-test, two-tailed $P = 0.947$) and cerebellum (WT n = 5; *Cyfip1*$^{+/-}$ n = 5; two-tailed Mann-Whitney *U*- test, $U = 7.000$, $P = 0.310$) (**Figure 5.3A**). In addition, we probed for the CYFIP1-WAVE1 interaction in the motor cortex using CYFIP1 immunoprecitation. Quantification of CYFIP1 co-immuoprecipitated WAVE1 relative to input WAVE1

protein levels revealed comparable ratios of co-immunoprecipated WAVE1 from motor cortical *Cyfip1*$^{+/-}$ and wild type lysates (WT n = 2; *Cyfip1*$^{+/-}$ n = 2) (**Figure 5.3B**).

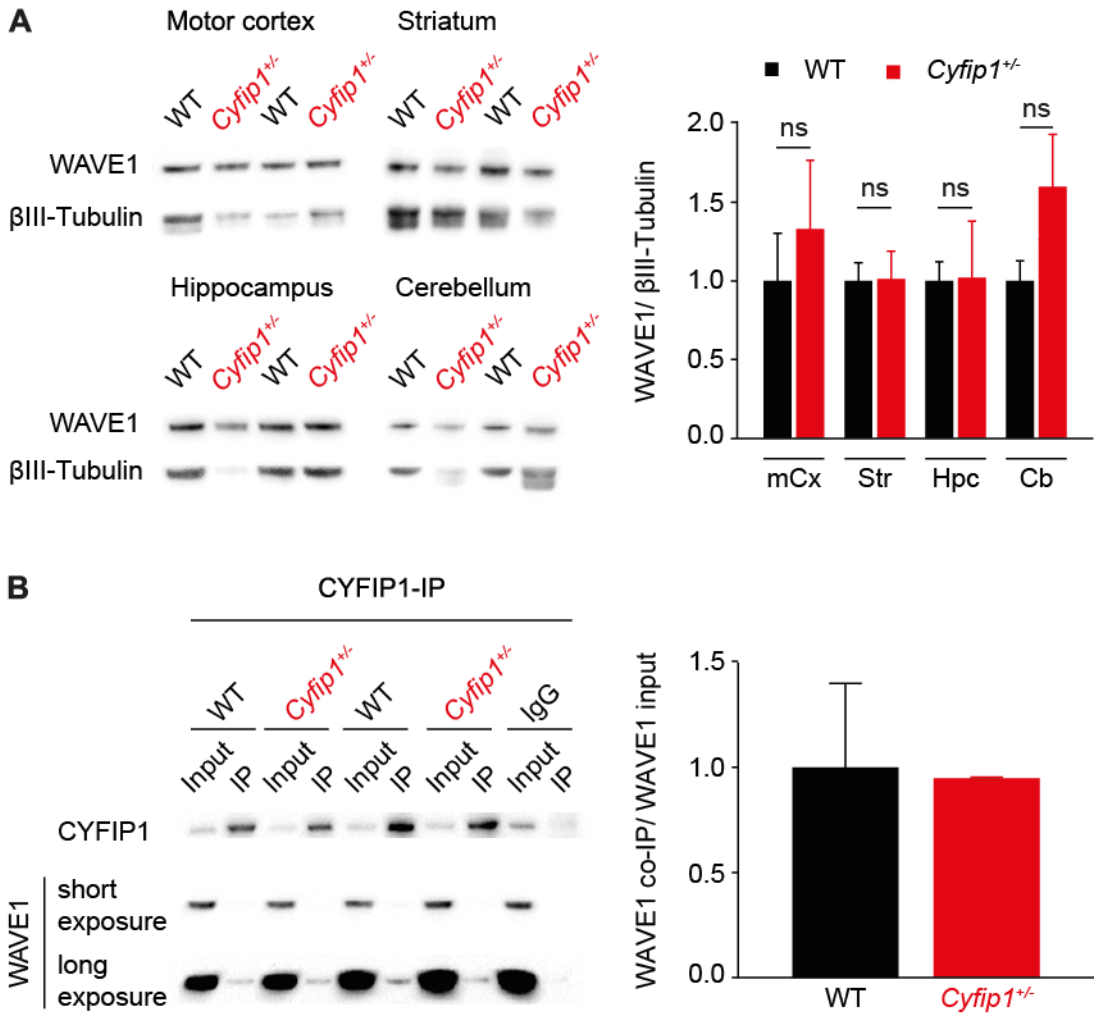

Figure 5.3 WAVE1 protein levels and WAVE1-CYFIP1 association in *Cyfip1*$^{+/-}$ and wild type brain tissues.

A, Western blots for WAVE1 and βIII-Tubulin of *Cyfip1*$^{+/-}$ and wild type motor cortex (mCx), striatum (Str), hippocampus (Hpc) and cerebellum (Cb) quantified by densitometry. Statistical significance was tested by two-tailed Student`s *t*-test or two-tailed Mann-Whitney *U*-test. ns $P > 0.05$. **B**, CYFIP1 co-immunoprecipitations of CYFIP1 and WAVE1 from *Cyfip1*$^{+/-}$ and wild type motor cortex. Co-immunoprecipitated levels of WAVE1 were normalised to WAVE1 levels in the input. Values represented as mean ± SEM.

5.2.3 Discussion

Despite a suboptimal quality of the βIII-Tubulin signal for some of the samples WAVE1 protein levels in the *Cyfip1*$^{+/-}$ motor cortex, striatum and hippocampus were similar to the WAVE1 protein levels in the corresponding wild type control tissues. This suggests that the heterozygous loss of *Cyfip1* and the consequently reduced CYFIP1 protein levels in the motor cortex, striatum and hippocampus had no effect on the WAVE1 protein levels. However, cerebellar WAVE1 levels showed a trend for an increase in *Cyfip1*$^{+/-}$ tissue compared to wild type control tissue but the quality of the obtained βIII-Tubulin signal is not sufficient to conclude with certainty that the trend does exist. Further experiments would be required to clarify the WAVE1 protein levels in the *Cyfip1*$^{+/-}$ and wild type cerebellum.

In the motor cortex, similar WAVE1 protein levels were detected in CYFIP1 co-immunoprecipitates of *Cyfip1*$^{+/-}$ and wild type tissues. Therefore, the heterozygous loss of *Cyfip1* had no detectable consequences on the interaction between CYFIP1 and WAVE1. Therefore, we conclude that CYFIP1 levels in the *Cyfip1*$^{+/-}$ motor cortex are sufficient to maintain a CYFIP1-WAVE1 association similar to the wild type condition. Given the complexity and dynamics of the WRC, the intact CYFIP1-WAVE1 interaction alone does not exclude WRC perturbations or functional consequences upon heterozygous *Cyfip1* deletion. Therefore testing other components of the WRC for their association (Chen et al. 2011) could support the finding of an intact interaction between CYIP1 and WAVE1 in *Cyfip1*$^{+/-}$ mice.

Chapter 6

Protein translation in *Cyfip1*$^{+/-}$ mice

6.1 Introduction

CYFIP1 was identified as a FMRP-interacting protein (Schenck et al. 2001). FMRP is a RNA-binding protein (Ashley et al. 1993; Siomi et al. 1993) involved in localisation and stabilisation of target RNAs (Kanai et al. 2004; Zalfa et al. 2007). Moreover FMRP is a suggested to be a translational repressor (Bassell & Warren 2008; Darnell et al. 2011; Brown et al. 2001). The role of FMRP as a translational repressor is strongly supported by *in vivo* studies demonstrating an increased protein synthesis rate in adult *Fmr* knockout mice (Qin et al. 2005; Michalon et al. 2012). Consequences of *Cyfip1*$^{+/-}$ deletion on the rate of mRNA translation *in vivo* has not been characterised yet and we hypothesised that reduced CYFIP1 protein levels may lead to a decreased repression of mRNA translation resulting in an increased rate of protein synthesis. To test this hypothesis we first assessed levels of eIF4E phosphorylation in the adult *Cyfip1*$^{+/-}$ and wild type motor cortex and second determined the protein synthesis rate *in vivo* using adult *Cyfip1*$^{+/-}$ and wild type male mice.

Phosphorylation of eIF4E has been reported to correlate with protein synthesis rate, at which phosphorylation promoted protein synthesis (Joshi et al. 1995; Lamphear & Panniers 1989; Kleijn et al. 1998). Hence, we used eIF4E phosphorylation as an indirect read-out for the protein synthesis rate. In addition, we used puromycin incorporation as a measure for the bulk protein synthesis rate *in vivo* (Liu et al. 2012). Puromycin is an aminonucleoside antibiotic and a structural analogue of aminoacyl tRNAs which is a substrate of the ribosomal machinery synthesising proteins *de novo* (Nathans 1964; Schmidt et al. 2009). Puromycin is randomly incorporated into elongating polypeptide chains, which induces termination of mRNA translation. As a

result, truncated puromycin labelled peptides are released from the ribosome (Nathans 1964). In order to deliver puromycin into the CNS *in vivo,* we used unilateral ventricular injections and allowed puromycin to diffuse and incorporate into nascent polypeptide chains across the brain. The levels of puromycin labelled peptides in brain tissue extracts from *Cyfip1*$^{+/-}$ and wild type adult male mice were determined by Western blotting, anti-puromycin antibody detection and subsequent quantification by densitometry.

6.2 Results

Obtained ratios of phosphorylated eIF4E over eIF4E were similar between motor cortical tissues for adult *Cyfip1*$^{+/-}$ and wild type male mice (WT n = 7; *Cyfip1*$^{+/-}$ n = 7; two-tailed Student`s *t*-test, *P* = 0.408) (**Figure 6.1**).

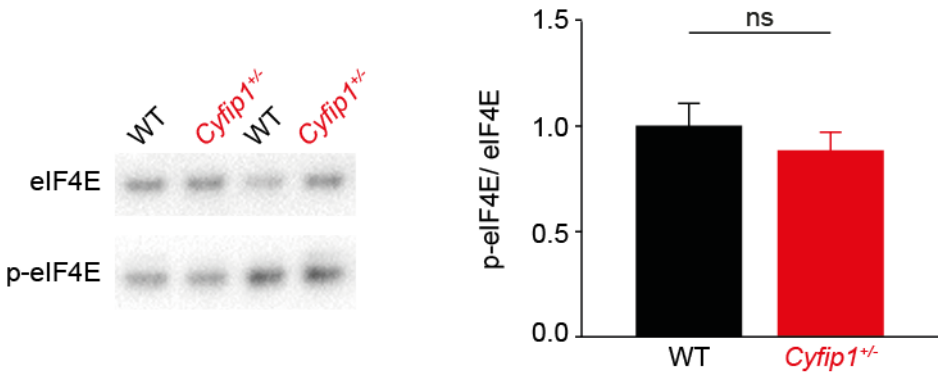

Figure 6.1 Phosphorylation of eIF4E in *Cyfip1*$^{+/-}$ and wild type male mice
Levels of phosphorylated eIF4E (p-eIF4E) were normalised to eIF4E levels. All values presented as mean ± SEM. Statistical significance was tested by two-tailed Student`s *t*-test. ns *P* > 0.05.

The obtained levels of puromycin labelling were similar between puromycin injected adult *Cyfip1*$^{+/-}$ and wild type male mice in the motor cortex (WT n = 5; *Cyfip1*$^{+/-}$ n = 5; two-tailed Mann-Whitney *U*-test, $U = 8.000$, $P = 0.421$), striatum (WT n = 5; *Cyfip1*$^{+/-}$ n = 5; two-tailed Student`s *t*-test, $P = 0.866$), hippocampus (WT n = 5; *Cyfip1*$^{+/-}$ n = 5; two-tailed Mann-Whitney *U*-test, $U = 7.000$, $P = 0.310$) and cerebellum (WT n = 5; *Cyfip1*$^{+/-}$ n = 5; two-tailed Mann-Whitney *U*-test, $U = 8.000$, $P = 0.421$). Importantly, the detected puromycin levels were in all tissues were above the background puromycin signal obtained from control tissues of mice that were not injected with puromycin.

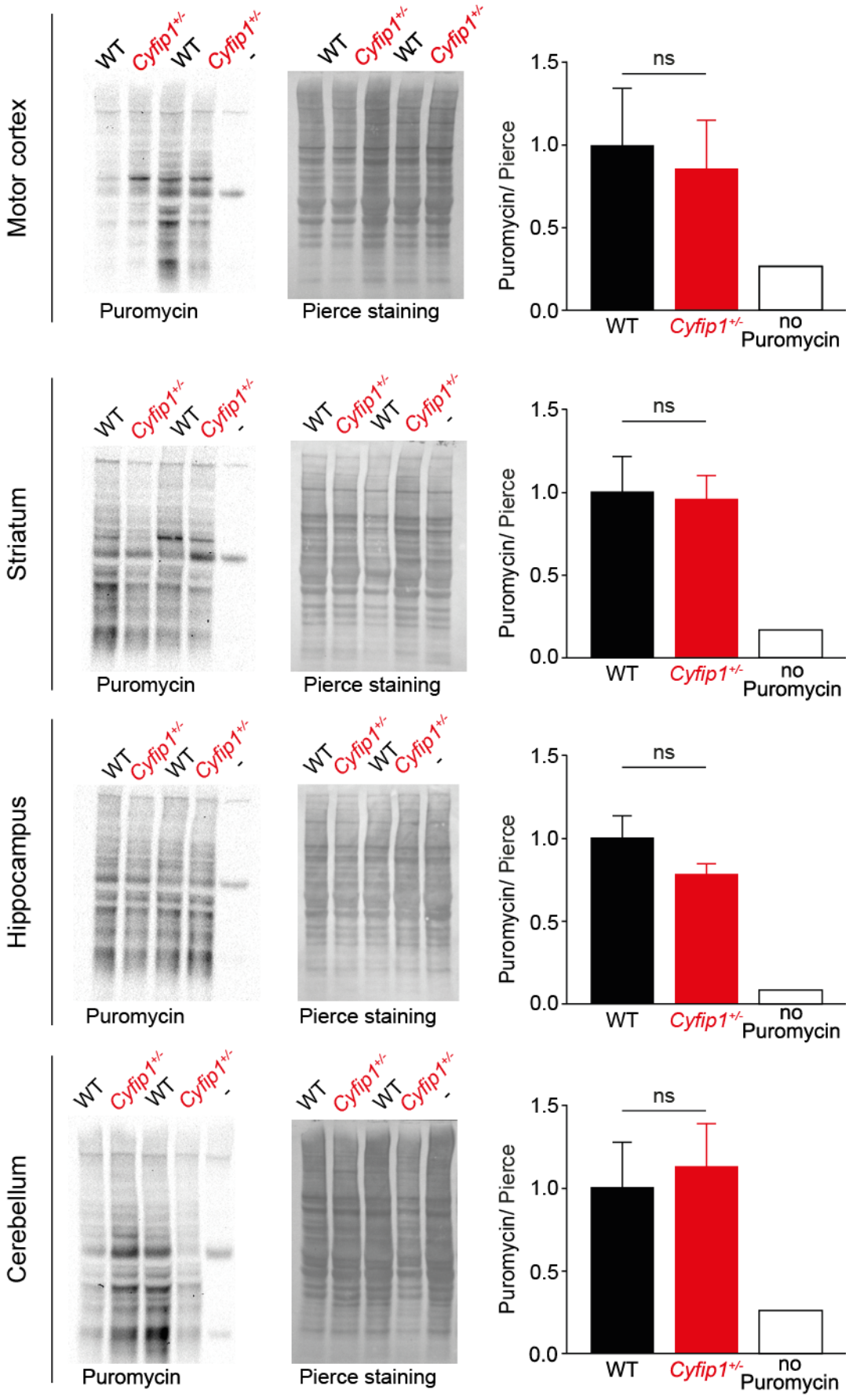

Figure 6.2 *Cyfip1*$^{+/-}$ and wild type protein synthesis rate *in vivo*.

Brain tissues of puromycin injected adult *Cyfip1*$^{+/-}$ and wild type male mice were analysed by Western blotting. Tissue lysates from a control mouse that had not been injected with puromycin served as a negative control (-). The puromycin levels were normalised to the Pierce staining which served as a loading control. Except from the negative control, values are presented as mean ± SEM. Statistical significance was tested by two-tailed Student`s *t*-test or two-tailed Mann-Whitney *U*-test. ns $P > 0.05$.

6.3 Discussion

Our results revealed similar levels of eIF4E phosphorylation in the adult *Cyfip1*$^{+/-}$ and wild type motor cortex. In addition, baseline protein synthesis rates between adult *Cyfip1*$^{+/-}$ and wild type male mice were similar in the motor cortex, striatum, hippocampus and cerebellum. Therefore, we conclude that the basal bulk protein synthesis rate was not affected by the heterozygous loss of *Cyfip1*. Despite decreased CYFIP1 protein levels in the *Cyfip1*$^{+/-}$ motor cortex and hippocampus the protein synthesis rate was comparable to the wild type protein synthesis rate. This result indicates that the decreased CYFIP1 protein levels were sufficient to regulate translation as in the wild type condition.

From a technical point of view, puromycin incorporation allows concluding on protein synthesis only to a certain degree. Puromycin crosses the cell membrane passively and is consequently an available substrate for the translation machinery (Nathans 1964). This mode of action gives rise to the cell-unspecific incorporation of puromycin. In tissues with different cellular subpopulations, such as the brain (Masland 2004), puromycin incorporation represents the mRNA translation rate of a given cell population as a ratio to the mRNA translation rate of the entire cell population. Therefore, small cell populations are underrepresented whereas large cell populations are overrepresented with regards to the bulk mRNA translation rate. This

limitation could mask a cell-specific effect of *Cyfip1* haploinsufficiency on the mRNA translation rate. Moreover, neurons are highly polarised cells where protein synthesis is not only occurring in the cell soma but also in axons and dendrites. RNA transport and local translation are thought to be critical for the site-specific regulation of the proteome (Steward & Schuman 2003; Glock et al. 2017). A potential effect of *Cyfip1* loss on local translation has not been characterised yet and can`t be ruled out. The metabolic labelling allows the quantification of the total rate of protein synthesis. However, the total rate of protein synthesis does not take the identity of translated mRNA in account. Thus, the heterozygous loss of *Cyfip1* might have an effect on the identity of translated mRNAs without detectable consequences on the rate of protein synthesis.

Chapter 7

Alteration of spine density and stability in *Cyfip1*$^{+/-}$ mice

7.1 Introduction

One of the main findings of the behavioural characterisation of *Cyfip1*$^{+/-}$ mice was an impaired motor learning behaviour in adult *Cyfip1*$^{+/-}$ male mice. Interestingly, motor learning in mice has been correlated with neuronal activity (Costa et al. 2004) and structural plasticity (Yang et al. 2009) in the motor cortex. More precisely, Yang et al. identified dendritic spine formation of layer V neurons in the forelimb representing area of the mouse motor cortex as a cellular correlate for rotarod-related motor learning.

Moreover, *Cyfip1* encodes a key regulator of actin dynamics and consequences of *Cyfip1* haploinsufficiency on actin dynamics and structural dendritic properties have been characterised by Pathania et. al 2004. The authors demonstrated increased mobile filamentous actin, reduced dendritic complexity, diminished activity-dependent changes in spine volume and an increased number of immature spines in cultured hippocampal *Cyfip1*$^{+/-}$ neurons compared to wild type control neurons. In agreement, hippocampal slices from *Cyfip1*$^{+/-}$ mice revealed a decreased dendritic complexity and increased numbers of immature spines compared to wild type control slices (Pathania et al. 2014). These findings highlight implications of *Cyfip1* haploinsufficiency on the dendritic spine morphology. We hypothesised that an aberrant dendritic spine plasticity in adult *Cyfip1*$^{+/-}$ males could underlie the observed motor learning impairment.

The aim was to assess first the dendritic spine density, with the help of a rotation student in the laboratory, and second to assess the dendritic spine plasticity in the

motor cortex of *Cyfip1*$^{+/-}$ and wild type male mice. To achieve this aim, we crossed *Cyfip1*$^{+/-}$ mice with animals from the Thy1-EGFP M-line to obtain *Cyfip1*$^{+/-}$*Thy1EGFP* and *Cyfip1*$^{+/+}$*Thy1EGFP* offspring with sparsely enhanced green fluorescent (EGFP) labelled neurons. Cortical dendrites from adult *Cyfip1*$^{+/-}$*Thy1EGFP* and *Cyfip1*$^{+/+}$*Thy1EGFP* male mice were imaged *ex vivo* and *in vivo* and analysed for spine density and structural plasticity.

7.2 Dendritic spine density and structural plasticity in adult *Cyfip1*$^{+/-}$ male mice

To investigate the dendritic spine organisation, we first analysed paraformaldehyde fixed tissue from different brain regions of adult *Cyfip1*$^{+/-}$*Thy1EGFP* and *Cyfip1*$^{+/+}$*Thy1EGFP* male mice for dendritic spine density by histology and fluorescent microscopy (**Figure 7.1A)**. The dendritic spine density in the primary motor cortex (M1) was significantly decreased in adult *Cyfip1*$^{+/-}$*Thy1EGFP* male mice compared to *Cyfip1*$^{+/+}$*Thy1EGFP* mice (*Cyfip1*$^{+/+}$*Thy1EGFP* n = 24 dendrites from 4 mice, *Cyfip1*$^{+/-}$*Thy1EGFP* n = 24 dendrites from 4 mice; two-tailed Student`s *t*-test, $P = 0.008$). In contrast, dendritic spine densities were similar between *Cyfip1*$^{+/-}$*Thy1EGFP* and *Cyfip1*$^{+/+}$*Thy1EGFP* mice in the primary visual area (V1) of the visual cortex (*Cyfip1*$^{+/+}$*Thy1EGFP* n = 24 dendrites from 4 mice, *Cyfip1*$^{+/-}$*Thy1EGFP* n = 24 dendrites from 4 mice; two-tailed Mann Whitney *U*-test, $U = 166.000$, $P = 0.174$), in the hippocampal CA1 area (*Cyfip1*$^{+/+}$*Thy1EGFP* n = 20 dendrites from 4 mice, *Cyfip1*$^{+/-}$*Thy1EGFP* n = 21 dendrites from 4 mice; two-tailed Student`s *t*-test, $P = 0.376$) and in the hippocampal CA3 area (*Cyfip1*$^{+/+}$*Thy1EGFP* n = 20 dendrites from 4 mice, *Cyfip1*$^{+/-}$*Thy1EGFP* n = 20 dendrites from 4 mice; two-tailed Student`s *t*-test, $P = 0.067$) (**Figure 7.1A**).

The reduced spine density in the adult *Cyfip1*$^{+/-}$*Thy1EGFP* motor cortex could be due to a deficit in forming new spines. Thus, the structural spine plasticity was assessed *in vivo*. In awake *Cyfip1*$^{+/-}$*Thy1EGFP* and *Cyfip1*$^{+/+}$*Thy1EGFP* mice, EGFP positive dendrites from layer V neurons in the forelimb representing area of the motor cortex were imaged. Two-photon microscopy over the period of nine days allowed determining the number of newly formed and eliminated dendritic spines (**Figure 7.1B**). The analysis revealed a significant increase in dendritic spine turnover, with increased formation (1.63 fold) and elimination (1.40 fold) of dendritic spines in the motor cortex of *Cyfip1*$^{+/-}$*Thy1EGFP* males compared to *Cyfip1*$^{+/+}$*Thy1EGFP* male mice (*Cyfip1*$^{+/+}$*Thy1EGFP* n = 40 dendrites from 4 mice, *Cyfip1*$^{+/-}$*Thy1EGFP* n = 36 dendrites from 4 mice; two-way ANOVA, main effect of genotype $F_{1, 148} = 4.718$, $P = 0.031$) (**Figure 7.1C**).

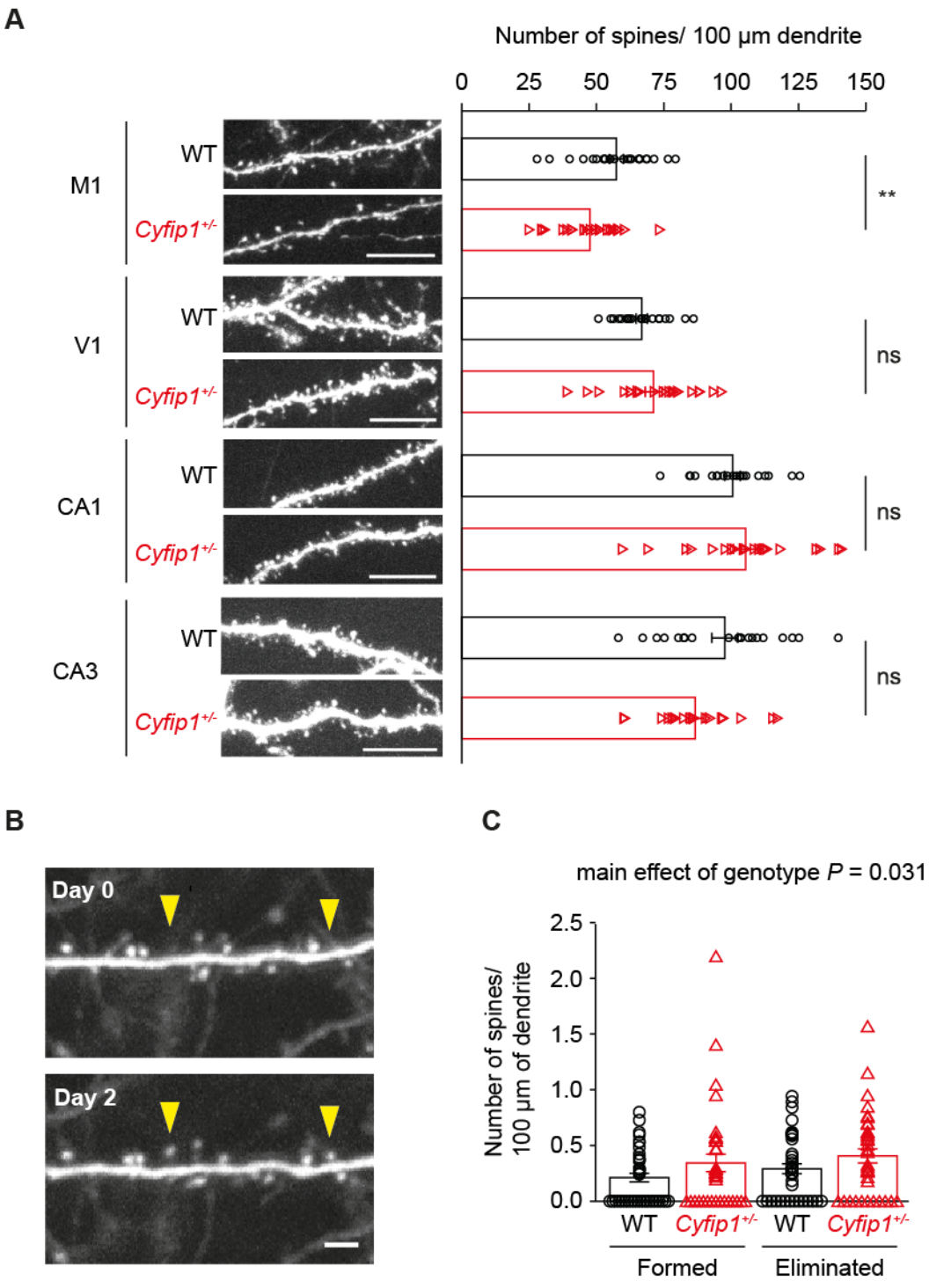

Figure 7.1 Reduced spine density and increased dendritic spine turnover in the male *Cyfip1*$^{+/-}$*Thy1EGFP* motor cortex.

A, Histologic preparations from adult *Cyfip1*$^{+/-}$*Thy1EGFP* (annotated as *Cyfip1*$^{+/-}$) and *Cyfip1*$^{+/+}$*Thy1EGFP* (annotated as WT) imaged for EGFP positive neurons in the primary motor cortex (M1), primary visual cortex (V1) and the hippocampal areas CA1 and CA3 and quantified for the number of spines per 100 µm of dendrite. Scale bar,

10 µm. **B** Repeated *in vivo* two-photo imaging of EGFP positive apical dendrite from layer V neuron in the forelimb representing area of the adult motor cortex over two days. Arrowheads indicate newly formed spines. Scale bar, 2 µm. **C**, Analysis of dendritic spine formation and elimination per 100 µm of dendrite over nine days for *Cyfip1*$^{+/-}$*Thy1EGFP* and *Cyfip1*$^{+/+}$*Thy1EGFP* male mice. Values represented as mean ± SEM. Statistical significance was tested by two-tailed Student`s *t*-test (B) or two-way ANOVA (D). ns > 0.05; ** $P < 0.01$.

7.3 Motor learning mediated structural plasticity in adult *Cyfip1*$^{+/-}$ male mice

According to the behavioural characterisation, adult male wild type mice increased their rotarod performance with training whereas *Cyfip1*$^{+/-}$ showed a motor learning deficit (Chapter 4.5). This observation led to the hypothesis that wild type neurons associated with motor learning form new spines whereas *Cyfip1*$^{+/-}$ neurons fail to form new spines.

Cyfip1$^{+/-}$*Thy1EGFP* and *Cyfip1*$^{+/+}$*Thy1EGFP* mice were trained using the rotarod protocol and structural imaging of apical dendrites from layer V neurons were acquired two days later. Image analysis and spine counting of *Cyfip1*$^{+/+}$*Thy1EGFP* dendrites revealed a 3.73 fold increase in dendritic spine formation upon rotarod training (Baseline 0.209 ± 0.038; after training 0.780 ± 0.163 n = 40 dendrites from 4 mice) whereas *Cyfip1*$^{+/-}$*Thy1EGFP* dendrites showed a 3.047 fold increase in dendritic spine formation following the rotarod paradigm (Baseline *Cyfip1*$^{+/-}$ *Thy1EGFP* 0.341 ± 0.078; after training 1.039 ± 0.179; n = 36 dendrites from 4 mice) (Repeated measures ANOVA, main effect of spine formation $F_{1, 74} = 25.737$, $P = 0.000$) (**Figure 7.2A**). Dendritic spine formation within each individual *Cyfip1*$^{+/-}$ *Thy1EGFP* and *Cyfip1*$^{+/+}$*Thy1EGFP* mouse showed a trend for an increase upon rotarod training except for one *Cyfip1*$^{+/+}$*Thy1EGFP* animal. (**Figure 7.2B**). Motor training had no effect on spine elimination of *Cyfip1*$^{+/-}$*Thy1EGFP* (Baseline: 0.404 ±

0.063; after training 0.532 ± 0.116, n = 40 dendrites from 4 mice) and *Cyfip1*$^{+/+}$*Thy1EGFP* dendrites (Baseline: 0.288 ± 0.044 after training 0.217 ± 0.077, n = 36 dendrites from 4 mice) (Repeated measures ANOVA, main effect of spine elimination $F_{1, 74}$ = 0.135, P = 0.715) (**Figure 7.2C**). On the level of the individual *Cyfip1*$^{+/-}$*Thy1EGFP* mice three out of four animals showed no trend of a changed spine elimination following training whereas spine elimination within *Cyfip1*$^{+/+}$*Thy1EGFP* mice was not detected or unchanged upon rotarod training (**Figure 7.2D**). In summary, rotarod training increased dendritic spine formation of layer V neurons in the forelimb representing area of the male *Cyfip1*$^{+/-}$*Thy1EGFP* and *Cyfip1*$^{+/+}$*Thy1EGFP* motor cortex whereas spine elimination was not affected by motor learning.

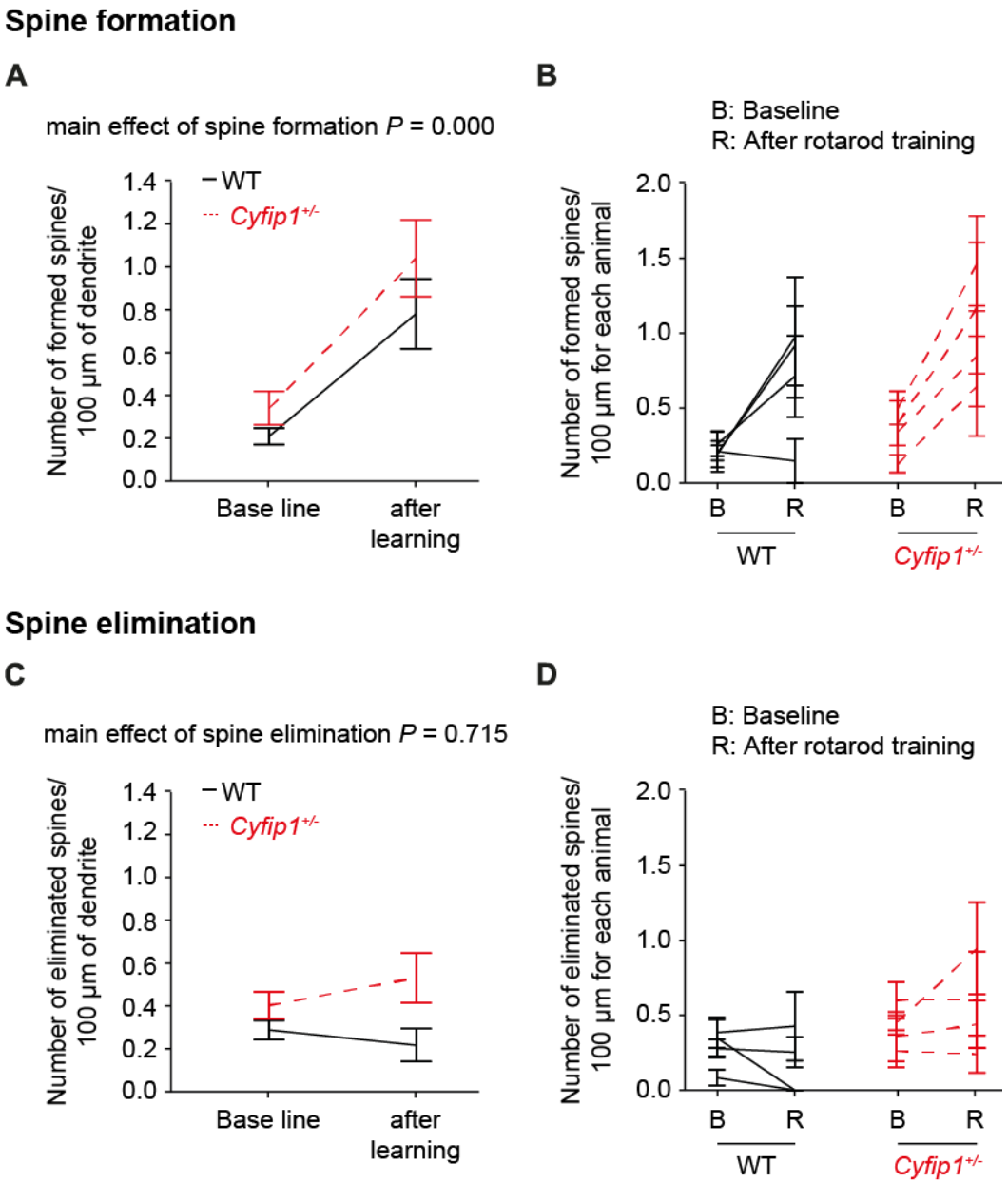

Figure 7.2 Motor learning increased dendritic spine formation in the male *Cyfip1*$^{+/-}$*Thy1EGFP* and *Cyfip1*$^{+/+}$*Thy1EGFP* forelimb representation of the motor cortex.

A, Increased spine formation of *Cyfip1*$^{+/-}$*Thy1EGFP* (annotated as *Cyfip1*$^{+/-}$) and *Cyfip1*$^{+/+}$*Thy1EGFP* (annotated as WT) dendrites following the motor learning. **B,** Majority of analysed dendrites within individual animals increased spine formation upon motor learning. **C,** Rotarod training had no effect on spine elimination in *Cyfip1*$^{+/-}$*Thy1EGFP* and *Cyfip1*$^{+/+}$*Thy1EGFP* mice. **D**, Spine elimination was unchanged in the majority of analysed dendrites following motor learning. Values in A and C represented as mean per dendrite ± SEM and values in B and D as mean of per

animal ± SEM. Statistical significance of A and C was tested by repeated measures ANOVA.

7.4 Discussion

Histological analysis of motor cortical sections revealed a decreased dendritic spine density in *Cyfip1*$^{+/-}$*Thy1EGFP* male mice compared to *Cyfip1*$^{+/+}$*Thy1EGFP* mice in the primary motor cortex but not in the V1 of the visual cortex and the hippocampal areas CA1 and CA3. These findings suggest that heterozygous *Cyfip1* loss had a brain region-specific effect on the dendritic spine density in adult mice. To characterise the dynamics underlying the decreased spine density in the primary motor cortex we performed structural imaging of apical dendrites originating from layer V neurons in the in the forelimb representing area of the motor cortex. The obtained results indicated an increased dendritic spine formation and elimination of *Cyfip1*$^{+/-}$ *Thy1EGFP* layer V neurons compared to *Cyfip1*$^{+/-}$*Thy1EGFP* control neurons. Thus, the aberrant dendritic spine density in the motor cortex of *Cyfip1*$^{+/-}$ mice is explained by the absence of dendritic spine stability and not by a defect in the formation of new spines. Reminiscent to our observations, reduced synaptic stability in the cortex associated with experience-dependent and learning-induced spine remodelling was reported in a mouse model lacking FMRP (Nakai et al. 2018).

Chapter 8

The social environment as a regulator of physiologic features in a mouse model for ASD

8.1 Introduction

A collaborative project with other PhD students of the lab was aiming to determine the effect of social environment on the behaviour and physiology of mouse models for autism and wild type mice (Kalbassi et al. 2017). For this project, we used a model of nonsyndromic ASD in which mice lack the X-linked gene *Nlgn3*, coding for the postsynaptic adhesion protein Neuroligin-3 exclusively expressed in the brain (Tanaka et al. 2010; Baudouin et al. 2012). In humans, *NLGN3* deletion is associated with nonsyndromic ASD (Jamain et al. 2003; Ylisaukko-oja et al. 2005; Levy et al. 2011; Sanders et al. 2011; Yuen et al. 2017). The deletion of *Nlgn3* in mice leads to distinct measurable phenotypes, including social behaviour and courtship deficits (Radyushkin et al. 2009; Rothwell et al. 2014; Baudouin et al. 2012; Fischer & Hammerschmidt 2011). To investigate the role of the social environment on mouse behaviour and physiology, we analysed the behaviour of mice from litters consisting of both genotypes (mixed genotype housing, MGH) in comparison to litters in which male mice were all of the same *Nlgn3*$^{y/+}$ genotype (single genotype housing, SGH). In this context, I analysed the expression level of pheromones in these differently housed *Nlgn3*$^{y/+}$ and wild type mice. In particular, I investigated major urinary proteins (MUPs), which are pheromone proteins synthesised in the liver and excreted in the urine (Sheehan et al. 2016).

8.2 Social environment of *Nlgn3$^{y/-}$* male mice

The adult male behaviour was analysed using males from litters consisting of *Nlgn3$^{y/-}$* and *Nlgn3$^{y/+}$* mice (mixed genotype housing, MGH) in comparison to litters in which all mice from the same genotype (*Nlgn3$^{y/-}$* or *Nlgn3$^{y/+}$*) (single genotype housing, SGH). The assessment of social environmental effects on social behaviour included the use of behavioural assays such as the tube test and the ultrasonic courtship vocalisation paradigm.

We used the tube test as a paradigm to test *Nlgn3$^{y/+}$* and *Nlgn3$^{y/-}$* male mice from MGH for their social dominance behaviour. Direct encounters between *Nlgn3$^{y/-}$* and *Nlgn3$^{y/+}$* mice from MGH revealed that *Nlgn3$^{y/-}$* mice lost more frequently encounters with *Nlgn3$^{y/+}$* mice (*Nlgn3$^{y/+}$* 72.9% ± 9.8%; *Nlgn3$^{y/-}$* 29.4% ± 10.3%; $P = 0.007$) (**Figure 8.1A**). Tube test wins were demonstrated to be a measure for social dominance whereas losing in the tube test was associated with social submission (Wang et al. 2011). Ranks in tube test behaviour and courtship vocalisation were described to correlate in group-housed mice with stable social hierarchies. More precisely the dominant animal with highest level of courtship vocalisation wins the tube test whereas the most submissive mouse vocalises the least and loses in tube test encounters (Wang et al. 2011). Therefore, we tested *Nlgn3$^{y/-}$* male mice from MGH and SGH for their courtship vocalisation and tube test behaviour. Results from MGH and SGH were analysed separately for correlation between rank in courtship vocalisation and tube test behaviour. In cages of SGH *Nlgn3$^{y/-}$* male mice observed ranks in courtship vocalisation and tube test behaviour correlated (13 cages; correlation test, $r^2 = 0.90$) whereas no correlation was obtained in MGH *Nlgn3$^{y/-}$* male mice (6 cages; correlation test, $r^2 = 0.25$) (**Figure 8.1B**).

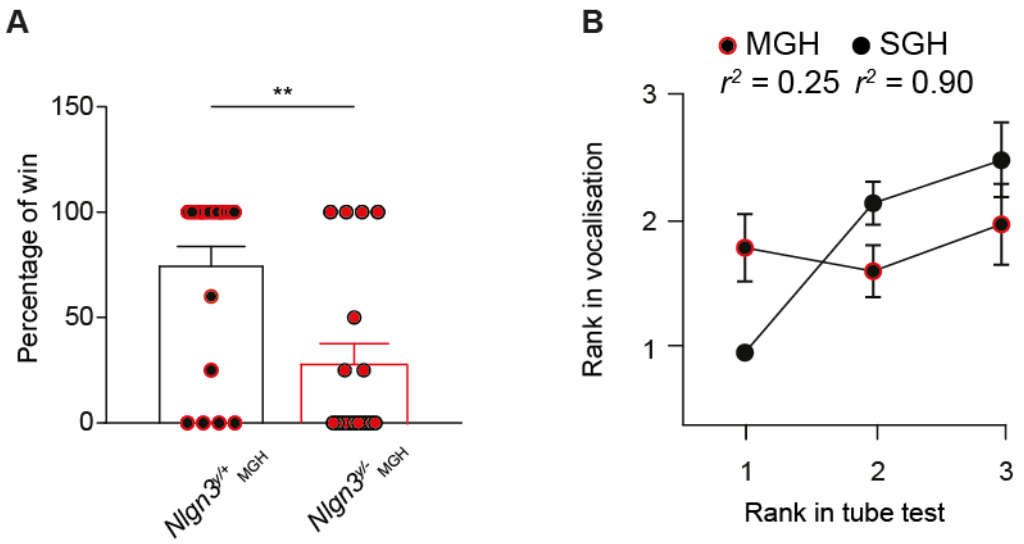

Figure 8.1 Social submission and unstable social hierarchy in *Nlgn3*$^{y/-}$ MGH mice.

A, *Nlgn3*$^{y/-}$ mice form MGH lost more frequently direct encounters against their *Nlgn3*$^{y/+}$ littermates. **B**, *Nlgn3*$^{y/-}$ MGH specific absence of correlation between rank in the tube test and rank of courtship vocalisation. All values are represented as mean ± SEM. Statistical significance was tested by two-tailed Mann-Whitney *U*-test. ** $P < 0.01$.

8.3 Effect of social environment on gene expression in *Nlgn3*$^{y/-}$ male mice

The social environment modulated social behaviours and ultimately the social hierarchy of adult male *Nlgn3*$^{y/-}$ mice. We next addressed whether the social environment modified the expression of genes encoding pheromones. Major urinary proteins (MUPs) are pheromones representing important social cues for mice.

In order to assess *Mup4*, *Mup6* and *Mup20* (also known as *Darcin*) mRNA levels quantitative real-time PCR was performed using the $2^{-\Delta\Delta CT}$ method. Obtained *Mup4*, *Mup6* and *Mup20* mRNA levels relative to *18S* mRNA levels were higher in the liver of *Nlgn3*$^{y/+}$ MGH mice compared to *Nlgn3*$^{y/+}$ SGH mice. In contrast, relative *Mup4*,

Mup6 and *Mup20* mRNA levels were similar in the liver of *Nlgn3*$^{y/-}$ from SGH and MGH (SGH: *Nlgn3*$^{y/+}$ n = 8 and *Nlgn3*$^{y/-}$ n = 7; MGH: *Nlgn3*$^{y/+}$ n = 8 and *Nlgn3*$^{y/-}$ n = 7; two-way ANOVA, main effect of housing, $F_{1, 78} = 6.30$, $P = 0.014$, interaction housing x genotype, $F_{1, 78} = 4.15$, $P = 0.045$, Sidak's post hoc test) (**Figure 8.2A**). Corticotropin release hormone receptor 2 (*Crhr2*) mRNA levels in liver tissues from adult male *Nlgn3*$^{y/+}$ and *Nlgn3*$^{y/-}$ mice from MGH and SGH and *18S* ribosomal RNA (rRNA) specific primers were used to perform quantitative real-time PCR. The obtained *Crhr2* mRNA levels were normalised to the *18S* mRNA levels and analysed for effects of genotype and housing condition. The normalised *Crhr2* mRNA levels were significantly increased in the liver of *Nlgn3*$^{y/+}$ and *Nlgn3*$^{y/-}$ mice from MGH compared to *Nlgn3*$^{y/+}$ and *Nlgn3*$^{y/-}$ from SGH (SGH: *Nlgn3*$^{y/+}$ n = 8 and *Nlgn3*$^{y/-}$n = 6; MGH: *Nlgn3*$^{y/+}$ n = 5 and *Nlgn3*$^{y/-}$ n = 5; Two-way ANOVA, main effect of housing $F_{1, 20} = 4.9$, $P = 0.038$) (**Figure 8.2B**). In addition, *cytochrome P450 2D9* (*Cyp2d9*) was used as a marker for effects of the social environment on sexual dimorphism of the liver. Hepatic *Cyp2d9* mRNA levels were determined in *Nlgn3*$^{y/+}$ and *Nlgn3*$^{y/-}$ male mice from MGH and SGH. *Cyfp2d9* mRNA levels relative to 18S mRNA levels were similar between *Nlgn3*$^{y/+}$ and *Nlgn3*$^{y/-}$ male mice from MGH and SGH (SGH: *Nlgn3*$^{y/+}$ n = 7 and *Nlgn3*$^{y/-}$n = 6; MGH: *Nlgn3*$^{y/+}$ n = 5 and *Nlgn3*$^{y/-}$ n = 5; one-way ANOVA $P > 0.05$) (**Figure 8.2C**). In summary, the social environment had an effect on *Mup4*, *Mup6* and *Mup20* mRNA levels in *Nlgn3*$^{y/+}$ mice and on *Crhr2* mRNA levels of *Nlgn3*$^{y/+}$ and *Nlgn3*$^{y/-}$ mice whereas *Cyp2d9* mRNA levels were similar between the tested genotypes and housing conditions.

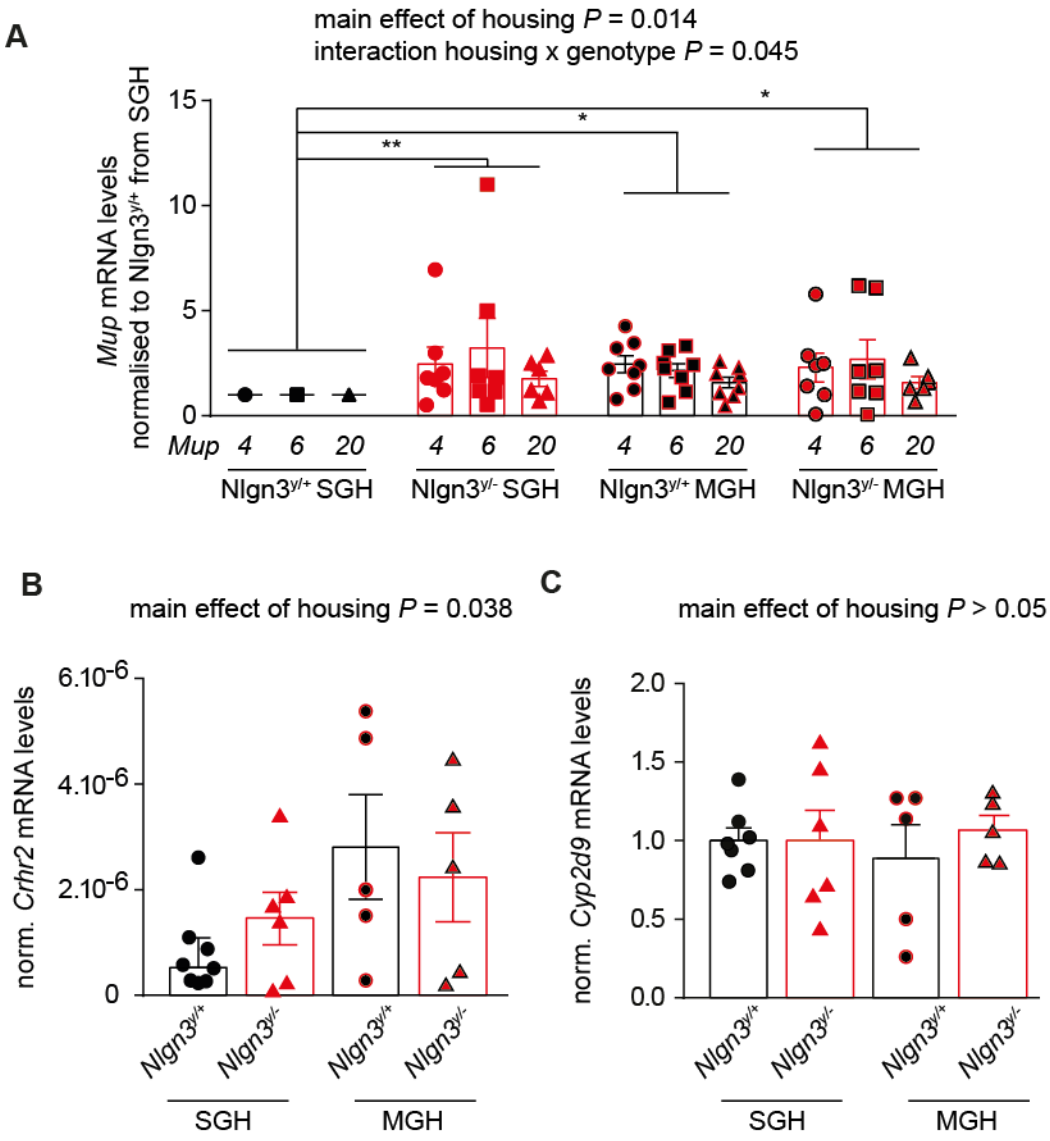

Figure 8.2 Effect of housing on hepatic mRNA levels in *Nlgn3$^{y/+}$* and *Nlgn3$^{y/-}$* mice.

A, Hepatic *Mup4*, *Mup6* and *Mup20* mRNA levels were reduced in *Nlgn3$^{y/+}$* mice from SGH compared to *Nlgn3$^{y/+}$* from SGH and *Nlgn3$^{y/-}$* mice from SGH and MGH. **B**, *Nlgn3$^{y/+}$* and *Nlgn3$^{y/-}$* mice from MGH had increased hepatic *Crhr2* mRNA levels compared to *Nlgn3$^{y/+}$* and *Nlgn3$^{y/-}$* mice from SGH **C**, Hepatic *Cyp2d9* mRNA levels were similar between mice from MGH and SGH. All values are represented as mean ± SEM. Statistical significance was tested by one-way or two-way ANOVA. * $P < 0.05$, ** $P < 0.01$.

8.4 Discussion

Our results demonstrate a submissive phenotype of adult *Nlgn3*$^{y/-}$ male mice in litters with *Nlgn3*$^{y/-}$ and *Nlgn3*$^{y/+}$ male mice and an absence in structured social hierarchy within litters of *Nlgn3*$^{y/-}$ and *Nlgn3*$^{y/+}$ male mice. In addition, the social environment of male *Nlgn3*$^{y/-}$ and *Nlgn3*$^{y/+}$ regulated the mRNA levels of hepatic *Crhr2.* Moreover, *Mup4*, *Mup6* and *Mup20* mRNA levels were modified by the social environment in *Nlgn3*$^{y/+}$ mice. These findings contribute to the characterisation of the *Nlgn3*$^{y/-}$ mouse model and further highlight the importance of the social environment.

Social paradigms have been widely used to characterise mouse models for psychiatric conditions. However, the social environment can have fundamental consequences on behaviour and physiology (Vargas-Pérez et al. 2009; Van Loo et al. 2003). In order to generalise these observations made in *Nlgn3*$^{y/-}$ mice, we considered testing whether the social environment had effects on the social behaviour of *Cyfip1*$^{+/-}$ mice. However, the phenotypic characterisation of *Cyfip1*$^{+/-}$ mice revealed tube test and courtship vocalisation behaviours similar to wild type control mice (Chapter 4.2).

Social environments are not standardised for experimental mice, which according to the presented results can affect the physiology of mice. Therefore, refined laboratory practice should take the social environment in account by including controls from different housing conditions.

Chapter 9

General discussion

9.1 Summary of results

Taken together, the obtained results showed that *Cyfip1* haploinsufficiency leads to sex-specific defects in motor learning and social behaviour accompanied by alteration of dendritic spine stability, providing new insights to understand the relationship between cellular and behavioural phenotypes in mouse models for ASD.

Adult male *Cyfip1*$^{+/-}$ mice showed a significantly decreased interest in social odours compared to control wild type mice. However, the discrimination of social odours, courtship vocalization and dominance behaviour were comparable between adult *Cyfip1*$^{+/-}$ and wild type male mice. Adult female *Cyfip1*$^{+/-}$ and wild type mice showed similar interest towards social odours but *Cyfip1*$^{+/-}$ and wild type mice did not discriminate social odours. This indicated a male-specific defect in social interest. General locomotor activity, anxiety and repetitive behaviours were comparable between *Cyfip1*$^{+/-}$ and wild type mice. In contrast, motor learning behaviour of adult *Cyfip1*$^{+/-}$ male mice was impaired. On the other hand, adult female *Cyfip1*$^{+/-}$ and wild type mice showed similar motor learning behaviours. Interestingly, earlier in development at P40 male *Cyfip1*$^{+/-}$ mice showed motor learning behaviour similar to age-matched wild type male mice. The motor learning performance of male *Cyfip1*$^{+/-}$ at P40 was higher than the performance of adult *Cyfip1*$^{+/-}$ male mice. Repeated motor training at P40, P50 and P51 increased the motor performance of male *Cyfip1*$^{+/-}$ and wild type mice when the animals were retested at early adulthood (P60). Hence, the adult *Cyfip1*$^{+/-}$ male-specific motor learning deficit is manifested in a critical window at the beginning of adolescence. Intact motor learning earlier in the development of *Cyfip1*$^{+/-}$ mice results in sustained motor ability up to the adult stage. This result also

indicates that the effect of *Cyfip1* haploinsufficiency on motor learning can be partially compensated by training of the mice.

In neurons, we found that the dendritic spine density in the *Cyfip1*$^{+/-}$ primary motor cortex was reduced compared to wild type controls whereas dendritic densities in the V1 area of the visual cortex and in the hippocampal areas CA1 and CA3 were comparable between *Cyfip1*$^{+/-}$ and wild type tissues. Further analysis of the underlying structural plasticity in the motor cortex revealed an increased spine turnover in *Cyfip1*$^{+/-}$ mice compared to wild type controls. In addition, motor learning induced spine formation in *Cyfip1*$^{+/-}$ and wild type. Thus, motor cortical *Cyfip1*$^{+/-}$ neurons have the potential to form new spines but the dendritic spine turnover is increased. In addition, we did not detect any major change in the protein synthesis rate or any defect of association between CYFIP1 and WAVE1, suggesting that the association between CYFIP1 and FMRP or the WAVE regulatory complex are not grossly affected by *Cyfip1* haploinsufficiency.

Interestingly, we found that although *Cyfip1* haploinsufficiency led to a significant reduction of *Cyfip1* mRNA levels in all analysed brain regions, CYFIP1 protein levels were significantly reduced in motor cortex and hippocampus but not in other brain regions and organs at the periphery. These results suggest an uncharacterised post-translational compensation of CYFIP1 protein levels in the motor cortex and hippocampus, through a yet uncharacterized mechanism.

In the following subchapters we discuss the potential molecular mechanisms underlying the neuronal phenotype, its implication in the behaviour phenotype, the impact of this results on the study of ASD and present potential future development of this work.

9.2 Molecular mechanisms underlying dendritic spine instability

In vivo imaging analysis revealed a decreased stability of dendritic spines based on increased spine formation and elimination of motor cortical *Cyfip1*$^{+/-}$ neurons. This finding is consistent with that of Pathania et al. showing that defects of dendritic spine morphology in hippocampal neurons of *Cyfip1*$^{+/-}$ mice. The working model in the following is an attempt to link CYFIP1 associated functions and mechanisms with the dendritic phenotype associated with *Cyfip1* haploinsufficiency (**Figure 9.1**).

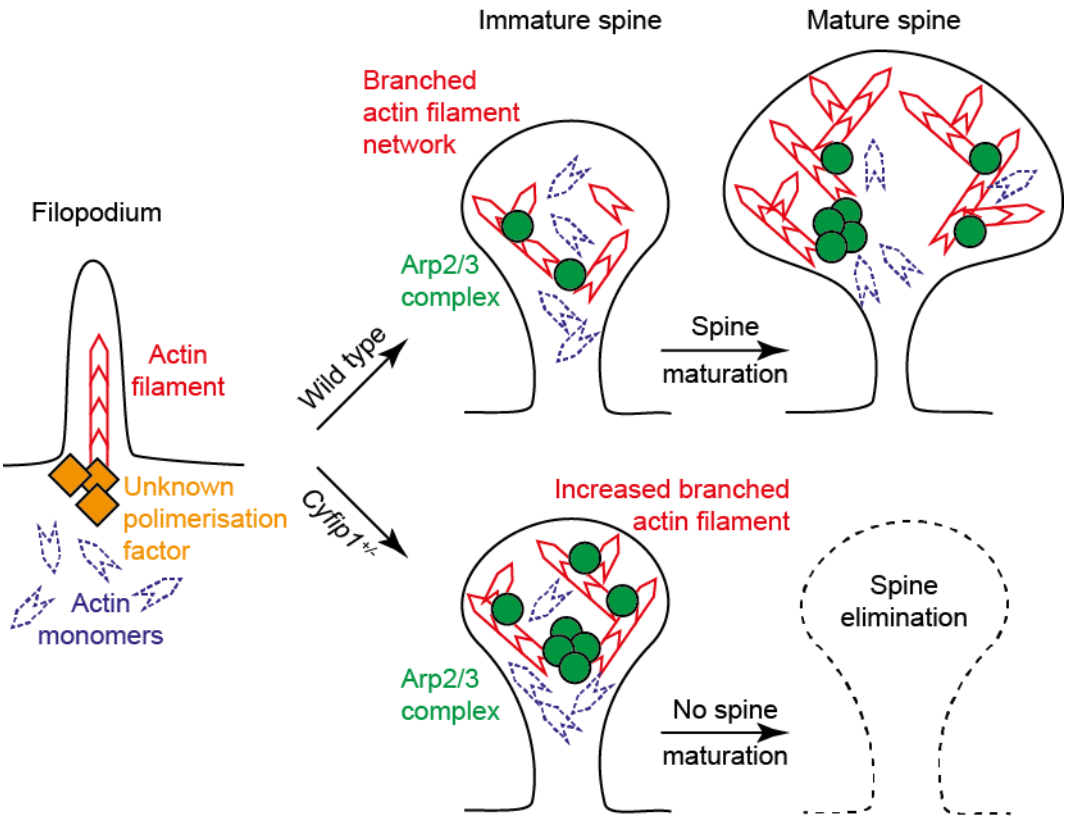

Figure 9.1 Model of defective spine maturation in *Cyfip1*$^{+/-}$ mice.
Filopodium formation occurs independently from Arp2/3 and CYFIP1 whereas the actin network of the immature spine is prematurely stable which prevents further spine maturation.

The Rho family of GTPases comprises different signalling G proteins such as RhoA, Cdc42 and Rac1. Rac1 has numerous downstream effectors but CYFIP1 is exclusively activated by GTP-Rac1 (Kobayashi et al. 1998). CYFIP1 activation downstream of Rac1 abolishes CYFIP1 mediated inhibition of the WAVE regulatory complex. Accordingly, *Cyfip1* deletion or reduced CYFIP1 levels can lead to disinhibition of the WAVE regulatory complex (Chen et al. 2011). Enhanced WRC activity consequently enhances actin nucleation through Arp2/3 (Takenawa & Suetsugu 2007). Increased actin polymerisation can facilitate morphological changes including spine formation (Cingolani & Goda 2008). This mechanism can explain the observed increased dynamics of spine formation and increased number of newly formed spines in *Cyfip1*$^{+/-}$ neurons (Pathania et al. 2014). As illustrated at the presynapse, CYFIP1 controls also protein synthesis and neuronal activity (Hsiao et al. 2016) which might affect formation and stabilisation of *Cyfip1*$^{+/-}$ dendritic spines. Our results from whole tissue lysates did not reveal a gross defect in protein synthesis rate. Nevertheless, technical limitations don`t allow excluding cell-specific changes in protein synthesis, altered rates of local translation or dysregulation of FMRP targets following *Cyfip1* haploinsufficiency.

Histologic analysis revealed a decreased dendritic spine density in the *Cyfip1*$^{+/-}$ motor cortex. Contrasting with this result, hippocampal *Cyfip1*$^{+/-}$ neurons in culture and in histologic preparations show similar spine densities compared to wild type control neurons (Pathania et al. 2014). Importantly, CYFIP protein levels were significantly decreased in these two brain regions. This suggests that depending on the brain region or the cell type, increased spine immaturity can have different consequences on the dendritic spine density. Results obtained from hippocampal neurons in culture suggest that decreased spine stability is largely independent of the physiological context and therefore cell autonomous (Pathania et al. 2014). It would be interesting to determine whether neurons from the motor cortex show a similar phenotype in culture, and in particular if the spine density is affected in these neurons. This would

allow determining if the decreased spine density is a phenotype dependent on the neuronal identity or the physiological context of the brain region.

Interestingly, hippocampal *Cyfip1*$^{+/-}$ neurons were demonstrated to show an altered dendritic spine morphology associated with spine immaturity (Pathania et al. 2014). The authors concluded that heterozygous *Cyfip1* deletion leads to an increased ratio immature over mature dendritic spines whereas the net spine density remains unchanged. Performing structural *in vivo* imaging we found an increased spine turnover in neurons of the *Cyfip1*$^{+/-}$ motor cortex. The increased spine turnover might explain an increased proportion of immature spines. However, the direct link between increased spine turnover in the motor cortex and immaturity related morphology of dendritic spines observed in the hippocampus remains elusive. Structural imaging *in vivo* is restricted to technically accessible brain regions excluding the hippocampus as a compatible structure of interest. Alternatively, classification of morphological spine subtypes in the motor cortex is technically feasible using super-resolution imaging (Wijetunge et al. 2014) but such experiments were not done.

Structural *in vivo* imaging revealed that cortical *Cyfip1*$^{+/-}$ neurons form new spines but yet show a decreased spine density. This suggests that actin filament nucleation for the formation of new filopodia is intact in *Cyfip1*$^{+/-}$ mice whereas spine stability is altered. Filopodia formation requires unbranched actin filaments which are nucleated by mammalian Diaphanous-related (mDia) formins (Hotulainen et al. 2009). On the other hand, networks of branched actin stabilise spines and promote spine growth downstream of Arp2/3. (Wegner et al. 2008; Hotulainen et al. 2009). Hence, the maturation of a filopodium to mature spine goes through a transition from mDia to Arp2/3 mediated actin nucleation. This indicates that filopodium formation is independent of Arp2/3 and its upstream regulator CYFIP1. However, Arp2/3 is crucial for the formation of branched actin filaments. Since CYFIP1 regulates Arp2/3 activity we propose that later stages of spine formation are affected in *Cyfip1*$^{+/-}$ spines. The loss of Arp2/3 inhibition in *Cyfip1*$^{+/-}$ spines leads to an increased network of branched

actin. This may lead to a premature increase in spine stability which in turn may compromise structural plasticity required for further maturation. This mechanism can interfere with spine maturation and could lead to spine elimination.

In addition, presynaptic functions such as neuronal activity or bouton formation in *Cyfip1*$^{+/-}$ mice might also contribute to the increased spine instability (Bury & Sabo 2015; Rust & Maritzen 2015; Hsiao et al. 2016). Moreover, *Cyfip1* is expressed in non-neuronal cells and possibly in microglia (Kobayashi et al. 1998; Davenport et al. 2018). Microglia are involved in synaptic pruning which is important for the control of synaptic maturation (Paolicelli et al. 2011). Microglial activity and control of spine elimination might be altered in *Cyfip1*$^{+/-}$ mice. Increased synaptic pruning may allow filopodia formation but would eliminate dendritic spines explaining the decreased spine density. Neuronal activity can promote microglial activity (Hung et al. 2010) which might lead to brain region-specific spine elimination.

9.3 Dendritic spines and motor learning

Motor learning was demonstrated to mediate structural plasticity in wild type mice. Rotarod training induced a 2.61 fold increase in spine formation whereas spine elimination remained unchanged. We replicated the increase in dendritic spine formation in layer V neurons and validated our experimental design combining the motor learning paradigm with structural *in vivo* imaging of dendritic plasticity. More specifically, we found a significant 3.73 fold increase in spine formation and no significant effect on spine elimination in adult *Cyfip1*$^{+/+}$*Thy1EGFP* male mice, comparable to the reported 2.61 fold increase found by (Yang et al. 2009). In their studies, Yang et al reported that stably maintained dendritic spines are associated with lifelong memories. This finding may implicate that motor learning is dependent

on the formation of new dendritic spines. *Cyfip1*$^{+/-}$ male mice show an absence in motor learning and so we thought to address this question and hypothesised that the absence of motor learning found in *Cyfip1*$^{+/-}$ mice would be associated with an absence of dendritic spine formation. We found that dendritic spine formation was significantly increased where dendritic spine elimination was unchanged in rotarod trained adult *Cyfip1*$^{+/-}$*Thy1EGFP* mice. This observation indicates that formation of dendritic spines in layer V neurons can still occur in mice showing an absence of motor learning on the rotarod. The molecular and cellular events triggering dendritic spine formation upon rotarod training in the motor cortex of *Cyfip1*$^{+/-}$ mice remain unknown. Nevertheless, these results lead us to speculate that the increased *Cyfip1*$^{+/-}$ spine turnover at baseline could lead to the motor learning impairment. The spine turnover at baseline could have consequences on the neuronal circuitry. Changes in the circuitry could result in an altered behavioural output.

This result has important consequences for the design of therapeutic strategies. The objective of a treatment would be to stabilise spines and not to promote their formation. Interestingly, female mice and young mice do not show such behavioural phenotype. The comparison of the cellular and molecular mechanisms controlled by *Cyfip1* over the development between females to the males could lead to a better understanding of the defective mechanism to be targeted. Motor learning in wild type mice has been associated with neuronal activity (Costa et al. 2004). Therefore, investigating the neuronal activity phenotype of *Cyfip1*$^{+/-}$ associated with motor learning would lead to a broader view on the *Cyfip1*$^{+/-}$ pathophysiology. Since motor training during the development improved the behavioural performance in adult *Cyfip1*$^{+/-}$ mice it would be interesting to test whether physical motor training could be mimicked by neuronal stimulation of the motor cortex. The effect of transcranial current stimulation (tDCS) on the *Cyfip1*$^{+/-}$ and wild type motor cortex could be investigated as well as the consequences on motor learning behaviour (Pedron et al. 2014; Waters et al. 2017). In addition, the integration of neuronal activity across the

neuronal network is determined by structural connectivity (Roudi et al. 2015; Ocker et al. 2017; Peters et al. 2017). Thus, structural connectivity alterations could be involved in the observed motor learning deficit. To address this possibility diffusor tensor imaging (DTI) (Wu et al. 2013) could be performed on *Cyfip1*$^{+/-}$ and wild type mice.

Insights on neuronal activity and connectivity by methods such as tDCS and DTI in a mouse model of *Cyfip1* deletion might be very valuable since the techniques are translationally applicable to human.

9.4 The necessity to better understand the function of *Cyfip1* in neurons

The mouse model for *Cyfip1* deletion used for the presented experiments is based on heterozygous deletion of *Cyfip1*. This genetic construct gives rise to reduced but not fully abolished *Cyfip1* expression. The remaining monoallelic *Cyfip1* expression can still contribute to physiologic CYFIP1 functions. Thus, CYFIP1 functions might not be compromised in the model for *Cyfip1* haploinsufficiency. In addition, the assessment of CYFIP1 protein levels in *Cyfip1*$^{+/-}$ mice revealed in some brain tissues CYFIP1 protein levels similar to levels found in wild type controls. *Cyfip1* mRNA levels were decreased by 50% reflecting the heterozygous deletion. These observations lead to the conclusion of a post-transcriptional compensation of CYFIP1 protein levels. As a result, CYFIP1 functions in *Cyfip1*$^{+/-}$ mice can still occur similar to the wild type condition due to monoallelic *Cyfip1* expression and compensation of CYFIP1 protein levels. Thus, the detection of pathological features of the *Cyfip1*$^{+/-}$ mouse model relies on the threshold of *Cyfip1* mRNA and CYFIP1 protein levels required for biological function. A complete knockout of *Cyfip1* would be preferred but the homozygous

Cyfip1 deletion was reported to be embryonically lethal in the mouse (Bozdagi et al. 2012; Pathania et al. 2014) and fly (Schenck et al. 2003; Zhao et al. 2013). A conditional *Cyfip1* knockout could circumvent early embryonic lethality and the limitations of a heterozygous mouse model. However, it remains to be tested which cell types are viable upon homozygous *Cyfip1* deletion and whether these cells underlie a critical developmental window for *Cyfip1* expression. Such a characterisation by itself would contribute to a better understanding of cell type-specific CYFIP1 functions.

Concerning the main findings described here, a conditional knockout of *Cyfip1* would be beneficial to strengthen the correlation between cellular and behavioural *Cyfip1*$^{+/-}$ phenotypes. Increased dendritic spine turnover in a population of motor cortical neurons associated with motor learning was correlated with motor learning impairment in adult *Cyfip1*$^{+/-}$ mice. A selective *Cyfip1* knockout specific for layer V neurons in the motor cortex would allow demonstrating causality between *Cyfip1* loss in these particular cells, increased dendritic spine turnover and defective motor learning behaviour.

The *Cyfip1*$^{+/-}$ mice used for the presented experiments were generated using a knockout first allele (Skarnes et al. 2013). This construct has the potential to be turned into a floxed allele upon flippase recombination and subsequent manipulation by Cre recombination would generate a conditional knockout allele for *Cyfip1*. Using this strategy a conditional *Cyfip1* knockout mouse line with a specific *Cyfip1* loss in excitatory neurons of the neocortex and hippocampus has been recently generated (Davenport et al. 2018). However, time constraints limited the generation of a conditional *Cyfip1* knockout mutant to further investigate the relationship between increased dendritic spine turnover and phenotypic motor learning behaviour.

9.5 Future directions

Studies in humans and mouse models have begun to explore the heterogeneity of ASD and identified convergent pathophysiological mechanisms, in particular deficits in structural and functional plasticity of dendritic spines, the postsynaptic structures docking most excitatory synapses. Analyses of post-mortem tissue of individuals with idiopathic ASD have shown higher-than-normal spine densities on the apical dendrites of layer II pyramidal neurons in frontal, parietal and temporal tissue (Hutsler & Zhang 2010; Tang et al. 2014). By contrast, decreased dendritic spine density has been consistently reported in human cortical tissue from individuals affected by monogenic disorders comorbid with autism, including Fragile-X (Rudelli et al. 1985; Hinton et al. 1991; Irwin et al. 2001), Angelman (Jay et al. 1991), and Rett's syndromes (Belichenko et al. 1994; Kaufmann et al. 1997; Chapleau et al. 2009) (for comprehensive review see Phillips and Miller (Phillips & Pozzo-Miller 2014)). The main finding of the behavioural characterisation of *Cyfip1*$^{+/-}$ mice was a motor learning impairment specific to adult male mice. Investigating the pathophysiology underlying the phenotypic *Cyfip1*$^{+/-}$ motor learning behaviour we observed an increased spine formation in described cellular correlates for motor learning (Yang et al. 2009). The correlation between aberrant structural plasticity phenotype and defective motor learning is an interesting starting point for further dissection of *Cyfip1* function and the pathophysiologic consequences upon *Cyfip1* deletion. CYFIP1 interacts at the synapse with Neuroligin-3, which has been associated with ASD. In addition, behavioural *Cyfip1*$^{+/-}$ phenotypes were male-specific in analogy to higher ASD prevalence in male individuals that in female individuals. Interestingly, motor deficits are comorbid symptoms of ASD (Moraes et al. 2017; Colombo-Dougovito & Reeve 2017).

The *Cyfip1*$^{+/-}$ male-specific motor learning deficit was instructive for the subsequent assessment for potential mechanisms contributing towards the altered behavioural output. Following this top-down approach, an increased spine turnover was identified in a cell type associated with motor learning. The correlation between motor learning deficit and increased spine turn over described here in male *Cyfip1*$^{+/-}$ mice raises the question of causality. Motor learning behaviour in adult female mice was not affected by the heterozygous loss of *Cyfip1*. Therefore, assessing the structural plasticity of dendritic spines in *Cyfip1*$^{+/-}$ and wild type female mice would help to evaluate the causality between altered structural plasticity and motor learning phenotype described here. Overcoming technical limitations, a mouse line with *Cyfip1* deletion from layer V neurons associated with motor learning would serve as a powerful model to assess the relationship between structural plastic and behavioural consequences. Unlike female *Cyfip1*$^{+/-}$ mice as a model, a cell type-selective *Cyfip1* deletion model would allow to cell-autonomous effects of structural plasticity on the behaviour isolated from potential effects of *Cyfip1* deletion on other cell types and neuronal circuits. This line of experiments would further outline the contribution of dendritic structural plasticity towards the motor learning behaviour.

Protein synthesis rates obtained from *Cyfip1*$^{+/-}$ and wild type mice were similar overall. Nevertheless, effects of *Cyfip1* haploinsufficiency on mRNA translation might occur in a confined manner. Increased dendritic spine formation over would suggest a higher demand of newly synthesised proteins in accordance with strong evidence associating protein synthesis and synaptic plasticity (Zukin et al. 2009). Therefore, the interest of the *Cyfip1* field of research in mRNA translation could be followed up by assessing the local mRNA translation in the identified layer V neurons showing increased spine turnover. Techniques involving *in vivo* labelling of newly synthesised proteins and quantification from histological slices (Hinz et al. 2013) would permit a refined characterisation of protein synthesis related CYFIP1 function.

9.6 Concluding remarks

Most insights into the function of *Cyfip1* and consequences upon its deletion originate from studies focussing on cellular aspect. The work presented here contributes to the characterisation of phenotypic behaviours of the *Cyfip1*$^{+/-}$ mice and the evaluation of the underlying pathophysiology *in vivo*.

The behavioural phenotype of *Cyfip1*$^{+/-}$ mouse model was characterised, including social behaviours. The assessment of social behaviours in *Cyfip1*$^{+/-}$ mice is an important aspect considering the association of *CYFIP1* with ASD in human (Nishimura et al. 2007; Van Der Zwaag et al. 2010; Leblond et al. 2012; Pinto et al. 2014). A phenotypic motor learning impairment in male *Cyfip1*$^{+/-}$ mice was identified and potential pathophysiologic mechanisms were evaluated. Importantly the identified phenotypic behaviour is reminiscent to symptoms comorbid to ASD (Moraes et al. 2017). This finding can be instructive for the clinical assessment of genetic predispositions with regards to *CYFIP1* deletion given that aspects of neuronal activity and connectivity can be translational.

Moreover, using a *Nlgn3*$^{y/-}$ mouse line as a model for social submission the fundamental effect the social environment on the behaviour and physiology on other mice within the same environment was demonstrated.

Bibliography

Aakalu, G. et al., 2001. Dynamic visualization of local protein synthesis in hippocampal neurons. *Neuron*, 30, pp.489–502.

Abekhoukh, S. & Bardoni, B., 2014. CYFIP family proteins between autism and intellectual disability: links with Fragile X syndrome. *Frontiers in Cellular Neuroscience*, 8(March), pp.1–9.

Allison, D.W. et al., 1998. Role of Actin in Anchoring Postsynaptic Receptors in Cultured Hippocampal Neurons: Differential Attachment of NMDA versus AMPA Receptors. *J. Neurosci.*, 18(7), pp.2423–2436.

Amos-Landgraf, J.M. et al., 1999. Chromosome breakage in the Prader-Willi and Angelman syndromes involves recombination between large, transcribed repeats at proximal and distal breakpoints. *American journal of human genetics*, 65(2), pp.370–86.

Antharavally, B.S. et al., 2004. A high-affinity reversible protein stain for Western blots. *Analytical Biochemistry*, 329(2), pp.276–280.

Arbuckle, E.P. et al., 2015. Testing for odor discrimination and habituation in mice. *Journal of visualized experiments*, (May), pp.1–7.

Ashley, C.T. et al., 1993. FMR1 protein: conserved RNP family domains and selective RNA binding. *Science (New York, N.Y.)*, 262(5133), pp.563–566.

Barbacid, M., 1994. The Trk family of neurotrophin receptors. *Journal of Neurobiology*, 25(11), pp.1386–1403.

Bassell, G.J. & Warren, S.T., 2008. Fragile X Syndrome: Loss of Local mRNA Regulation Alters Synaptic Development and Function. *Neuron*, 60(2), pp.201–214.

Baudouin, S.J. et al., 2012. Shared synaptic pathophysiology in syndromic and nonsyndromic rodent models of autism. *Science (New York, N.Y.)*, 338(6103), pp.128–32.

Beggs, J.E. et al., 2015. The MAP kinase-interacting kinases regulate cell migration, vimentin expression and eIF4E/CYFIP1 binding. *Biochem. J*, 467, pp.63–76.

Belichenko, P. V et al., 1994. Rett syndrome: 3-D confocal microscopy of cortical pyramidal dendrites and afferents. *Neuroreport: An International Journal for the Rapid Communication of Research in Neuroscience*, 5(12), pp.1509–1513.

Benítez-Burraco, A. et al., 2017. Variable Penetrance of the 15q11.2 BP1-BP2 Microduplication in a Family with Cognitive and Language Impairment. *Molecular Syndromology*, 8(3), pp.139–147.

Bittel, D.C., Kibiryeva, N. & Butler, M.G., 2006. Expression of 4 genes between chromosome 15 breakpoints 1 and 2 and behavioral outcomes in Prader-Willi syndrome. *Pediatrics*, 118(4), pp.1276–1283.

Bothwell, S. et al., 2001. Neuronal hypertrophy in the neocortex of patients with temporal lobe epilepsy. *The Journal of Neuroscience*, 21(13), pp.4789–800.

Bozdagi, O. et al., 2012. Haploinsufficiency of Cyfip1 produces fragile X-like phenotypes in mice. *PLoS ONE*, 7(8).

Broekkamp, C.L. et al., 1986. Major tranquillizers can be distinguished from minor tranquillizers on the basis of effects on marble burying and swim-induced grooming in mice. *European Journal of Pharmacology*, 126(3), pp.223–229.

Brooks, S.P. & Dunnett, S.B., 2009. Tests to assess motor phenotype in mice: A user's guide. *Nature Reviews Neuroscience*, 10(7), pp.519–529.

Brown, V. et al., 2001. Microarray identification of FMRP-associated brain mRNAs and altered mRNA translational profiles in fragile X syndrome. *Cell*, 107(4),

pp.477–487.

Browne, C.E. et al., 1997. Inherited Interstitial Duplications of Proximal 15q: Genotype-Phenotype Correlations. *The American Journal of Human Genetics*, 61(6), pp.1342–1352.

Burnside, R.D. et al., 2011. Microdeletion/microduplication of proximal 15q11.2 between BP1 and BP2: A susceptibility region for neurological dysfunction including developmental and language delay. *Human Genetics*, 130(4), pp.517–528.

Bury, L.A.D. & Sabo, S.L., 2015. Building a terminal: mechanisms of presynaptic development in the CNS. *The Neuroscientist*, pp.1–20.

Butler, M.G. et al., 2008. Array comparative genomic hybridization (aCGH) analysis in Prader-Willi syndrome. *American Journal of Medical Genetics, Part A*, 146(7), pp.854–860.

Butler, M.G. et al., 2004. Behavioral differences among subjects with Prader-Willi syndrome and type I or type II deletion and maternal disomy. *Pediatrics*, 113(3), pp.565–573.

Caligioni, C.S., 2009. Assessing reproductive status/stages in mice. *Curr Protoc Neurosci*, p.Appendix 4:Appendix 4I.

Catalanotto, C., Cogoni, C. & Zardo, G., 2016. MicroRNA in control of gene expression: an overview of nuclear functions. *International Journal of Molecular Sciences*, 17(1712).

Chai, J.-H. et al., 2003. Identification of four highly conserved Genes between breakpoint hotspots BP1 and BP2 of the Prader-Willi/Angelman syndromes deletion region that have undergone evolutionary transposition mediated by flanking duplicons. *The American Journal of Human Genetics*, 73(4), pp.898–

925.

Chapleau, C.A. et al., 2009. Modulation of dendritic spine development and plasticity by BDNF and vesicular trafficking: Fundamental roles in neurodevelopmental disorders associated with mental retardation and autism. *Journal of Neurodevelopmental Disorders*, 1(3), pp.185–196.

Che, E. et al., 2015. Fragile X Mental Retardation Protein Regulates Translation by Binding Directly to the Ribosome. *Molecular cell*, 54(3), pp.407–417.

Chen, B. et al., 2014. The WAVE regulatory complex links diverse receptors to the actin cytoskeleton. *Cell*, 16(156), pp.195–207.

Chen, Z. et al., 2010. Structure and control of the actin regulatory WAVE complex. *Nature*, 468(7323), pp.533–538.

Chen, Z. et al., 2011. Structure and control of the actin regulatory WAVE complex. , 468(7323), pp.533–538.

Christensen, D.L. et al., 2016. Prevalence and characteristics of autism spectrum disorder among 4-year-old children in the autism and developmental disabilities monitoring network. *Journal of Developmental Behavior Pediatrics*, 037(1), pp.1–8.

Chung, L. et al., 2015. Parental origin impairment of synaptic functions and behaviors in cytoplasmic FMRP interacting protein 1 (Cyfip1) deficient mice. *Brain Research*, 1629, pp.340–350.

Cingolani, L.A. & Goda, Y., 2008. Actin in action: The interplay between the actin cytoskeleton and synaptic efficacy. *Nature Reviews Neuroscience*, 9(5), pp.344–356.

Cioni, J.M. et al., 2018. Axon-Axon Interactions Regulate Topographic Optic Tract Sorting via CYFIP2-Dependent WAVE Complex Function. *Neuron*, 97(5),

p.1078–1093.e6.

Colombo-Dougovito, A.M. & Reeve, R.E., 2017. Exploring the Interaction of Motor and Social Skills With Autism Severity Using the SFARI Dataset. *Perceptual and Motor Skills*, 124(2), pp.413–424.

Cory, G.O.C. & Ridley, A.J., 2002. Braking WAVEs. *Nature*, 418(August), pp.732–734.

Costa, R.M., Cohen, D. & Nicolesis, M.A.L., 2004. Differential Corticostriatal Plasticity during Fast and Slow Motor Skill Learning in Mice Rui. *Current Biology*, 14, pp.1124–1134.

Cox, D. & Butler, M., 2015. The 15q11.2 BP1–BP2 Microdeletion Syndrome: A Review. *International Journal of Molecular Sciences*, 16(2), pp.4068–4082.

Dai, Z. & Pendergast, A.M., 1995. Abi-2, a novel SH3-containing protein interacts with the c-Abl tyrosine kinase and modulates c-Abl transforming activity. *Genes and Development*, 9(21), pp.2569–2582.

Darnell, J.C. et al., 2011. FMRP stalls ribosomal translocation on mRNAs linked to synaptic function and autism. *Cell*, 146(2), pp.247–261.

Davenport, E.C. et al., 2018. Correct CYFIP1 dosage is essential for synaptic inhibition and the excitatory / inhibitory balance. *bioRxiv*.

Debaere, F. et al., 2004. Changes in brain activation during the acquisition of a new bimanual coodination task. *Neuropsychologia*, 42(7), pp.855–67.

Eden, S. et al., 2002. Mechanism of regulation of WAVE1-induced actin nucleation by Rac1 and Nck. *Nature*, 418(6899), pp.790–793.

Fabian, M.R., Sonenberg, N. & Filipowicz, W., 2018. Regulation of mRNA translation and stability by microRNAs. *Annual Review of Biochemistry*, 79, pp.351–79.

Faul, F. et al., 2007. G * Power 3 : A flexible statistical power analysis program for the social , behavioral , and biomedical sciences. *Behaviour Research Methods*, 39(2), pp.175–191.

Ferkin, M.H. & Li, H.Z., 2005. A battery of olfactory-based screens for phenotyping the social and sexual behaviors of mice. *Physiology and behavior*, 85, pp.489–499.

Fischer, J. & Hammerschmidt, K., 2011. Ultrasonic vocalizations in mouse models for speech and socio-cognitive disorders: insights into the evolution of vocal communication. *Genes, brain, and behavior*, 10(1), pp.17–27.

Föcking, M. et al., 2015. Proteomic and genomic evidence implicates the postsynaptic density in schizophrenia. *Molecular Psychiatry*, 20(4), pp.424–432.

Forrest, M.P., Parnell, E. & Penzes, P., 2018. Dendritic structural plasticity and neuropsychiatric disease. *Nature Reviews Neuroscience*, 19(4), pp.215–234.

Gandolfo, F. et al., 2000. Cortical correlates of learning in monkeys adapting to a new dynamical environment. *Proceedings of the National Academy of Sciences*, 97(5), pp.2259–2263.

Genheden, M. et al., 2015. BDNF Stimulation of Protein Synthesis in Cortical Neurons Requires the MAP Kinase-Interacting Kinase MNK1. *Journal of Neuroscience*, 35(3), pp.972–984.

Glausier, J.R. & Lewis, D.A., 2013. Dendritic spine pathology in schizophrenia. *Neuroscience*, 251, pp.90–107.

Glock, C., Heumüller, M. & Schuman, E.M., 2017. mRNA transport & local translation in neurons. *Current Opinion in Neurobiology*, 45, pp.169–177.

Goldey, G.J. et al., 2014. Removable cranial windows for long-term imaging in awake mice. *Nature Protocols*, 9(11), pp.2515–2538.

Goley, E.D. et al., 2004. Critical conformational changes in the Arp2/3 complex are induced by nucleotide and nucleation promoting factor. *Molecular Cell*, 16(2), pp.269–279.

Gomez, T.M. & Letourneau, P.C., 2014. Actin Dynamics in Growth Cone Motility and Navigation. *J Neurochem*, 129(2), pp.221–234.

Goytain, A. et al., 2007. NIPA1(SPG6), the basis for autosomal dominant form of hereditary spastic paraplegia, encodes a functional Mg2+transporter. *Journal of Biological Chemistry*, 282(11), pp.8060–8068.

Guizar-Sicairos, M., Thurman, S.T. & Fienup, J.R., 2008. Efficient subpixel image registration algorithms. *Optics Letters*, 33(2), p.156.

Guo, H. et al., 2015. Social dominance-related major urinary proteins and the regulatory mechanism in mice. *Integrative Zoology*, 10(6), pp.543–554.

Hall, A., 1998. Rho GTPases and the Actin Cytoskeleton. , 509(1998).

Hall, C.S., 1934. Emotional behavior in the rat: defecation and urination as measures of individual differences in emotionality. *J. Comp. Psychol.*, 18, pp.385–403.

Halpain, S., 2000. Actin and the agile spine: How and why do dendritic spines dance? *Trends in Neurosciences*, 23(4), pp.141–146.

Han, K. et al., 2014. Fragile X-like behaviors and abnormal cortical dendritic spines in Cytoplasmic FMR1-interacting protein 2-mutant mice. *Human Molecular Genetics*, 24(7), pp.1813–1823.

Hinton, V.J. et al., 1991. Analysis of neocortex in three males with the fragile X syndrome. *American Journal of Medical Genetics*, 41(3), pp.289–94.

Hinz, F.I., Dieterich, D.C. & Schuman, E.M., 2013. Teaching old NCATs new tricks: Using non-canonical amino acid tagging to study neuronal plasticity. *Current*

Opinion in Chemical Biology, 17(5), pp.738–746.

Holy, T.E. & Guo, Z., 2005. Ultrasonic songs of male mice. *PLoS biology*, 3(12), p.e386.

Hotulainen, P. et al., 2009. Defning mechanisms of actin polymerization and depolymerization during Dendritic spine morphogenesis. *Journal of Cell Biology*, 185(2), pp.323–339.

Hsiao, K. et al., 2016. Cyfip1 Regulates Presynaptic Activity during Development. *Journal of Neuroscience*, 36(5), pp.1564–1576.

Hung, J. et al., 2010. Activation of microglia by neuronal activity: Results from a new in vitro paradigm based on neuronal-silicon interfacing technology. *Brain, Behavior, and Immunity*, 24(1), pp.31–40.

Hutsler, J.J. & Zhang, H., 2010. Increased dendritic spine densities on cortical projection neurons in autism spectrum disorders. *Brain Research*, 1309, pp.83–94.

Irwin, S.A. et al., 2001. Abnormal dendritic spine characteristics in the temporal and visual cortices of patients with fragile-X syndrome: a quantitative examination. *American Journal of Medical Genetics*, 98(2), pp.161–7.

Ismail, A.M. et al., 2009. The WAVE regulatory complex is inhibited. *Nature Structural and Molecular Biology*, 16(5), pp.561–563.

Jackson, R.S. et al., 2007. CYFIP2, a direct p53 target, is leptomycin-B sensitive. *Cell Cycle*, 6(1), pp.95–103.

Jamain, S. et al., 2003. Mutations of the X-linked genes encoding neuroligins NLGN3 and NLGN4 are associated with autism. *Nature Genetics*, 34(1), pp.27–29.

Jay, V. et al., 1991. Puppet-like syndrome of Angelman: a pathologic and

neurochemical study. *Neurology*, 41(3), pp.416–22.

Jenkins, I.H. et al., 1994. Motor sequence learning: a study with positron emission tomography. *J Neurosci*, 14(June), pp.3775–3790.

Jiao, S. et al., 2017. Inhibition of CYFIP2 promotes gastric cancer cell proliferation and chemoresistance to 5-fluorouracil through activation of the Akt signaling pathway. *Oncology Letters*, 13(4), pp.2133–2140.

Joshi, B. et al., 1995. Phosphorylation of eukaryotic protein synthesis initiation factor 4E at Ser-209. *Journal of Biochemical Chemistry*, 270(24), pp.14597–603.

Kalbassi, S. et al., 2017. Male and Female Mice Lacking Neuroligin-3 Modify the Behavior of Their Wild-Type Littermates. *Eneuro*, 4(4), p.ENEURO.0145-17.2017.

Kanai, Y., Dohmae, N. & Hirokawa, N., 2004. Kinesin transports RNA: Isolation and characterization of an RNA-transporting granule. *Neuron*, 43(4), pp.513–525.

Karni, A. et al., 1995. Functional Mri Evidence for Adult Motor Cortex Plasticity During Motor Skill Learning. *Nature*, 377(6545), pp.155–158.

Kaufmann, W. et al., 1997. Abnormalities in neuronal maturation in Rett syndrome neocortex: preliminary molecular correlates. *European child & adolescent psychiatry*, (6), p.Suppl 1:75-7.

Kim, I.H. et al., 2013. Disruption of Arp2/3 Results in Asymmetric Structural Plasticity of Dendritic Spines and Progressive Synaptic and Behavioral Abnormalities. *Journal of Neuroscience*, 33(14), pp.6081–6092.

Kirov, G. et al., 2009. Support for the involvement of large copy number variants in the pathogenesis of schizophrenia. *Human Molecular Genetics*, 18(8), pp.1497–1503.

Kleijn, M. et al., 1998. Regulation of translation initiation factors by signal transduction. *Eur J Biochem*, 253(3), pp.531–544.

Kobayashi, K. et al., 1998. p140Sra-1 (specifically Rac1-associated protein) is a novel specific target for Rac1 small GTPase. *Journal of Biological Chemistry*, 273(1), pp.291–295.

Köster, F. et al., 1998. Identification of shyc, a novel gene expressed in the murine developing and adult nervous system. *Neuroscience Letters*, 252(1), pp.69–71.

Kunda, P. et al., 2003. Abi, Sra1, and Kette Control the Stability and Localization of SCAR/WAVE to Regulate the Formation of Actin-Based Protrusions. *Current Biology*, 13(21), pp.1867–1875.

Lamphear, B.J. & Panniers, R., 1989. Cap binding protein complex that restores protein synthesis in heat-shocked ehrlich cell lysates contains highly phosphorylated eIF-4E. *Journal of Biochemical Chemistry*, 265, pp.5333–5337.

Leblond, C.S. et al., 2012. Genetic and functional analyses of SHANK2 mutations suggest a multiple hit model of autism spectrum disorders. *PLoS Genetics*, 8(2).

Lee, Y. et al., 2017. Phosphorylation of CYFIP2, a component of the WAVE-regulatory complex, regulates dendritic spine density and neurite outgrowth in cultured hippocampal neurons potentially by affecting the complex assembly. *NeuroReport*, 28(12), pp.749–754.

Levy, D. et al., 2011. Rare De Novo and Transmitted Copy-Number Variation in Autistic Spectrum Disorders. *Neuron*, 70(5), pp.886–897.

Lindzey, G., Winston, H. & Manosevitz, M., 1961. Social dominance in inbred mouse strains. *Nature*, 191, pp.474–476.

Liu, J. et al., 2012. Imaging protein synthesis in cells and tissues with an alkyne analog of puromycin. *Proceedings of the National Academy of Sciences*, 109(2),

pp.413–418.

Lonstein, J.S. & De Vries, G.J., 2000. Sex differences in the parental behavior of rodents. *Neuroscience & Biobehavioral Reviews*, 24(6), pp.669–686.

Van Loo, P.L.P., Van Zutphen, L.F.M. & Baumans, V., 2003. Male management: Coping with aggression problems in male laboratory mice. *Laboratory Animals*, 37(4), pp.300–313.

Luo, L. et al., 1996. Differential effects of the Rac GTPase on Purkinje cell axons and dendritic trunks and spines. *Nature*, 379(6568), pp.837–840.

Lüscher, B., Fuchs, T. & Kilpatrick, C.L., 2011. GABAAReceptor Trafficking-Mediated Plasticity of Inhibitory Synapses. *Neuron*, 70(3), pp.385–409.

Madrigal, I. et al., 2012. 15q11.2 microdeletion and FMR1 premutation in a family with intellectual disabilities and autism. *Gene*, 508(1), pp.92–95.

Marchand, J.B. et al., 2001. Interaction of WASP/Scar proteins with actin and vertebrate Arp2/3 complex. *Nature Cell Biology*, 3(1), pp.76–82.

Marsden, K.C. et al., 2018. A Cyfip2-Dependent Excitatory Interneuron Pathway Establishes the Innate Startle Threshold. *Cell Reports*, 23(3), pp.878–887.

Martin, K.C., Barad, M. & Kandel, E.R., 2000. Local protein synthesis and its role in synapse-specific plasticity. *Current Opinion in Neurobiology*, 10(5), pp.587–592.

Masland, R.H., 2004. Neuronal cell types. *Current Biology*, 14(13), pp.497–500.

Matus, a et al., 1982. High actin concentrations in brain dendritic spines and postsynaptic densities. *Proceedings of the National Academy of Sciences of the United States of America*, 79(23), pp.7590–7594.

Matus, A. et al., 2000. Actin-Based Plasticity in Dendritic Spines. *Source: Science, New Series Exp. Cell Res. Suppl. Science Nature Neurosci. Cell Science*

ScienceJ. Biot. Chem. Curr. Opin. Neurobiol. F. A. Edwards Physiol. Rev. Nature Neurosci. Trends Neurosci. Curr. Opin. Neurobiol, 290(6), pp.754–758.

Michalon, A. et al., 2012. Chronic Pharmacological mGlu5 Inhibition Corrects Fragile X in Adult Mice. *Neuron*, 74(1), pp.49–56.

Mihalick, S.M. et al., 2000. An olfactory discrimination procedure for mice. *Journal of the experimental analysis of behavior*, 3(3), pp.305–318.

Milner, K.M. et al., 2005. Prader-Willi syndrome: Intellectual abilities and behavioural features by genetic subtype. *Journal of Child Psychology and Psychiatry and Allied Disciplines*, 46(10), pp.1089–1096.

Moraes, Í.A.P. de et al., 2017. Motor learning characterization in people with autism spectrum disorder: A systematic review. *Dementia & Neuropsychologia*, 11(3), pp.276–286.

Moy, S.S. et al., 2004. Sociability and preference for social novelty in five inbred strains : an approach to assess autistic-like behavior in mice. *Genes, Brain and Behavior*, 3, pp.287–302.

Murphy, S.M. et al., 2001. GCP5 and GCP6: two new members of the human gamma-tubulin complex. *Molecular biology of the cell*, 12(11), pp.3340–52.

Nagase, Y. et al., 1995. Prediction of the coding sequences of unidentified human genes. IV. The coding sequences of 40 new genes (KIAA0121-KIAA1060) deducted by analysis of cDNA clones from the human cell line KG-1. *DNA Res.*, 2(January), pp.199–210.

Nakai, N. et al., 2018. Common defects of spine dynamics and circuit function in neurodevelopmental disorders: a systematic review of findings from in vivo optical imaging of mouse models. *Frontiers in Neuroscience*, 12(June), pp.1–18.

Nakao, S. et al., 2008. Contact-dependent promotion of cell migration by the OL-

protocadherin-Nap1 interaction. *Journal of Cell Biology*, 182(2), pp.395–410.

Nakashima, M. et al., 2018. De novo hotspot variants in CYFIP2 cause early-onset epileptic encephalopathy. *Annals of Neurology*, 83(4), pp.794–806.

Nakayama, a Y., Harms, M.B. & Luo, L., 2000. Small GTPases Rac and Rho in the maintenance of dendritic spines and branches in hippocampal pyramidal neurons. *The Journal of neuroscience : the official journal of the Society for Neuroscience*, 20(14), pp.5329–38.

Napoli, I. et al., 2008. The Fragile X Syndrome Protein Represses Activity-Dependent Translation through CYFIP1, a New 4E-BP. *Cell*, 134(6), pp.1042–1054.

Nathans, D., 1964. Puromcyin inhibion of protein synthesis: incorporation of puromycin into peptide chains. *Pnas*, 51(1963), pp.585–592.

Nicholls, R.D. & Knepper, J.L., 2001. Genome organisation, function, and imprinting in Prader-Willi and Angelman syndromes. *Annual review of human genetics*.

Nishimura, Y. et al., 2007. Genome-wide expression profiling of lymphoblastoid cell lines distinguishes different forms of autism and reveals shared pathways. *Human Molecular Genetics*, 16(14), pp.1682–1698.

Nishiyama, T. et al., 1994. rac p21 is involved in insulin-induced membrane ruffling and rho p21 is involved in hepatocyte growth factor- and 12-O-tetradecanoylphorbol-13-acetate (TPA)-induced membrane ruffling in KB cells. *Mol.Cell Biol.*, 14(4), pp.2447–2456.

Noroozi, R. et al., 2018. Cytoplasmic FMRP interacting protein 1/2 (CYFIP1/2) expression analysis in autism. *Metabolic Brain Disease*, 2, pp.1–6.

Nowicki, S.T. et al., 2007. The Prader-Willi phenotype of fragile X syndrome. *Journal of developmental and behavioral pediatrics : JDBP*, 28(2), pp.133–8.

Ocker, G.K. et al., 2017. From the statistics of connectivity to the statistics of spike times in neuronal networks. *Current Opinion in Neurobiology*, 46, pp.109–119.

Oguro-Ando, A. et al., 2014. Increased CYFIP1 dosage alters cellular and dendritic morphology and dysregulates mTOR. *Molecular psychiatry*, 20(April), pp.1–10.

Padrick, S.B. & Rosen, M.K., 2010. Physical Mechanisms of Signal Integration by WASP Family Proteins. *Annual Review of Biochemistry*, 79(1), pp.707–735.

Panja, D. et al., 2014. Two-Stage Translational Control of Dentate Gyrus LTP Consolidation Is Mediated by Sustained BDNF-TrkB Signaling to MNK. *Cell Reports*, 9(4), pp.1430–1445.

Paolicelli, R.C. et al., 2011. Synaptic Pruning by Microglia Is Necessary for Normal Brain Synaptic Pruning by Microglia Is Necessary for Normal Brain Development. *Science*, 333(September), pp.1456–1459.

Pathania, M. et al., 2014. The autism and schizophrenia associated gene CYFIP1 is critical for the maintenance of dendritic complexity and the stabilization of mature spines. *Translational psychiatry*, 4(February), p.e374.

Pedron, S. et al., 2014. Repeated transcranial direct current stimulation prevents abnormal behaviors associated with abstinence from chronic nicotine consumption. *Neuropsychopharmacology*, 39, pp.981–988.

Peters, A.J., Liu, H. & Komiyama, T., 2017. Learning in the Rodent Motor Cortex. *Annual review of neuroscience*, (March), pp.77–97.

Pfeiffer, B.E. & Huber, K.M., 2006. Current Advances in Local Protein Synthesis and Synaptic Plasticity. *Journal of Neuroscience*, 26(27), pp.7147–7150.

Phillips, M. & Pozzo-Miller, L., 2014. Dendritic spine dysgenesis in autism related disorders. *Neuroscience Letters*, 601, pp.30–40.

Pinto, D. et al., 2014. Convergence of genes and cellular pathways dysregulated in autism spectrum disorders. *American Journal of Human Genetics*, 94(5), pp.677–694.

Pollard, T.D. & Borisy, G.G., 2003. Cellular motility driven by assembly and disassembly of actin filaments. *Cell*, 112(4), pp.453–465.

Qin, M. et al., 2005. Postadolescent changes in regional cerebral protein synthesis: an in vivo study in the FMR1 null mouse. *The Journal of neuroscience : the official journal of the Society for Neuroscience*, 25(20), pp.5087–5095.

Radyushkin, K. et al., 2009. Neuroligin-3-deficient mice: model of a monogenic heritable form of autism with an olfactory deficit. *Genes, brain, and behavior*, 8(4), pp.416–25.

Ranson, A., 2017. Stability and Plasticity of Contextual Modulation in the Mouse Visual Cortex. *Cell Reports*, 18(4), pp.840–848.

Raynaud-Messina, B. & Merdes, A., 2007. Gamma-tubulin complexes and microtubule organization. *Current Opinion in Cell Biology*, 19(1), pp.24–30.

Rees, E. et al., 2014. Analysis of copy number variations at 15 schizophrenia-associated loci. *British Journal of Psychiatry*, 204(2), pp.108–114.

Richter, J.D. & Sonenberg, N., 2005. Regulation of cap-dependent translation by eIF4E inhibitory proteins. *Nature*, 433(7025), pp.477–480.

Ridley, A.J. et al., 1992. The small GTP-binding protein rac regulates growth factor-induced membrane ruffling. *Cell*, 70(3), pp.401–410.

Roberts, S.E. et al., 2002. Characterisation of interstitial duplications and triplications of chromosome 15q11-q13. *Human Genetics*, 110(3), pp.227–234.

Rothwell, P.E. et al., 2014. Autism-Associated Neuroligin-3 Mutations Commonly

Impair Striatal Circuits to Boost Repetitive Behaviors. *Cell*, 158(1), pp.198–212.

Roudi, Y., Dunn, B. & Hertz, J., 2015. Multi-neuronal activity and functional connectivity in cell assemblies. *Current Opinion in Neurobiology*, 32, pp.38–44.

De Rubeis, S. et al., 2013. CYFIP1 coordinates mRNA translation and cytoskeleton remodeling to ensure proper dendritic spine formation. *Neuron*, 79(6), pp.1169–82.

Rudelli, R.D. et al., 1985. Adult fragile X syndrome. Clinico-neuropathologic findings. *Acta Neuropathologica*, 67(3–4), pp.289–95.

Rust, M.B. & Maritzen, T., 2015. Relevance of presynaptic actin dynamics for synapse function and mouse behavior. *Experimental Cell Research*, pp.1–7.

Sahoo, T. et al., 2007. Identification of novel deletions of 15q11q13 in Angelman syndrome by array-CGH: molecular characterization and genotype-phenotype correlations. *European journal of human genetics : EJHG*, 15(9), pp.943–949.

Saller, E. et al., 1999. Increased apoptosis induction by 121F mutant p53. *The EMBO Journal*, 18(16), pp.4424–37.

Sanders, S.J. et al., 2011. Multiple Recurrent De Novo CNVs, Including Duplications of the 7q11.23 Williams Syndrome Region, Are Strongly Associated with Autism. *Neuron*, 70(5), pp.863–885.

Santini, E. et al., 2013. Exaggerated translation causes synaptic and behavioural aberrations associated with autism. *Nature*, 493(7432), pp.411–5.

Sato, Y. et al., 2017. Prolactin upregulates female-predominant P450 gene expressions and downregulates male-predominant gene expressions in mouse liver. *Drug Metabolism and Disposition*, 45(6), pp.586–592.

Schenck, A. et al., 2001. A highly conserved protein family interacting with the fragile

X mental retardation protein (FMRP) and displaying selective interactions with FMRP-related proteins FXR1P and FXR2P. *Proceedings of the National Academy of Sciences of the United States of America*, 98(15), pp.8844–9.

Schenck, A. et al., 2003. CYFIP/Sra-1 controls neuronal connectivity in Drosophila and links the Rac1 GTPase pathway to the fragile X protein. *Neuron*, 38(6), pp.887–898.

Schindelin, J. et al., 2012. Fiji: An open-source platform for biological-image analysis. *Nature Methods*, 9(7), pp.676–682.

Schmidt, E.K. et al., 2009. SUnSET , a nonradioactive method to monitor protein synthesis. *Nature methods*, 6(4), pp.275–277.

Schratt, G.M. et al., 2004. BDNF regulates the translation of a select group of mRNAs by a mammalian target of rapamycin-phosphatidylinositol 3-kinase-dependent pathway during neuronal development. *Journal of Neuroscience*, 24(33), pp.7366–7377.

Seitz, R.J. et al., 1990. Motor learning in man: a positron emission tomographic study. *Neuroreport*, 1(1), pp.57–60.

Sheehan, M.J. et al., 2016. Selection on Coding and Regulatory Variation Maintains Individuality in Major Urinary Protein Scent Marks in Wild Mice. *PLoS Genetics*, 12(3), pp.1–33.

Shi, Y., Ålin, K. & Goff, S.P., 1995. Abl-interactor-1, a novel SH3 protein binding to the carboxy-terminal portion of the Abl protein, suppresses v-abl transforming activity. *Genes and Development*, 9(21), pp.2583–2597.

Simon, P., Dupuis, R. & Costentin, J., 1994. Thigmotaxis as an index of anxiety in mice. Influence of dopaminergic transmissions. *Behavioural Brain Research*, 61(1), pp.59–64.

Siomi, H. et al., 1993. The protein product of the fragile X gene, FMR1, has characteristics of an RNA-binding protein. *Cell*, 74(2), pp.291–298.

Skarnes, W.C. et al., 2013. A conditional knockout resource for the genome – wide study of mouse gene function. *Nature*, 474(7351), pp.337–342.

Sonenberg, N. & Hinnebusch, A.G., 2009. Regulation of Translation Initiation in Eukaryotes: Mechanisms and Biological Targets. *Cell*, 136(4), pp.731–745.

Stavoe, A.K.H. et al., 2012. Synaptic vesicle clustering requires a distinct MIG-10/lamellipodin isoform and ABI-1 downstream from Netrin. *Genes and Development*, 26(19), pp.2206–2221.

Stefansson, H. et al., 2014. CNVs conferring risk of autism or schizophrenia affect cognition in controls. *Nature*, 505(7483), pp.361–366.

Steward, O. & Schuman, E.M., 2003. Compartmentalized synthesis and degradation of proteins in neurons. *Neuron*, 40(2), pp.347–359.

Tai, K. et al., 2010. Adhesion properties and retinofugal expression of chicken protocadherin-19. *Brain Research*, 1344(1994), pp.13–24.

Takenawa, T. & Suetsugu, S., 2007. The WASP–WAVE protein network: connecting the membrane to the cytoskeleton. *Nature Reviews Molecular Cell Biology*, 8(1), pp.37–48.

Tanaka, K.F. et al., 2010. Flexible Accelerated STOP Tetracycline Operator-Knockin (FAST): A Versatile and Efficient New Gene Modulating System. *Biological Psychiatry*, 67(8), pp.770–773.

Tang, G. et al., 2014. Loss of mTOR-Dependent Macroautophagy Causes Autistic-like Synaptic Pruning Deficits. *Neuron*, 83(5), pp.1131–1143.

Thomas, A. et al., 2009. Marble burying reflects a repetitive and perseverative

behavior more than novelty-induced anxiety. *Psychopharmacology*, 204(2), pp.361–373.

Tiwari, S.S. et al., 2016. Alzheimer-related decrease in CYFIP2 links amyloid production to tau hyperphosphorylation and memory loss. *Brain*, 139(10), pp.2751–2765.

Valente, K.D. et al., 2013. Angelman syndrome caused by deletion: A genotype-phenotype correlation determined by breakpoint. *Epilepsy Research*, 105(1–2), pp.234–239.

Varela, M.C. et al., 2005. Impact of molecular mechanisms, including deletion size, on Prader-Willi syndrome phenotype: Study of 75 patients. *Clinical Genetics*, 67(1), pp.47–52.

Vargas-Pérez, H. et al., 2009. Social dominance rank influences wheel running behavior in mice. *Neuroscience letters*, 457(3), pp.137–140.

Verkerk, A.J.M.H. et al., 1991. Identification of a gene (FMR-1) containing a CGG repeat coincident with a breakpoint cluster region exhibiting length variation in fragile X syndrome. *Cell*, 65(5), pp.905–914.

Wang, F. et al., 2011. Bidirectional control of social hierarchy by synaptic efficacy in medial prefrontal cortex. *Science (New York, N.Y.)*, 334(6056), pp.693–7.

Waters, S., Wiestler, T. & Diedrichsen, J., 2017. Cooperation not competition: bihemispheric tDCS and fMRI show role for ipsilateral hemisphere in motor learning. , 37(31), pp.7500–7512.

Wegner, A.M. et al., 2008. N-WASP and the Arp2/3 complex are critical regulators of actin in the development of dendritic spines and synapses. *Journal of Biological Chemistry*, 283(23), pp.15912–15920.

Weiler, I.J. & Greenough, W.T., 1993. Metabotropic glutamate receptors trigger

postsynaptic protein synthesis. *Proceedings of the National Academy of Sciences of the United States of America*, 90(15), pp.7168–7171.

Wijetunge, L.S. et al., 2014. Stimulated Emission Depletion (STED) Microscopy Reveals Nanoscale Defects in the Developmental Trajectory of Dendritic Spine Morphogenesis in a Mouse Model of Fragile X Syndrome. *Journal of Neuroscience*, 34(18), pp.6405–6412.

Wise, S.P. et al., 1998. Changes in motor cortical activity during visuomotor adaptation. *Exp Brain Res*, 121(3), pp.285–299.

Wu, D. et al., 2013. In vivo high-resolution diffusion tensor imaging of the mouse brain. *NeuroImage*, 83, pp.18–26.

Wu, M. V et al., 2009. Estrogen masculinizes neural pathways and sex-specific behaviors. *Cell*, 139(1), pp.61–72.

Yang, G., Pan, F. & Gan, W.B., 2009. Stably maintained dendritic spines are associated with lifelong memories. *Nature*, 462(7275), pp.920–924.

Yang, M. & Crawley, J.N., 2009. Simple behavioral assessment of mouse olfaction. *Curr Protoc Neurosci*, pp.1–14.

Yin, Y., Edelman, G.M. & Vanderklish, P.W., 2002. The brain-derived neurotrophic factor enhances synthesis of Arc in synaptoneurosomes. *Proceedings of the National Academy of Sciences*, 99(4), pp.2368–2373.

Ylisaukko-oja, T. et al., 2005. Analysis of four neuroligin genes as candidates for autism. *European journal of human genetics : EJHG*, 13(12), pp.1285–92.

Yuen, R.K.C. et al., 2017. Whole genome sequencing resource identifies 18 new candidate genes for autism spectrum disorder. *Nature Neuroscience*, 20(4), pp.602–611.

Zalfa, F. et al., 2007. A new function for the fragile X mental retardation protein in regulation of PSD-95 mRNA stability. *Nature Neuroscience*, 10(5), pp.578–587.

Zhao, L. et al., 2013. Drosophila cyfip Regulates Synaptic Development and Endocytosis by Suppressing Filamentous Actin Assembly. *PLoS Genetics*, 9(4).

Zukin, R.S., Richter, J.D. & Bagni, C., 2009. Signals, synapses, and synthesis: how new proteins control plasticity. *Frontiers in Neural Circuits*, 3(October), pp.1–8.

Van Der Zwaag, B. et al., 2010. A co-segregating microduplication of chromosome 15q11.2 pinpoints two risk genes for autism spectrum disorder. *American Journal of Medical Genetics, Part B: Neuropsychiatric Genetics*, 153(4), pp.960–966.

Appendix

Figure	Shapiro-Wilk test of normality	Test for Equality of variances	Type of test	Power	Sample size
3.1, Motor cortex	WT: W = 0.931, P = 0.422 *CyfiP1*$^{+/-}$: W = 0.946, P = 0.592	Levene`s test F = 0.980, P = 0.758	Student`s t-test, one-tailed F = 0.098, P = 0.006	NA	WT n = 11 *Cyfip1*$^{+/-}$ n = 11
3.1, Striatum	WT: W = 0.674, P = 0.000 *CyfiP1*$^{+/-}$: W = 0.602, P = 0.000	Levene`s test F = 0.910, P = 0.766	Mann-Whitney, one-tailed U = 11.000, P = 0.000	NA	WT n = 12 *Cyfip1*$^{+/-}$ n = 12
3.1, Cerebellum	WT: W = 0.956, P = 0.720 *CyfiP1*$^{+/-}$: W = 0.944, P = 0.624	Levene`s test F = 2.961, P = 0.102	Student`s t-test, one-tailed F = 2.961, P = 0.006	NA	WT n = 11 *Cyfip1*$^{+/-}$ n = 9
3.1, Liver	WT: W = 0.926, P = 0.413 *CyfiP1*$^{+/-}$: W = 0.956, P = 0.758	Levene`s test F = 15.906, P = 0.001	Mann-Whitney, one-tailed U = 13.000, P = 0.004	NA	WT n = 10 *Cyfip1*$^{+/-}$ n=9
3.2B, Motor cortex	WT: W = 0.928, P = 0.139 *CyfiP1*$^{+/-}$: W = 0.910, P = 0.064	Levene`s test F = 0.967, P = 0.332	Student`s t-test, one-tailed F = 0.967, P = 0.017	NA	WT n = 20 *Cyfip1*$^{+/-}$ n = 20
3.2B, Hippocampus	WT: W = 0.895, P = 0.116 *CyfiP1*$^{+/-}$: W = 0.916, P = 0.254	Levene`s test F = 2.682, P = 0.115	Student`s t-test, one-tailed F = 2.682, P = 0.002	NA	WT n = 13 *Cyfip1*$^{+/-}$: n = 12
3.2B, Striatum	WT: W = 0.499, P = 0.396 *CyfiP1*$^{+/-}$: W = 0.881, P = 0.040	Levene`s test F = 0.441, P = 0.512	Mann-Whitney, one-tailed U = 88.000, P = 0.069	NA	WT n = 16 *Cyfip1*$^{+/-}$: n = 16

3.2B, Thalamus	WT: W = 0.836, P = 0.091 *CyfiP1*$^{+/-}$: W = 0.840, P = 0.099	Levene`s test F = 0.703, P = 0.418	Student`s *t*-test, one-tailed F = 0.703, P = 0.332	NA	WT n = 7 *Cyfip1*$^{+/-}$ n = 7
3.2B, Somato-sensory cortex	WT: W = 0.809, P = 0.096 *CyfiP1*$^{+/-}$: W = 0.757, P = 0.007	Levene`s test F = 0.774, P = 0.396	Mann-Whitney, one-tailed U = 22.000, P = 0.500	NA	WT n=5 *Cyfip1*$^{+/-}$ n=9
3.2B, Cerebellum	WT: W = 0.911, P = 0.189 *CyfiP1*$^{+/-}$: W = 0.812, P = 0.013	Levene`s test F = 0.000, P = 0.987	Mann-Whitney, one-tailed U = 58.000, P = 0.148	NA	WT n = 13 *Cyfip1*$^{+/-}$: n = 12
3.2B, Liver	WT: W = 0.838, P = 0.030 *CyfiP1*$^{+/-}$: W = 0.972, P = 0.911	Levene`s test F = 1.447, P = 0.245	Mann-Whitney, one-tailed U = 48.500, P = 0.471	NA	WT n = 11, *Cyfip1*$^{+/-}$ n = 9
3.2B, Spleen	WT: W = 0.905, P = 0.213 *CyfiP1*$^{+/-}$: W = 0.838, P = 0.055	Levene`s test F = 1.721, P = 0.206	Student`s *t*-test, one-tailed F = 1.721, P = 0.478	NA	WT: n=11 *Cyfip1*$^{+/-}$ n = 9
4.1A	WT Control: W = 0.917, P = 0.371 S1: W = 0.960, P = 0.801 S2: W = 0.925, P = 0.432 *Cyfip1*$^{+/-}$ Control: W = 0.924, P = 0.323 S1: W = 0.835, P = 0.024 S2: W = 0.937, P = 0.466	Mauchly`s Test of Sphericity W = 0.904, χ^2 = 1.819, P = 0.403	Repeated measures ANOVA Pillai`s trance Main effect of odour $F_{2, 18}$ = 11.177, P = 0.001 Interaction odour x genotype $F_{2, 18}$ = 3.776, P = 0.043 Followed by Bonferroni corrected pairwise comparison	0.979 0.612	WT n = 9 *Cyfip1*$^{+/-}$ n = 12

4.1B	WT S1: W = 0.924, P = 0.423 S2: W = 0.926, P = 0.442 *Cyfip1*$^{+/-}$ S1: W = 0.927, P = 0.353 S2: W = 0.931, P = 0.389	Levene`s test F = 3.755, P = 0.019	Repeated measures ANOVA Pillai`s trance Main effect of odour $F_{1, 19}$ = 27.792, P = 0.000 Interaction odour x genotype $F_{1, 19}$ = 0.657, P = 0.428	 0.999 0.657	WT n = 9, *Cyfip1*$^{+/-}$ n = 12
4.1C	WT W = 0.969, P = 0.770 *Cyfip1*$^{+/-}$ W = 0.898, P = 0.207	Levene`s test F = 0.367, P = 0.550	Student`s *t*-test, two-tailed P = 0.698	NA	WT n = 18 *Cyfip1*$^{+/-}$ n = 10
4.1E	WT Control: W = 0.877, P = 0.176 S1: W = 0.862, P = 0.125 S2: W = 0.901, P = 0.297 *Cyfip1*$^{+/-}$ Control: W = 0.901, P = 0.225 S1: W = 0.897, P = 0.203 S2: W = 0.933, P = 0.452	Mauchly`s Test of Sphericity W = 0.550, χ^2 = 8.959, P = 0.011 Greenhouse-Geisser ε = 0.690	Repeated measures ANOVA Pillai`s trance Main effect of odour $F_{2, 15}$ = 6.306, P = 0.010 Interaction odour x genotype $F_{2, 15}$ = 0.654, P = 0.534	 0.825 0.139	WT n = 8, *Cyfip1*$^{+/-}$ n = 10

4.1F	WT S1: W = 0.949, P = 0.698 S2: W = 0.960, P = 0.816 *Cyfip1*$^{+/-}$ S1: W = 0.805, P = 0.011 S2: W = 0.954, P = 0.720	Levene`s test F = 0.338, P = 0.798	Repeated measures ANOVA Pillai`s trance Main effect of odour $F_{1, 16}$ = 1.601, P = 0.224 Interaction odour x genotype $F_{1, 16}$ = 0.031, P = 0.862	 0.825 0.139	WT n = 8 for S1 *Cyfip1*$^{+/-}$ n = 11 for S1
4.2A	WT; W = 0.939, P = 0.539 *Cyfip1*$^{+/-}$*;* W = 0.909, P = 0.098	Levene`s test F = 0.005, P = 0.947	Student`s *t*-test, two-tailed, P = 0.540	NA	WT n = 10 *Cyfip1*$^{+/-}$ n = 17
4.2B	WT; W = 0.907, P = 0.296 *Cyfip1*$^{+/-}$*;* W = 0.887, P = 0.107	Levene`s test F = 5.320, P = 0.033	Mann-Whitney *U*-test, two-tailed U = 47.000, P = 0.651	NA	WT n = 9 *Cyfip1*$^{+/-}$ n = 12
4.2C	WT; W = 0.917, P = 0.173 *Cyfip1*$^{+/-}$*;* W = 0.896, P = 0.083	Levene`s test F = 0.502, P = 0.485	Student`s *t*-test, two-tailed, P = 0.243	NA	WT n = 15 *Cyfip1*$^{+/-}$ n = 15
4.2D	WT; W = 0.955, P = 0.747 *Cyfip1*$^{+/-}$*;* W = 0.811, P = 0.038	Levene`s test F = 1.076, P = 0.316	Mann-Whitney *U*-test, two-tailed U = 18.000, P = 0.093	NA	WT n = 9, *Cyfip1*$^{+/-}$ n = 8
4.2E	WT; W = 0.919, P = 0.346 *Cyfip1*$^{+/-}$*;* W = 0.939, P = 0.572	Levene`s test F = 0.015, P = 0.903	Student`s *t*-test, two-tailed, P = 0.806	NA	WT n = 10 *Cyfip1*$^{+/-}$ n = 9

4.2F	WT; W = 0.880, P = 0.048 *Cyfip1*$^{+/-}$; W = 0.914, P = 0.157	Levene`s test F = 3.817, P = 0.061	Mann-Whitney U-test, two-tailed U = 102.500, P = 0.683	NA	WT n = 15 *Cyfip1*$^{+/-}$ n = 15
4.3A, WT	Trial 1; W = 0.934, P = 0.254 Trial 2; W = 0.950, P = 0.458 Trial 3; W = 0.983, P = 0.052 Trial 4; W = 0.853, P = 0.012 Trial 5; W = 0.906, P = 0.087 Trial 6; W = 0.905, P = 0.083 Trial 7; W = 0.922, P = 0.160	W = 0.362, χ^2 = 14.018, P = 0.836	Repeated measures ANOVA Main effect of Trial, Pillai`s Trace $F_{6, 11}$ = 16.094, P = 0.000 Followed by Bonferroni corrected pairwise comparison	1.000	WT n = 17
4.3A, *Cyfip1*$^{+/-}$	Trial 1; W = 0.956, P = 0.628 Trial 2; W = 0.938, P = 0.359 Trial 3; W = 0.945, P = 0.445 Trial 4; W = 0.907, P = 0.124 Trial 5; W = 0.924, P = 0.219 Trial 6; W = 0.976, P = 0.938 Trial 7; W = 0.934, P = 0.312	W = 0.069, χ^2 = 31.521, P = 0.055	Repeated measures ANOVA Main effect of Trial, Pillai`s Trace $F_{6, 9}$ = 1.092, P = 0.434	0.247	*Cyfip1*$^{+/-}$ n = 15
4.3B	WT W = 0.934, P = 0.254 *Cyfip1*$^{+/-}$ W = 0.956, P = 0.624	Levene`s test F = 0.706, P = 0.407	Student`s t-test, two-tailed, P = 0.169	NA	WT n = 17 *Cyfip1*$^{+/-}$ n = 15

4.3C, WT	Trial 1; W = 0.905, P = 0.184 Trial 2; W = 0.926, P = 0.335 Trial 3; W = 0.859, P = 0.048 Trial 4; W = 0.912, P = 0.226 Trial 5; W = 0.924, P = 0.318 Trial 6; W = 0.886, P = 0.103 Trial 7; W = 0.819, P = 0.016	Mauchly`s Test of Sphericity W = 0.025, χ^2 = 32.504, P = 0.048, Greenhouse-Geisser ε = 0.576	Repeated measures ANOVA Within-Subject Effects Greenhouse-Geisser $F_{6, 66}$ = 15.395, P = 0.000 (same values obtained with test assuming sphericity) Followed by Bonferroni corrected pairwise comparison	1.000	WT n = 12
4.3C ***Cyfip1*$^{+/-}$**	Trial 1; W = 0.932, P = 0.463 Trial 2; W = 0.991, P = 0.998 Trial 3; W = 0.947, P = 0.629 Trial 4; W = 0.851, P = 0.059 Trial 5; W = 0.886, P = 0.154 Trial 6; W = 0.877, P = 0.120 Trial 7; W = 0.918, P = 0.340	Mauchly`s Test of Sphericity W = 0.024, χ^2 = 25.193, P = 0.239	Repeated measures ANOVA Within-Subject Effects Sphericity assumed $F_{6, 54}$ = 3.409, P = 0.006 Followed by Bonferroni corrected pairwise comparison	0.915	*Cyfip1*$^{+/-}$ n = 10
4.3D	WT W = 0.905, P = 0.184 *Cyfip1*$^{+/-}$ W = 0.932, P = 0.463	Levene`s test F = 0.458, P = 0.506	Student`s t-test, two-tailed, P = 0.332	NA	WT n = 12 *Cyfip1*$^{+/-}$ n = 10

4.4A	Trial 1; W = 0.959, P = 0.809 Trial 2; W = 0.991, P = 0.994 Trial 3; W = 0.947, P = 0.629 Trial 4; W = 0.928, P = 0.537 Trial 5; W = 0.936, P = 0.605 Trial 6; W = 0.967, P = 0.873 Trial 7; W = 0.734, P = 0.009	Mauchly`s Test of Sphericity W = 0.000, χ^2 = 30.757, P = 0.132	Repeated measures ANOVA Within-Subject Effects $F_{6, 36}$ = 15.261, P = 0.000	1.000	WT = 7
4.4B	Trial 1; W = 0.943, P = 0.702 Trial 2; W = 0.952, P = 0.574 Trial 3; W = 0.981, P = 0.629 Trial 4; W = 0.943, P = 0.546 Trial 5; W = 0.965, P = 0.605 Trial 6; W = 0.923, P = 0.068 Trial 7; W = 0.842, P = 0.080	Mauchly`s Test of Sphericity W = 0.038, χ^2 = 26.177, P = 0.123	Repeated measures ANOVA Within-Subject Effects $F_{6, 54}$ = 7.716, P = 0.000	1.000	*Cyfip1*$^{+/-}$ n = 10
4.4C	WT P40: see **4.4A** WT P60: see **4.3A**	Mauchly`s Test of Sphericity W = 0.389, χ^2 = 18.685, P = 0.548	Repeated measures ANOVA Pillai`s Trace, Main effect of trial $F_{6, 17}$ = 23.515, P = 0.000 Interaction trial x age $F_{6, 17}$ = 0.815, P = 0.573	1.000 0.238	WT P40 n = 7, WT P60 n = 17

4.4D	*Cyfip1*$^{+/-}$ P40: see **4.4B** *Cyfip1*$^{+/-}$ P60: see **4.3A**	Mauchly`s Test of Sphericity W = 0.131, χ^2 = 38.218, P = 0.009; Greenhouse-Geisser ε = 0.602	Repeated measures ANOVA Within-Subject Effects, Greenhouse-Geisser test main effect of trial $F_{6, 138}$ = 6.692, P = 0.000 interaction trial x age $F_{6, 138}$ = 3.000, P = 0.009 Followed by Bonferroni corrected pairwise comparison	 0.998 0.894	*Cyfip1*$^{+/-}$ P40 n = 8 *Cyfip1*$^{+/-}$ P60 n = 15
4.5A	Trained *WT* Trial 1; W = 0.921, P = 0.514 Trial 2; W = 0.924, P = 0.537 Trial 3; W = 0.879, P = 0.264 Trial 4; W = 0.916, P = 0.479 Trial 5; W = 0.693, P = 0.005 Trial 6; W = 0.798, P = 0.057 Trial 7; W = 0.815, P = 0.080	Mauchly`s Test of Sphericity W = 0.001 χ^2 = 25.109, P = 0.344	Repeated measures ANOVA, Pillai`s Trace Main effect of Trial, $F_{6, 36}$ = 2.053, P = 0.084	 0.076	Trained WT n = 7

4.5B	Trained WT see **4.5A** Untrained WT see **4.5C**	Mauchly`s Test of Sphericity W = 0.597 χ^2 = 10.199, P = 0.965	Repeated measures ANOVA, Pillai`s Trace Main effect of Trial, $F_{6, 17}$ = 3.260, P = 0.025; Interaction Trial x Training, $F_{6, 17}$ = 2.650, P = 0.047 Followed by Bonferroni corrected pairwise comparison	 0.805 0.723	Trained WT n = 7 Untrained WT n = 17
4.5C	Trained *Cyfip1*$^{+/-}$ Trial 1; W = 0.921, P = 0.514 Trial 2; W = 0.924, P = 0.537 Trial 3; W = 0.879, P = 0.264 Trial 4; W = 0.916, P = 0.479 Trial 5; W = 0.693, P = 0.005 Trial 6; W = 0.798, P = 0.057 Trial 7; W = 0.815, P = 0.080	Mauchly`s Test of Sphericity not obtained	Repeated measures ANOVA Within-Subject Effects, sphericity assumed Main effect of Trial $F_{6, 30}$ = 13.465, P = 0.000 Followed by Bonferroni corrected pairwise comparison	 1.000	Trained *Cyfip1*$^{+/-}$ n = 6,

4.5D	Trained *Cyfip1*$^{+/-}$ P60: see **4.5C** Untrained *Cyfip1*$^{+/-}$ P60: see **4.3A**	Mauchly`s Test of Sphericity W = 0.133, χ^2 = 33.893, P = 0.029; Greenhouse-Geisser ε = 0.641	Repeated measures ANOVA Within-Subject Effects, Greenhouse-Geisser test Main effect of Trial $F_{6, 114}$ = 6.269, P = 0.000 Interaction Trial x Training $F_{6, 114}$ = 2.872, P = 0.030 Followed by Bonferroni corrected pairwise comparison	 0.982 0.741	Trained *Cyfip1*$^{+/-}$ n = 6 Untrained *Cyfip1*$^{+/-}$ n = 15
5.1A, Motor cortex *Cyfip1*$^{+/-}$	female: W = 0.922, P = 0.520 male: W = 0.821, P = 0.119	Levene`s test F = 0.958, P = 0.353	Student`s *t*-test, two-tailed P = 0.003	NA	female: n = 6 male: n = 5
5.1A, Striatum *Cyfip1*$^{+/-}$	female: W = 0.953, P = 0.761 male: W = 0.626, P = 0.001	Levene`s test F = 2.776, P = 0.127	Mann-Whitney, two-tailed U = 16.000, P = 0.818	NA	female: n = 6 male: n = 6
5.1A, Cerebellum *Cyfip1*$^{+/-}$	female: W = 1.000, P = 0.987 male: W = 0.962, P = 0.832	Levene`s test F = 0.953, P = 0.361	Student`s *t*-test, two-tailed P = 0.643	NA	female: n = 3 male: n = 6
5.1A, Liver *Cyfip1*$^{+/-}$	female: W = 0.999, P = 0.927 male: W = 0.916, P = 0.478	Levene`s test F = 0.565, P = 0.477	Student`s *t*-test, two-tailed P = 0.192	NA	female: n = 3 male: n = 6

5.1B, Motor cortex WT	female: W = 0.857, P = 0.178 male: W = 0.890, P = 0.358	Levene`s test F = 2.798, P = 0.129	Student`s t-test, two-tailed P = 0.012	NA	female: n = 6 male: n = 5
5.1B, Striatum WT	female: W = 0.760, P = 0.025 male: W = 0.993, P = 0.603	Levene`s test F = 4.089, P = 0.071	Mann-Whitney, two-tailed U = 10.000, P = 0.240	NA	female: n = 6 male: n = 6
5.1B, Cerebellum WT	female: W = 0.931, P = 0.587 male: W = 0.891, P = 0.362	Levene`s test F = 0.043, P = 0.840	Student`s t-test, two-tailed P = 0.167	NA	female: n = 6 male: n = 4
5.1B, Liver WT	female: W = 0.859, P = 0.186 male: W = 0.959, P = 0.773	Levene`s test F = 0.402, P = 0.544	Student`s t-test, two-tailed P = 0.596	NA	female: n = 6 male: n = 4
5.2A, Motor cortex *Cyfip1*$^{+/-}$	female: W = 0.892, P = 0.327 male: W = 0.948, P = 0.713	Levene`s test F = 0.934, P = 0.355	Student`s t-test, two-tailed P = 0.715	NA	female: n = 6 male: n = 7
5.2A, Striatum *Cyfip1*$^{+/-}$	female: W = 0.712, P = 0.016 male: W = 0.897, P = 0.316	Levene`s test F = 0.000, P = 0.999	Mann-Whitney, two-tailed U = 12.000, P = 0.788	NA	female: n = 4 male: n = 7
5.2A, Hippocampus *Cyfip1*$^{+/-}$	female: W = 0.960, P = 0.816 male: W = 0.863, P = 0.161	Levene`s test F = 0.688, P = 0.423	Student`s t-test, two-tailed P = 0.182	NA	female: n = 7 male: n = 7

5.2A, Cerebellum *Cyfip1*$^{+/-}$	female: $W = 0.791$, $P = 0.034$ male: $W = 0.936$, $P = 0.606$	Levene`s test $F = 0.858$, $P = 0.372$	Mann-Whitney, two-tailed $U = 22.000$, $P = 0.805$	NA	female: n = 7 male: n = 7
5.2B, Motor cortex WT	female: $W = 0.849$, $P = 0.156$ male: $W = 0.912$, $P = 0.413$	Levene`s test $F = 8.987$, $P = 0.012$	Mann-Whitney, two-tailed $U = 14.000$, $P = 0.366$	NA	female: n = 6 male: n = 7
5.2B, Striatum WT	female: $W = 0.924$, $P = 0.503$ male: $W = 0.951$, $P = 0.736$	Levene`s test $F = 0.020$, $P = 0.889$	Student`s *t*-test, two-tailed $P = 0.261$	NA	female: n = 7 male: n = 7
5.2B, Hippocampus WT	female: $W = 0.855$, $P = 0.136$ male: $W = 0.946$, $P = 0.698$	Levene`s test $F = 2.355$, $P = 0.151$	Student`s *t*-test, two-tailed $P = 0.387$	NA	female: n = 7 male: n = 7
5.2B, Cerebellum WT	female: $W = 0.984$, $P = 0.978$ male: $W = 0.852$, $P = 0.127$	Levene`s test $F = 0.095$, $P = 0.763$	Student`s *t*-test, two-tailed $P = 0.749$	NA	female: n = 7 male: n = 7
5.3A, Motor cortex	WT: $W = 0.876$, $P = 0.290$ *Cyfip1*$^{+/-}$: $W = 0.888$, $P = 0.347$	Levene`s test $F = 0.267$, $P = 0.619$	Student`s *t*-test, two-tailed $P = 0.553$	NA	WT n = 5 *Cyfip1*$^{+/-}$ n = 5
5.3A, Striatum	WT: $W = 0.878$, $P = 0.299$ *Cyfip1*$^{+/-}$: $W = 0.936$, $P = 0.640$	Levene`s test $F = 1.491$, $P = 0.257$	Student`s *t*-test, two-tailed $P = 0.957$	NA	WT n = 5 *Cyfip1*$^{+/-}$ n = 5
5.3A, Hippocampus	WT: $W = 0.841$, $P = 0.166$ *Cyfip1*$^{+/-}$: $W = 0.969$, $P = 0.663$	Levene`s test $F = 2.711$, $P = 0.151$	Student`s t-test, two-tailed $P = 0.947$	NA	WT n = 5, *Cyfip1*$^{+/-}$ n = 3

5.3A, Cerebellum	WT: W = 0.831, P = 0.142 *Cyfip1*$^{+/-}$: W = 0.824, P = 0.126	Levene`s test F = 7.558, P = 0.025	Mann-Whitney, two-tailed U = 7.000, P = 0.310	NA	WT n = 5 *Cyfip1*$^{+/-}$ n = 5
5.3B	NA, too few samples	NA, too few samples	NA, too few samples	NA	WT n = 2 *Cyfip1*$^{+/-}$ n = 2
6.1	WT: W = 0.985, P = 0.980 *Cyfip1*$^{+/-}$: W = 0.944, P = 0.672	Levene`s test F = 0.76, P = 0.787	Student`s *t*-test, two-tailed P = 0.408	NA	WT n = 7, *Cyfip1*$^{+/-}$ n = 7
6.2, Motor cortex	WT: W = 0.712, P = 0.013 *CyfiP1*$^{+/-}$: W = 0.856, P = 0.214	Levene`s test F = 0.011, P = 0.921	Mann-Whitney, two-tailed U = 8.000, P = 0.421	NA	WT: n = 5, *Cyfip1*$^{+/-}$: n = 5
6.2, Striatum	WT: W = 0.781, P = 0.056 *CyfiP1*$^{+/-}$: W = 0.904, P = 0.431	Levene`s test F = 1.048, P = 0.336	Student`s *t*-test, two-tailed P = 0.866	NA	WT: n = 5, *Cyfip1*$^{+/-}$: n = 5
6.2, Hippocampus	WT: W = 0.893, P = 0.373 *CyfiP1*$^{+/-}$: W = 0.857, P = 0.217	Levene`s test F = 6.567, P = 0.034	Mann-Whitney, two-tailed U = 7.000, P = 0.310	NA	WT: n = 5, *Cyfip1*$^{+/-}$: n = 5
6.2, Cerebellum	WT: W = 0.864, P = 0.243 *CyfiP1*$^{+/-}$: W = 0.741, P = 0.024	Levene`s test F = 0.016, P = 0.903	Mann-Whitney, two-tailed U = 8.000, P = 0.421	NA	WT: n = 5, *Cyfip1*$^{+/-}$: n = 5
7.1A, M1	WT: W = 0.969, P = 0.645 *CyfiP1*$^{+/-}$: W = 0.957, P = 0.379	Levene`s test F = 0.028, P = 0.867	Student`s *t*-test, two-tailed P = 0.008	NA	WT: n = 24, *Cyfip1*$^{+/-}$: n = 24
7.1A, V1	WT: W = 0.980, P = 0.935 *CyfiP1*$^{+/-}$: W = 0.972, P = 0.755	Levene`s test F = 4.474, P = 0.041	Mann-Whitney, two-tailed U = 166.000, P = 0.174	NA	WT: n = 24, *Cyfip1*$^{+/-}$: n = 24

7.1A, CA1	WT: W = 0.984, P = 0.977 *CyfiP1*$^{+/-}$: W = 0.963, P = 0.569	Levene`s test F = 2.426, P = 0.127	Student`s *t*-test, two-tailed P = 0.376	NA	WT: n = 20, *Cyfip1*$^{+/-}$: n = 21
7.1A, CA3	WT: W = 0.975, P = 0.855 *CyfiP1*$^{+/-}$: W = 0.960, P = 0.546	Levene`s test F = 3.992, P = 0.053	Student`s *t*-test, two-tailed P = 0.067	NA	WT: n = 20, *Cyfip1*$^{+/-}$: n = 20
7.1C	Formation WT W = 0.814, P = 0.000 *Cyfip1*$^{+/-}$ W = 0.731, P = 0.000 Elimination WT W = 0.877, P = 0.000 *Cyfip1*$^{+/-}$ W = 0.894, P = 0.002	Levene`s test F = 2.762, P = 0.044	Two-way ANOVA Main effect of plasticity $F_{1, 148}$ = 1.567, P = 0.213 Main effect genotype $F_{1, 148}$ = 4.718, P = 0.031 Interaction plasticity x genotype $F_{1, 148}$ = 0.020, P = 0.887	 0.238 0.578 0.020	WT dendrites n = 40 *Cyfip1*$^{+/-}$ dendrites n = 36
7.2A	Base line WT W = 0.814, P = 0.000 *Cyfip1*$^{+/-}$ W = 0.731, P = 0.000 After training WT W = 0.761, P = 0.000 *Cyfip1*$^{+/-}$ W = 0.866, P = 0.000	Mauchly`s Test of Sphericity assumed	Repeated measures ANOVA Main effect of spine formation $F_{1, 74}$ = 25.737, P = 0.000 Interaction spine formation x genotype $F_{1, 74}$ = 0.260, P = 0.612	 0.999 0.079	WT dendrites n = 40 *Cyfip1*$^{+/-}$ dendrites n = 36
7.2C	Base line WT W = 0.877, P = 0.000 *Cyfip1*$^{+/-}$ W = 0.894, P = 0.002	Mauchly`s Test of Sphericity assumed	Repeated measures ANOVA Main effect of spine elimination		WT dendrites n = 40

	After training WT W = 0.515, P = 0.000 *Cyfip1*$^{+/-}$ W = 0.774, P = 0.000		$F_{1, 74}$ = 0.135, P = 0.715 Interaction spine elimination x genotype $F_{1, 74}$ = 1.649, P = 0.203	0.065 0.245	*Cyfip1*$^{+/-}$ dendrites n = 36
8.1A	nonparameteric		Mann-Whitney	NA	*Nlgn3*$^{y/+}$ MGH:17 *Nlgn3*$^{y/-}$ MGH:17
8.1B	Unknown	Unknown	Correlation test	NA	MGH: 13 cages SGH: 6 cages
8.2A	Normal distribution	Equal variances	Two-way ANOVA Effect of housing $F_{1, 78}$ = 6.30, P = 0.014 Interaction housing x genotype $F_{1, 78}$ = 4.150, P = 0.045 Sidak`s post hoc test	-	*Nlgn3*$^{y/+}$ SGH:8 *Nlgn3*$^{y/-}$ SGH:7 *Nlgn3*$^{y/+}$ MGH:8 *Nlgn3*$^{y/-}$ MGH:7

8.2B	Normal distribution	Equal variances	Two-way ANOVA Effect of housing $F_{1, 20}$ = 4.900, P = 0.038	-	*Nlgn3*$^{y/+}$ SGH:8 *Nlgn3*$^{y/-}$ SGH:6 *Nlgn3*$^{y/+}$ MGH:5 *Nlgn3*$^{y/-}$ MGH:5
8.2C	Normal distribution	Equal variances	One-way ANOVA	NA	*Nlgn3*$^{y/+}$ SGH:7 *Nlgn3*$^{y/-}$ SGH:6 *Nlgn3*$^{y/+}$ MGH:5 *Nlgn3*$^{y/-}$ MGH:5

Table A.1 Details of statistical analysis.